Supramolecular Iridium(III) Assemblies

Diego Rota Martir[a] *and Eli Zysman-Colman*[a]*

[a] Organic Semiconductor Centre, EaStCHEM School of Chemistry, University of St Andrews, St Andrews, Fife, KY16 9ST, UK, Fax: +44-1334 463808; Tel: +44-1334 463826; E-mail: eli.zysman-colman@st-andrews.ac.uk;
URL: http://www.zysman-colman.com

Abstract. Iridium(III) complexes exhibit remarkable photophysical properties such as high photoluminescence quantum yields, wide color tunability and high chemical stability. They have featured prominently in diverse applications such as sensing, bio-imaging, photoredox catalysis, solar fuels and solid-state lighting. In the vast majority of these reports the iridium complex is mononuclear in nature. The use of iridium complexes as components of self-assembled systems has garnered increasing attention and this review aims to comprehensively document the advances made in this area. Special emphasis will be devoted to describing the photophysical properties and applications of such photo-active supramolecular materials. Soft materials such as soft salts, liquid crystals, gels, colloids incorporating iridium are described as are hydrogen bonding- and π-π staking-directed assemblies, coordination-driven self-assembled materials such as coordination polymers and metal organic frameworks, macrocycles, capsules and cages. Finally, guest Ir(III) complexes encapsulated within the cavities of cage-type structures are presented.

Contents

1. Introduction

The term molecular self-assembly applies to pathways that produce a final product directly and spontaneously when the correct components are mixed under appropriate conditions.[1] Self-assembly plays an integral role in the structure and function of biological systems[2-4] and it is implicated in a variety of functional materials.[5] In Nature self-assembly is generally based on numerous hydrogen bounding, electrostatic, van der Waals, and other weak inter- and intra-molecular interaction working synergistically to assemble, for example, secondary and tertiary structures of proteins, which then provide well-defined local environments to mediate biochemical transformations.[6] Similarly, in natural photosynthesis organisms optimize solar energy conversion through the self-organized assembly of photofunctional chromophores.[7, 8] Over the last two decades, molecular self-assembly has played a key role in the construction of a variety of elegant and intricate synthetic nanostructures, including molecular crystals and liquid crystals,[9, 10] colloids[11] and micelles,[12] gels,[13, 14] polymers[15, 16] and nanoscale structures of high symmetry, such as 3D-frameworks,[17] metal-organic polygons and polyhedra.[18, 19] As the properties of these materials highly depend both on the nature of their components and the interactions between them, the explicit manipulation of the building blocks and the non-covalent forces that hold the constituents together has promoted the evolution of functional properties, which have been exploited in numerous advanced

technologies. For example, liquid crystals have found application as anisotropic organic semiconductors in organic field effect transistors (OFETs), Organic Light-Emitting Diodes (OLEDs) and Organic Photovoltaic devices (OPVs).[9, 10, 20] Due to their large surface area and biocompatibility, colloids and micelles are very important for water purification, cleansing action of soap and food formulation.[21, 22] Hydrogels and polymers are key components in materials for medicine, food science and cosmetics.[23-25] Nanostructured materials such as molecular crystals, frameworks or 3D-polyhedral structures exhibit interesting optical, magnetic and catalytic properties, which have been rapidly exploited in diverse applications such as in catalysis, magnetic devices and gas purification.[26-28]

In recent years, there has been an increasing interest in the construction of photoactive supramolecular assemblies through the incorporation of luminescent building blocks.[29-32] This immediately generates possibilities for assembling in very close proximity a high concentration of chromophoric units through non-covalent interactions, thereby achieving photophysical properties that are difficult to obtain in conventional molecular materials. Besides modulating the optoelectronic properties of the emissive compounds as a function of the assembly, their organization into ordered structures can also radically change the physical properties of the bulk materials.[33] As a result, nanomaterials that exhibit both fascinating physical and photoactive properties have been one of the main areas of interest in supramolecular chemistry in recent years.[29, 34, 35]

Cyclometalated iridium(III) complexes exhibit efficient phosphorescence, unprecedented facile emission color tunability across the visible spectrum, and high chemical and thermal stability.[36-40] They have thus found use in myriad applications such as in sensing,[41, 42] bio-imaging,[43] photoredox catalysis,[44] solar fuels[45, 46] and in electroluminescent

devices.[47, 48] The use of iridium complexes as luminescent components for self-assembly has also become increasingly popular. This review article provides an exhaustive summary on the development of photoactive self-assembled materials based on iridium(III) complexes, giving special emphasis to their photophysical properties, and highlighting their applications. Depending on the nature of the ligands, iridium(III) complexes can be cationic, neutral and anionic. The vast majority of cationic iridium(III) complexes possess the general motif $[Ir(C^N)_2(N^N)]^+$, where C^N is a cyclometalating ligand such as 2-phenylpyridinato (ppy) and N^N is a neutral ancillary ligand such as 2,2'-bipyridine (bpy). Homoleptic neutral iridium complexes possess the general formula $[Ir(C^N)_3]$ and are frequently studied as their facial geometric isomer. Heteroleptic neutral complexes generally possess the structural motif $[Ir(C^N)_2(X)]$, where X is an anionic bidentate ligand such as acetylacetonates, oxazolines or thiazolines whereas, negatively charged cyclometalated iridium(III) complexes typically possess the composition $[Ir(C^N)_2(Y)_2]^-$, where Y is typically an anionic monodentate ligand such as CN^-, NCS^- and NCO^-.

We begin by describing iridium-based soft materials such as ion-paired iridium complexes commonly known as soft-salts, liquid crystals, supramolecular gels, colloidal structures and assemblies developed through H-bonding and π-π-stacking interactions. Next, we turn our attention to describing luminescent iridium-based coordination polymers, metal-organic frameworks (MOFs) and discrete structures, followed by an overview of luminescent Ir-based macrocycles, capsules and cages. The last chapter of this review highlights the emerging field of dynamic encapsulation of mononuclear iridium complexes into the cavities of 3D MOFs and cages. In this chapter, emphasis will be placed in describing the changes of the luminescent properties of the guest iridium complexes due to their physical and optoelectronic interactions with the host materials. It is worth noting that a number of studies involving luminescent Ir(III)

complexes covalently assembled within multinuclear dyads, triads and arrays,[49-51] or covalently linked onto polymeric structures[52-54] have been reported. As these systems have been extensively described elsewhere, they are not included within the present review.

2. Soft materials

Molecular aggregation induced by non-covalent interactions between Ir(III) chromophores can have tremendous impact on the properties of materials. Desirable photophysical properties such as emission tuning, enhanced photoluminescence quantum yield, longer excited state lifetimes, and energy and electron transfer processes can be achieved by controlling the aggregation and organization of Ir(III) emitters in soft materials.

2.1. Soft salts

The term "soft salt" describes ionic materials that are composed of two or more organometallic components characterized by complementary charges and assembled into complex salts through Coulombic interactions. The majority of the reported soft salts incorporating iridium have consisted of a cationic iridium complex married with an anionic iridium complex.

The first examples of iridium soft salts were reported in 2010 by Thompson and co-workers[55] (Figure **1**) and De Cola and co-workers[56] (Figure **2a**) who assembled via salt metathesis reactions blue- and green-emitting anionic Ir(III) complexes with yellow- and orange-emitting cationic iridium complexes.

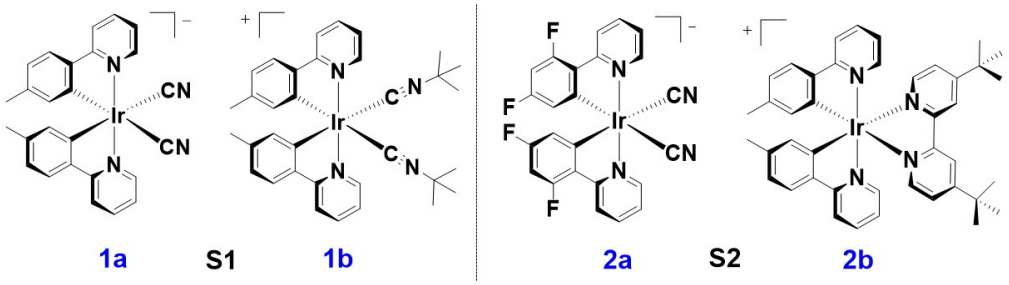

Figure **1**. Chemical structure of soft salt **S1** (left) and **S2** (right).

Soft salt **S1** was prepared by assembling the anionic green-emitting Ir(III) complex Na[Ir(mppyH)$_2$(CN)$_2$], Na**1a** with the cationic yellow-emitting Ir(III) complex [Ir(mppyH)$_2$(CNdt)$_2$]Cl, **1b**Cl (mppyH is 2-(*p*-tolyl)pyridine and CNdt is 2-methyl-*N*-methylydynepropan-2-aminium), while **S2** contains the anionic blue-emitting Ir(III) complex Na[Ir(dFppy)$_2$(CN)$_2$], Na**2a** (dFppyH is 4,6-difluorophenylpyridine) with the cationic orange-emitting Ir(III) complex [Ir(mppyH)$_2$(dtbubpy)]Cl, **2b**Cl (dtbubpy is 4,4'-di-*tert*-butyl-2,2'-bipyridine) (Figure **1**). In degassed MeCN the complexes Na**1a** and **1b**Cl exhibited vibronic ligand-centered (^{3}LC) emission profiles, respectively, at λ_{PL} = 472 nm and λ_{PL} = 458 nm with photoluminescence quantum yield of Φ_{PL} = 70% and Φ_{PL} = 38%, and photoluminescence lifetimes of τ_{PL} = 4.0 μs and τ_{PL} = 36.7 μs. Similarly, complex Na**2a** exhibited a vibronic ^{3}LC emission at λ_{PL} = 448 nm with a Φ_{PL} of 70% and a τ_{PL} = 4.1 μs, while complex **2b**Cl showed a broad mixed metal-to-ligand and ligand-to-ligand charge transfer (^{3}MLCT/^{3}LLCT) emission centered at λ_{PL} = 586 nm with a lower Φ_{PL} of 21% and a shorter τ_{PL} of 0.43 μs. The photoluminescence spectra of the soft salts **S1** and **S2** exhibited a concentration dependence, which impacted the degree of emission quenching of the anion by the cation *via* Dexter energy transfer. Taking **S2** as an example, at a relatively low concentration of 10^{-5} M its luminescence profile was dominated by the emission at λ_{PL} = 448 nm, characteristic of the blue-emitting anion **2a**. This high-energy emission gradually decreased as a function of increasing concentration of **S2** from 10^{-5} M to 10^{-3} M and, at a concentration greater than 10^{-3} M, only the

orange emission exhibited by the cation **2b** at λ_{PL} = 586 nm was observed. Based on a bimolecular quenching model, a quenching rate constant k_q of 1.71 x 10^{10} $M^{-1}s^{-1}$, close to the diffusion limit in acetonitrile (2 x 10^{10} $M^{-1}s^{-1}$), was calculated.

Similarly, De Cola and co-workers assembled the green-emitting anionic Ir(III) complex of composition $NBu_4[Ir(ppy)_2(CN)_2]$, NBu_4**3a**, with the yellow-emitting cationic Ir(III) complex $[Ir(dFppy)_2(bpy)]Cl$, **3b**Cl (**S3**, Figure **2**), and the blue-emitting anionic Ir(III) complex K**2a** with the orange-emitting cationic Ir(III) complex $[Ir(ppy)_2(bpy)]Cl$, **4b**Cl (**S4**, Figure **2a**).

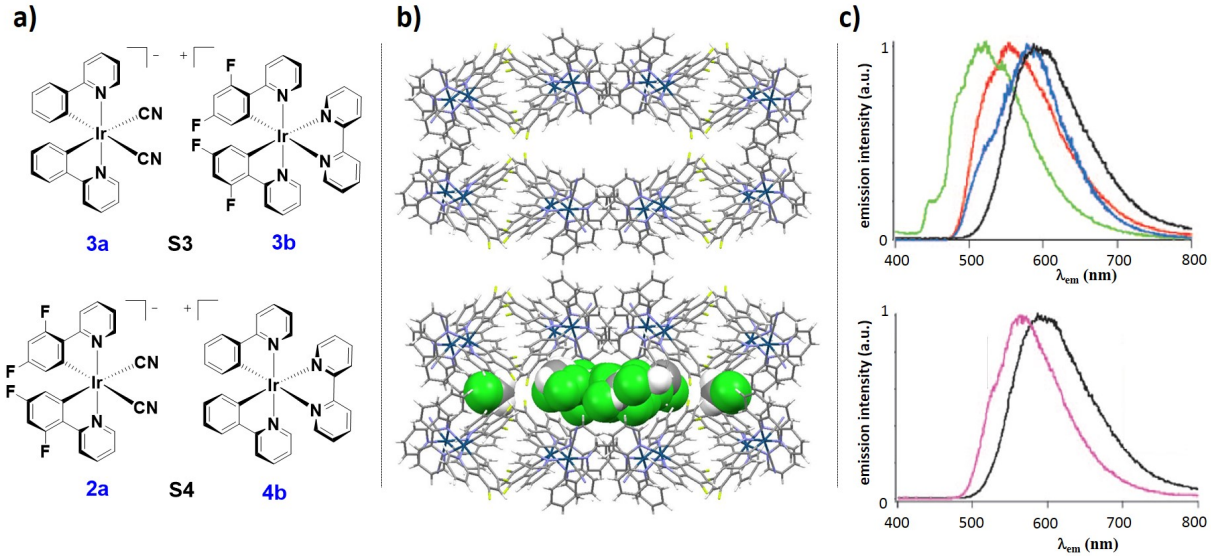

Figure **2**. **a)** Chemical structures of complex salts **S3** (top) and **S4** (bottom). **b)** crystal packing of salt **S3** highlighting the channel running along the crystallographic *c* axis (top) and illustration of the dichloromethane solvent molecules (space-filling representation) inside the channel and pockets of **S3** (bottom). The remaining solvent molecules are omitted for clarity. **c)** top: normalized emission spectra of dried **S4** (black line), **S4** with toluene intercalated (blue line), complexes **2a** (red line) and **4b** (green line); bottom: normalized emission spectra of **S4** (black line) and **S4** intercalating anthraquinone (pink line). Part **c)** is adapted with permission. Copyright 2010, Wiley-VCH.[56]

The X-ray single crystal structure of **S4** showed that this soft salt forms a 3D porous network where small solvent molecules such as dichloromethane, amyl acetate, ethyl acetate, diethyl ether, toluene or anthraquinone could be easily intercalated (Figure **2b**). The emission properties of the single crystals of the microcrystalline salts **S3** and **S4** were investigated both under vacuum in the absence of guest molecule inclusion and after loading guest molecules into their networks. In degassed DCM, complex NBu_4**3a** emitted yellow light with a λ_{PL} at 564 nm while **3b**Cl emitted in the blue-green with a λ_{PL} at 502 nm. The emission of the crystal of **S3** in its dry form exhibited a red-shifted emission at λ_{PL} = 591 nm. Analogously, the dried crystal of **S4** exhibited a red-shifted emission at λ_{PL} = 596 nm compared to the emission of both K**2a** and **4b**Cl, which exhibited, respectively, λ_{PL} = 554 nm and λ_{PL} = 460 nm. The red-shifted emission of both **S3** and **S4** compared to the corresponding mononuclear complexes were attributed to strong π-π interactions between the C^N ligands of complementary iridium complexes of opposite charge present in the crystal networks, promoting Dexter energy transfer from the high energy anionic Ir donors **3a** and **2a** to the low energy cationic Ir acceptors **3b** and **4b**, and additionally promoting exciplex formation and emission from correspondingly lower-energy excited states. Importantly, the emission properties of the crystals **S3** and **S4** could be efficiently modulated by trapping guest molecules within their porous networks. For example, the intercalation of toluene or anthraquinone into **S4** led to blue-shifted emission of the soft-salt, respectively, at λ_{PL} = 590 nm and λ_{max} = 580 nm, compared to the dried crystal. An enhanced emission was observed when toluene was absorbed into **S4** due to the disruption of the π-π interactions whereas the emission was quenched when anthraquinone was intercalated within the crystal of **S4** as a function of the photoinduced electron transfer from the **S4** donor to the anthraquinone acceptor (Figure **2c**).

Our group reported[57] the first example of a three component heterometallic ion-pair assembly, **S5** (Figure **3**) involving two equivalents of complex NBu_4**3a** (Figure **2**) associated with the red-emitting $[Ru(dtbubpy)_3]Cl_2$ **5b**Cl_2 (Figure **3a**). Upon photoexcitation into the ruthenium complex ^{1}MLCT absorption band in MeCN, **5b**Cl_2 exhibited the characteristic broad ^{3}MLCT emission centered at λ_{PL} = 630 nm, which is complementary in color compared to the ^{3}LC emission exhibited by complex NBu_4**3a** (λ_{PL} = 477 nm in degassed MeCN). Soft salt **S5** nicely illustrates how the emission properties can be modulated upon changes in concentration and medium. At low concentration, the emission of **S5** is dominated by the structured ^{3}LC emission of **3a**. As the concentration increases, due to increased efficiency of the Förster energy transfer from the anionic Ir(III) donor to the cationic Ru(II) acceptor, the emission profile of **S5** resembles increasingly that of the lower-energy emission of the Ru(II) complex **5b** (Figure **3b**). In contrast to the emission behavior observed for **S3** and **S4**, the emission of **S5** did not involve either excimers or exciplexes. Further, as a function of the solvent polarity, the electrostatic interaction of the cation and anion could be modulated and therefore the magnitude of the energy transfer between the two. Solvents of high polarity, such as DMSO, MeOH or EtOH, solvated strongly the ions, leading to their weak association, poor energy transfer and an emission dominated by **3a**. Less polar solvents such as DCM or MeCN promoted the formation of intimate ion pairs, resulting in shorter distance between the Ir and Ru ions and more efficient energy transfer, and an emission profile that resembles that of **5b**.

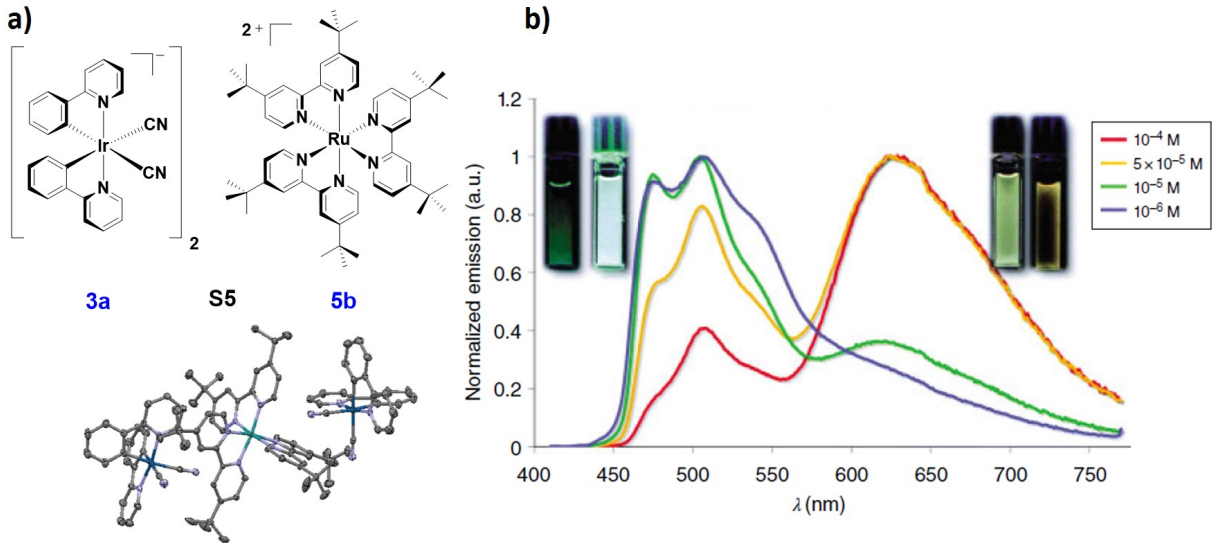

Figure **3**. **a)** Chemical structure of the soft salt **S5** with its single crystal x-ray structure; **b)** normalized emission spectra of **S5** recorded in deaerated MeCN at 298 K at different concentrations (λ_{exc} = 390 nm). Insets are images of MeCN solutions of **S5** at different concentrations. Image **b)** is adapted from ref [57] with permission from The Royal Society of Chemistry.

Soft salt **S5** exhibited a significantly enhanced ECL (electrochemiluminescence) signal at similar energy to **5b**.[58] This observation is rather unusual considering that for the vast majority of multichromophoric species, the ECL signals could be addressed at different potentials and thus produce multiple emissive readouts.[59-61] The ECL efficiency of **S5** was determined to be 2.51%, which is intermediate between the ECL efficiencies of the ionic components **3a** (2.83%) and **5b** (2.14%). The higher ECL efficiency for **S5** compared to **5b** is due to the $[Ir]^{\cdot -}$ - $[Ru]^{\cdot +}$ annihilation process, where $[Ir]^{-}$ acts as a co-reactant and thus reduces the energy required to emit light from the excited [Ru]*.

Godbert and co-workers[62] synthetized green-emitting anionic Ir complexes bearing an unsual bidentate orotate dianion as the ancillary ligand (NBu_4**4a** and NBu_4**4b** in Figure **4a**).

These complexes exhibited high photoluminescence quantum yields of Φ_{PL} = 69% and Φ_{PL} = 58%, respectively, with emission maxima, respectively, at 530 nm and 536 nm. When NBu_4**4a** and NBu_4**4b** were respectively assembled with the cationic complex $[Ir(ppy)_2(py\text{-}am)]Cl$ (**6b**Cl in Figure **4a**, py-am is 2-pycolylamine), which itself shows an emission at λ_{PL} = 490 nm with a Φ_{PL} of 52%, highly emissive soft salts, **S6a** and **S6b** (Figure **4a**) were obtained. **S6a** and **S6b** are unusual examples of soft salts in which the cation (**6b**) is the donor unit, while the anions (**4a** and **4b**) are the acceptors. The emission of **S6a** and **S6b** involved contributions from both ions with λ_{PL}, respectively, at 480, 525 nm and 486, 532 nm and high Φ_{PL} values of 81% and 83%, respectively.

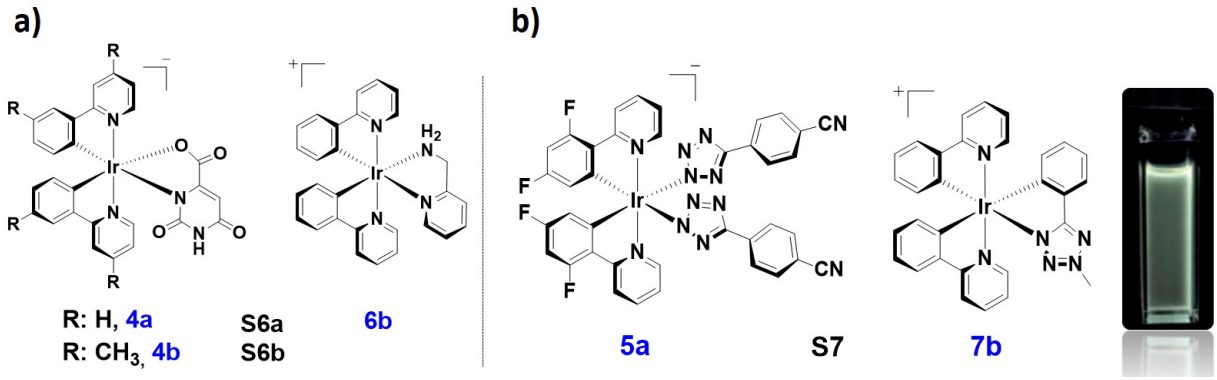

Figure **4**. **a)** chemical structure of soft salts **S6a** and **S6b** and **b)** chemical structure of the white-emitting soft salt **S7**. Inset is image of air-equilibrate DCM solution of **S7**. The inset image is adapted from ref [63] with permission from The Royal Society of Chemistry.

A white-emitting soft salt was obtained by Stagni and co-workers[63] by assembling the blue-emitting anionic Ir(III) complex NBu_4**5a** (Figure **4b**), bearing dFppy as C^N ligands and 4-benzonitrile tetrazolate as ancillary ligands, with the red-emitting $[Ir(ppy)_2(ptz\text{-}Me)]Cl$ complex (ptz-Me is 5-methyl-2-phenyltetrazole) (**7b**Cl, Figure **4b**). In aerated DCM, complex NBu_4**5a** exhibited a structured emission profile typical of emission from a ^{3}LC/^{3}MLCT state with λ_{PL} at 462 nm and 492 nm and a Φ_{PL} of 3.3%. Complex **7b**Cl, by contrast, exhibited a broad emission profile with λ_{PL} = 686 nm and a Φ_{PL} of 2.7%. As both the anionic and cationic

complexes **5a** and **7b** contributed almost equally to the emission of **S7** in aerated DCM, and energy transfer between the two ions played a minor role, an almost pure white-light (CIE: x = 0.3288, y = 0.3284) with λ_{PL} at 460 nm, 490 nm and 680 nm and a Φ_{PL} of 2.8% was emitted by the assembly. The poor energy transfer in **S7** is probably due to the presence of the bulky 4-benzonitrile tetrazolate in **5a** that restricts its interaction with the cation **7b**.

In the context of electroluminescence devices, neutral Ir complexes have been extensively used in Organic Light-Emitting Diodes (OLEDs),[64-66] whereas cationic Ir(III) complexes have been explored more explicitly as emitters in Light-Emitting Electrochemical Cells (LEECs).[47, 67] Covalently linked dinuclear iridium complexes have been scarcely investigated as emitters in solid-state lighting, with only one example available for use in LEECs[68] and few for OLEDs.[69-75] However, iridium-based soft salts have demonstrated reasonable performance as emitter materials in OLEDs. The main advantage of using soft salts in lighting devices relies on the capacity to introduce two phosphorescent centers in one complex ion, while controlling the intermolecular separation of the two metal centers through non-covalent interactions. The first examples of iridium soft salts used in OLEDs were reported by Thompson and co-workers.[55] Notably, OLEDs fabricated by using **S2** (Figure **1**) as the emitting material exhibited an external efficiency, EQE, of 4.7% and a luminance of over 7428 $cd \cdot m^2$ (λ_{PL} = 586 nm). The good performance of the OLED could be directly linked to the suitable alignment of the HOMO-LUMO levels of the two ionic components of the soft salt. Unfortunately, the relatively low Φ_{PL} of 18% exhibited by **S2** in thin films limited the efficiency of the device. When **S2** was used as the emitter in a single-layer LEEC, the device failed to turn on under voltages ranging from 2.5 V to 7 V, a result of the poor ionic mobility of the ions of **S2**.

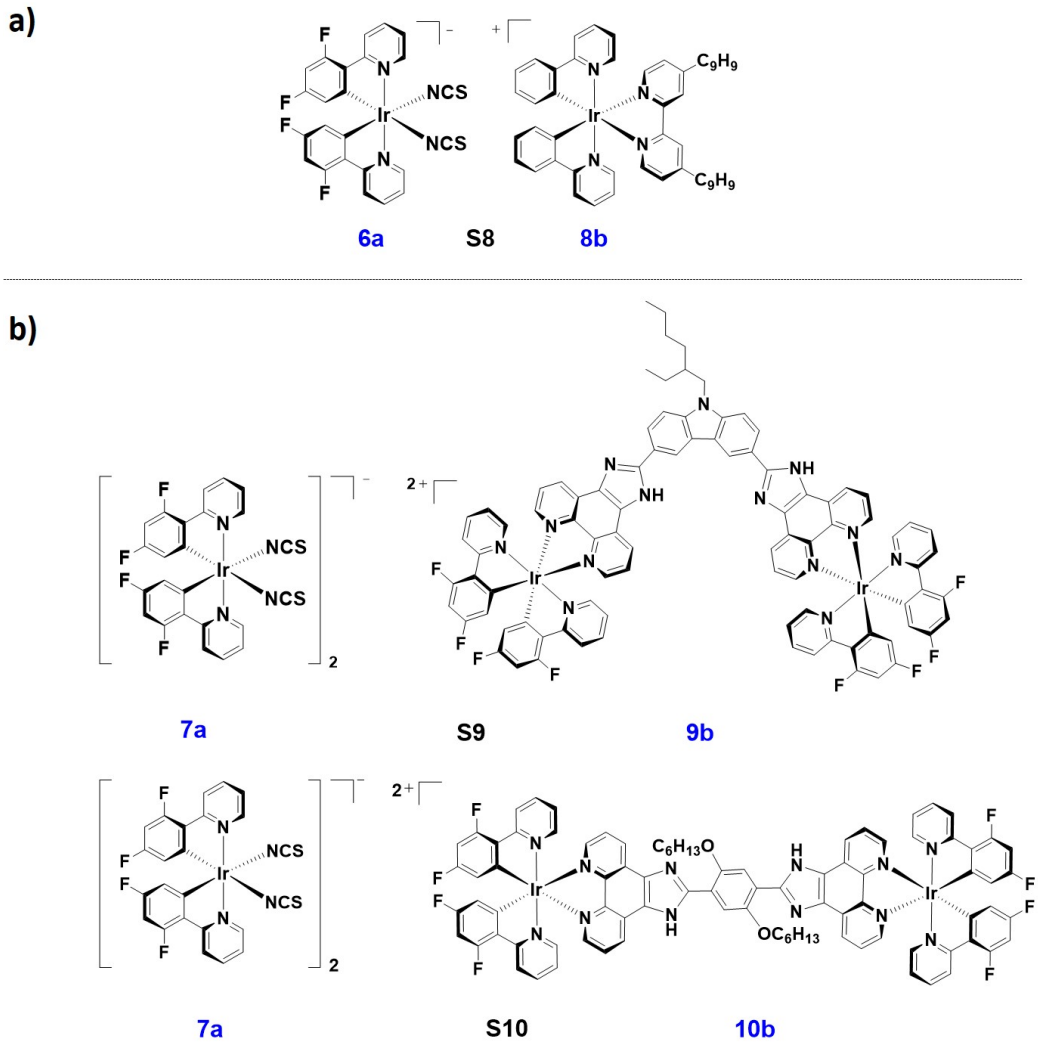

Figure **5**. Chemical structures of iridium soft salts used in OLEDs. **a) S8** and **b) S9** (top) and **S10** (bottom).

Dumur, Mayer and co-workers[76] also explored the use of a soft salt emitter in OLEDs, the composition of which consisted of the anionic $NBu_4[Ir(dFppy)_2(NCS)_2]$, NBu_4**6a**, with the cationic complex $[Ir(ppy)_2(bpy\text{-}non)]PF_6$ **8b**PF_6 (Figure **5a**, bpy-non is 4,4'-dinonyl-2,2'-bipyridine). The nonyl chains were introduced to **8b**PF_6 to enhance the solubility of the resultant **S8** in organic solvents and thus improve the thin film morphology in solution-processed devices. Soft salt **S8** exhibited luminescence centered at approximately 550 nm in DCM solution, thin film and in electroluminescent devices. The OLEDs fabricated with **S8** as

the emitting material exhibited a low external quantum efficiency of 0.66% and a luminance of 1114 $cd \cdot m^{-2}$ (λ_{EL} = 553 nm).

Two iridium soft salts based on ion-paired dinuclear cationic, and mononuclear anionic complexes were reported by Mayer and co-workers[77] and investigated as emitting materials in OLEDs (Figure **5b**). The unit bridging the two iridium centers in the dinuclear cationic complexes consisted either of a carbazole derivative for **9b**PF_6 or a phenylene group in the case of **10b**PF_6. Both dinuclear complexes **9b**PF_6 and **10b**PF_6 exhibited low Φ_{PL} in degassed DCM of 9.1% and 15.0%, respectively, attributed to intramolecular quenching between the two iridium luminophores. As the phenylene bridge favored the communication between the two iridium centers, the electroluminescence performance using **S10** was poorer than that using **S9** with respective maximum peak current efficiencies of 0.06 and 0.44 $cd \cdot A^{-1}$ and maximum brightness of 101 and 1022 $cd \cdot m^{-2}$.

Intracellular pH is a crucial parameter associated with cellular behavior and pathological conditions such as cell proliferation, apoptosis, drug resistance, enzymatic activity and ion transport.[78] Abnormal cellular pH is an indicator of inappropriate cellular function, which is associated with many diseases such as stroke, cancer, and Alzheimers.[79] It is thus pivotal to monitor pH alteration in biological cells and tissues to understand physiological and pathological processes.[80] In this context, Wong, Zhao and co-workers[81] recently illustrated that soft salts can also be rationally designed to act as efficient probes for lifetime imaging of intracellular pH. Indeed, they designed the soft salt **S11** (Figure **6a**) formed by the assembly of the cationic complex **11b**Cl, bearing a qpy (qpy = 4,4':2',2'':4'',4'''-quaterpyridine) as the ancillary ligand, with the anionic complex NBu_4**2a** (Figure **1**). Specifically, complex

11b Cl is pH sensitive as the protonation or deprotonation of its distal pyridine units gives rise to changes in the emission of **S11**, which can be easily detected by both steady-state and time-resolved luminescence spectroscopy. The cationic complex **11b**Cl showed a broad orange-red emission in deareated MeCN centered at λ_{PL} = 625 nm, which decreased dramatically in intensity with decreasing pH (Figure **6b**). By contrast, the structured blue-emission exhibited by the anionic counterpart NBu_4**2a** (λ_{PL} = 451, 475 nm) was not affected by changes in pH.

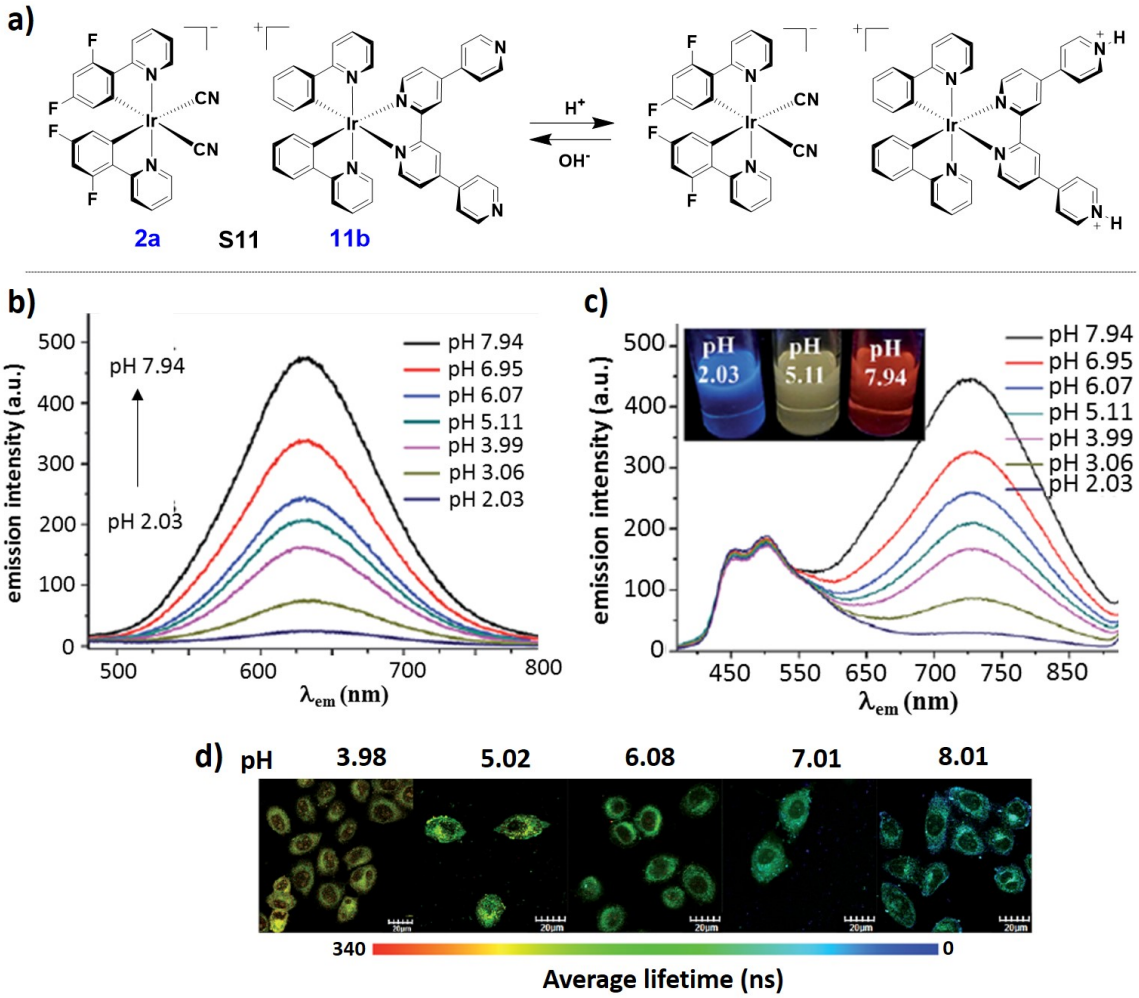

Figure **6**. **a)** Design concept of the ratiometric design probe and chemicals structures of **2a**, **11b** and soft salt **S11**. **b)** changes in the phosphorescence emission spectra of **11b** (2.0×10^{-5} M) in the pH range of 2.03 – 7.94 in MeCN/buffer (1:9, v/v). **c)** changes in the phosphorescence emission spectra of **S11** (2.0×10^{-5} M) in the pH range of 2.03 – 7.94 in MeCN/buffer (1:9, v/v). **d)** phosphorescence lifetime images of **S11** in living Hep-G2 cells (incubated at 37 ˚C for

1h) at different pH values. Images **b)**, **c)** and **d)** are adapted from Ref. [81] with permission from The Royal Society of Chemistry.

The phosphorescence spectral changes of **S11** at different pH values are illustrated in Figure **6c**. Enhanced phosphorescence at λ_{PL} = 625 nm was observed at basic pH, while at acidic pH the emission of **11b** was quenched due to the protonation of the qpy ligand. Thus, at basic pH the emission of **S11** was dominated by the orange emission of **11b**, the result of efficient energy transfer from **2a**, while at acidic pH the emission of **S11** was dominated by the structured blue emission of the donor anion. Such a change in phosphorescence from blue to orange with increasing pH values was also detected using confocal luminescence microscopy after incubation of **S11** in living HepG-2 cells (Figure **6d**).

Similarly, Zhao and co-workers[82] used an ion-paired iridium complex (**S12**, Figure **7a**), composed of a cationic complex functionalised with α,β-unsaturated ketone moieties (**12b**PF_6), and the anionic complex NBu_4**3a** (Figure **2a**), for ratiometric and time-resolved luminescence sensing and imaging of intracellular biothiols cysteine and homocysteine. These analytes were chosen as they participate in the process of cellular growth in living cells. The sensing capacity of **S12** towards thiol analytes is due to their rapid Michael addition with the α,β-unsaturated ketone moieties of **12b** thereby promoting a strong enhancement of the emission of the cation acceptor at λ_{PL} = 560 nm, while only slightly influencing the photophysics of the donor complex at λ_{PL} = 485, 505 nm (Figure **7b**,**c**).

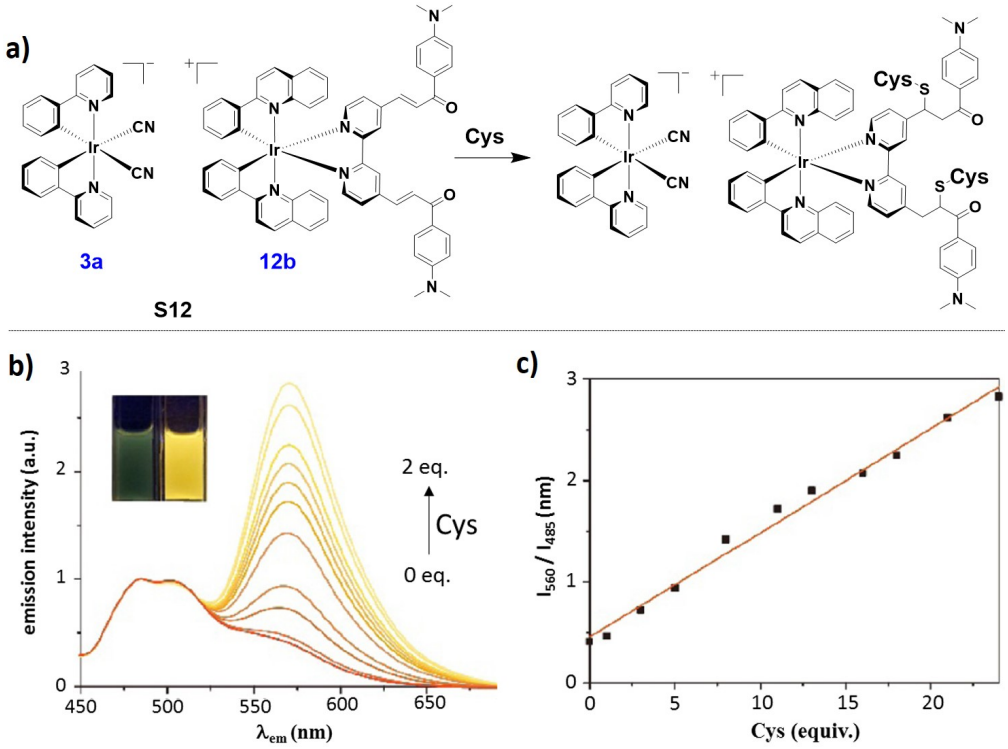

Figure **7**. **a)** chemical structures of **3a**, **12b** and soft salt **S12** and sensing mechanism of **S12**. **b)** changes in phosphorescence emission spectra of **S12** in MeCN/H_2O (3:2, v/v) with various amount of cysteine added (from 0 to 2 equivalents). Insets are images of **S12** without cysteine (left) and with two equivalent of cysteine (right). **c)** titration curve plotted with emission intensity at 560 nm over that at 485 nm as a function of cysteine equivalents. Images **b)** and **c)** are adapted from Ref. [82] - published by OSA publishing.

Schanze and co-workers[83] reported an ion-paired assembly between the anionic poly(phenyleneethynylene) electrolyte ($PPESO_3^-$) and the cationic Ir(III) complex **4b**Cl (Figure **2a**). Upon excitation of **4b**-$PPESO_3$ in methanol at 355 nm, the emission of $PPESO_3^-$ at λ_{PL} = 450 nm was completely quenched as a result of Dexter energy transfer from $PPESO_3^-$ to **4b** with a calculated quenching constant (k_q) of around 10^5 M^{-1}. A weak phosphorescence from **4b** was observed at λ_{PL} = 610 nm. Subsequent to the Dexter energy transfer, ultra-fast back-transfer from the triplet state of **4b** located at 2.25 eV to the triplet state of $PPESO_3^-$ located between

2.0 – 2.2 eV was detected by transient absorption spectroscopy. By contrast, back-energy transfer was not observed when $PPESO_3^-$ was assembled with the Ir(III) complex of composition $[Ir(hqx)_2(bpy)]Cl$ (hqx is 2,3-diphenylquinoxaline), which possesses a triplet state at 1.96 eV, which is too low in energy to sensitize the formation of the triplet state of $PPESO_3^-$. This study demonstrates that Ir(III) complexes with appropriate triplet energy can serve to sensitize the triplet state in conjugated polymers.

2.2. Liquid crystals

Liquid crystals (LC) are considered as the "fourth state of matter" as their properties are intermediate between those of crystalline solids and those of liquids. Most liquid crystals are neutral organic compounds.[10] However, ionic liquid crystals can also be formed by incorporating anions and cations into the molecule of the LC.[84] Ionic metallomesogens, for instance, are liquid crystals based on transition metal complexes.[85] The driving force for the formation of metallomesogens are the interactions, generally van der Waals, between the anisometric molecules promoting high self-organization of the materials into rod-like, disc-like or nematic columnar phases.[9, 10] Early examples of LC iridium complexes took advantage of the square-planar geometry or iridium(I) metal centers. Complex **LC1** (Figure **8**) is a dinuclear complex bearing a mesomorphic ligand that, due to its elongated shape, displayed a smectic phase at higher temperature (between 142 ˚C and 169 ˚C) compared to related mononuclear complexes (between 104 ˚C and 128 ˚C) of the composition of $[IrCl(CO)_2L]$, where L are 4-stilbazole or 4-styrylpyridine derivatives bearing long alkoxy chains.[86, 87] **LC2** (Figure **8**) is based on an iridium dicarbonyl β-ketonate functionalized with alkoxy chains that crystallized with a strict antiparallel arrangement of the Ir centers to produce one-dimensional chains that displayed disordered columnar hexagonal phases (Col_{hd}).[88, 89]

Interestingly, for $n = 3, 4, 5$, the complexes were liquid crystalline already at 0 °C and remained so up to 130 °C.

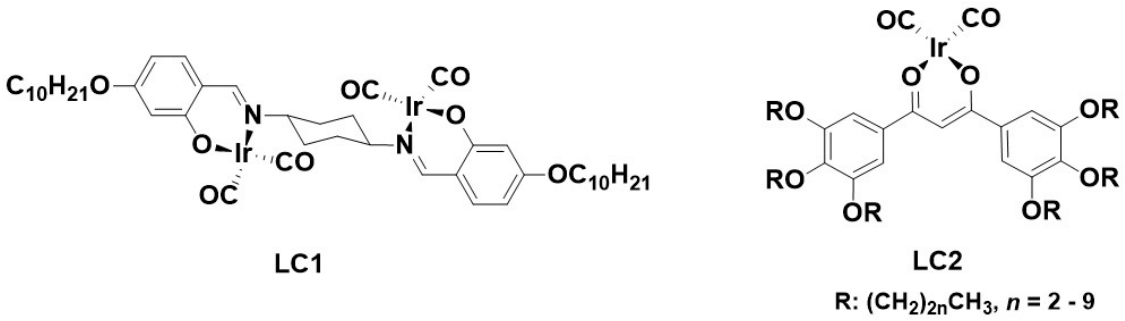

Figure **8**. Chemical structure of **LC1** (left) and **LC2** (right).

The first example of a LC based on a luminescent cyclometalated Ir(III) complex (**LC3**, Figure **9**) was reported by Ghedini and co-workers.[90] **LC3** is the cationic complex $[Ir(ppy)_2(bpy\text{-}C8)]PF_6$ bearing a bipyridine functionalized at the 4,4'-position with [3,4,5-(trioctyloxy)benzoyloxymethyl] units as the ancillary ligand. This complex exhibited a monotropic columnar hexagonal phase when the sample was cooled rapidly (>10 °C/min), and this mesophase was stable within the temperature range of 120 °C - 20 °C. Upon subsequent heating, crystallization was observed at 94 °C and isotropization occurred at 184 °C. When the sample was slowly cooled, only the crystalline phase was observed. Interestingly, the different phases exhibited different emission properties. In deaerated DCM **LC3** exhibited an orange-red emission at λ_{PL} = 600 nm with a Φ_{PL} of 12% and an emission lifetime, τ_{PL}, of 320 ns, corresponding to a mixed ^{3}LLCT/^{3}MLCT transition (LLCT = ligand-to-ligand charge transfer). Unlike the modest Φ_{PL} of **LC3** in solution, enhanced luminescence was detected in the two condensed phases. The emission of the liquid-crystalline and crystalline phases were both blue-shifted, respectively, at λ_{PL} = 560 nm and 520 nm, with significantly higher Φ_{PL} of 39% and 48%, respectively, compared to those observed in DCM (Figure **9**). The blue shifts accompanied by the enhanced emission intensities exhibited by **LC3** on moving from solution to the liquid-crystalline phase and finally to the crystalline solid are due to the reduced

aggregation quenching phenomena and the increasing molecular rigidity present in the condensed phases.

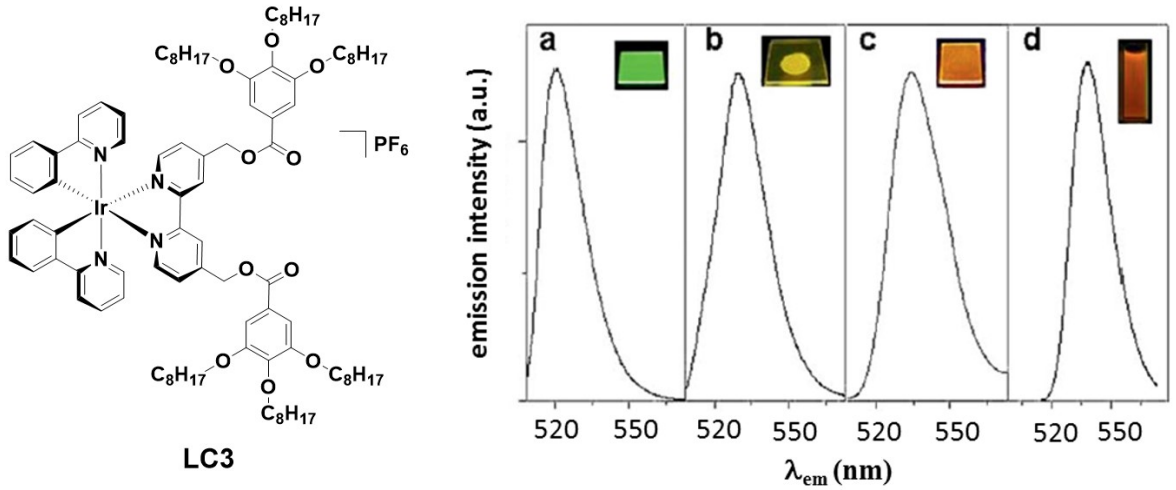

Figure **9**. Chemical structure of **LC3** (left) and its emission spectra (right) collected from **a)** crystalline film (green), **b)** mesophase film (yellow), **c)** amorphous film (orange-red) and **d)** DCM solution. Insets are images of samples under UV illumination. Images **a)**, **b)**, **c)** and **d)** are adapted with permission. Copyright 2010, Wiley-VCH.[90]

Bruce, Williams and co-workers[91] used cyclometalated Ir(III) complexes bearing anisotropic polycatenar 2,5-diphenylpyridine ligands to prepare the liquid crystalline complexes **LC4**-**LC9** illustrated in Figure **10**. Complex **LC4** was formed by cleavage of the corresponding μ-dichloro-bridged iridium dimers with dimethyl sulfoxide. Complex **LC4** showed both lamellar and columnar rectangular phases. However, **LC4** exhibited a weak emission at λ_{PL} = 580 nm with a low Φ_{PL} of 0.5% in degassed DCM and lacked chemical stability. The subsequent reaction of **LC4** with $AgPF_6$ in MeCN yielded **LC5**, which was found to be slightly more emissive and more stable than **LC4**. **LC5** exhibited a columnar mesophase between 145 ˚C and 163 ˚C, and emission in degassed DCM at λ_{PL} of 520 nm, with a Φ_{PL} of 1.3% and a τ_{PL} of 1750 ns. In search as additional luminescent iridium-based LCs, attention then turned to neutral complexes bearing acetylacetonate (acac) as the ancillary ligand.

Complexes **LC6** and **LC7** were not liquid crystalline. It was indeed discovered that three polycatenar chains on each of the C^N ligands were necessary to confer liquid crystallinity upon the complexes. Thus, **LC8** was both LC in nature and emissive, exhibiting a columnar hexagonal phase between 31 ˚C and 66 ˚C and emission at λ_{PL} = 582 nm with a Φ_{PL} of 9.1%; no emission lifetime was reported. The μ-dichloro-bridged iridium dimer **LC9** (Figure **10**) also exhibited a columnar liquid crystal phase from room temperature to 75 ˚C. This iridium dimer was, however, weakly emissive at λ_{PL} = 570 nm, exhibiting a low Φ_{PL} of 0.8% accompanied by a relatively long τ_{PL} of 5.1 μs.

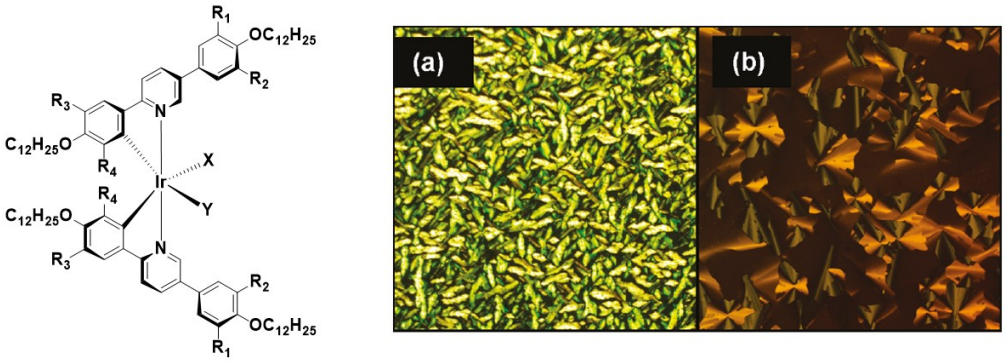

R_1, R_2, R_3, R_4 = H; X = Cl; Y = dmso: **LC4**
R_1, R_2, R_3, R_4 = H; X, Y = MeCN: **LC5**
R_1, R_3 = -$OC_{12}H_{25}$; R_2, R_4 = H; X, Y = acac: **LC6**
R_1, R_2, R_3 = -$OC_{12}H_{25}$; R_4 = H; X, Y = acac: **LC7**
R_1, R_2, R_3, R_4 = -$OC_{12}H_{25}$; X, Y = acac: **LC8**
R_1, R_2, R_3 = -$OC_{12}H_{25}$; R_4 = H; X, Y = Cl-dimer: **LC9**

Figure **10**. Chemical structure of the LC molecular complexes and optical texture of complexes (a) **LC5** (155 ˚C on cooling) and (b) **LC9** (43 ˚C on cooling). Images **a)** and **b)** are adapted with permission from Ref. [91]. Copyright 2011, American Chemical Society.

In a subsequent work[92] by the same authors, a series of dinuclear Ir(III) complexes were prepared based on ppy derivatives functionalized with four, five and six polycatenar chains as cyclometalating ligands, and 1,1,2,2-tetraacetylethane (tae) acting as both the ancillary and bridging ligand to connect two iridium centers (Figure **11a**). **LC10**, **LC11**, **LC12** and **LC13** were all similarly mesomorphic, showing a columnar hexagonal mesophase with a fern-like feature. Considering that the corresponding mononuclear acac complexes **LC6** and **LC7** were

not mesomorphic in nature, the bridging tae ligand changes the geometries of the molecules, making them more disc-like and inducing mesomorphism in the same manner as the bridging chlorides did in **LC9**. However, unlike **LC9**, complexes **LC10**, **LC11**, **LC12** and **LC13** were all very emissive in DCM solution at room temperature, all exhibiting similar orange luminescence between 578 nm and 588 nm with Φ_{PL} of approximately 50% and τ_{PL} of around 4.0 μs. As the two iridium centers in all of the dinuclear complexes are asymmetric, two diastereomeric forms, i.e. *meso*-form with Λ-, Δ-stereochemistry, and racemate-form with Δ,Δ- and Λ,Λ-stereochemistry, can be obtained. For μ-dichloro-bridged iridium dimers only the racemic form is generally obtained because of steric hindrance. However, as the tae bridging ligand keeps the iridium centers more distant compared to the chloro bridging ligands, the formation of both diastereomers (meso and racemic) was observed for complexes **LC10**, **LC11**, **LC12** and **LC13**. In the case of complex **LC11**, the two racemates were separated by column chromatography into the enantiopure analogs without identifying their respective absolute configuration. Despite both isomers exhibiting identical emission properties (λ_{PL} = 558, 663 nm, Φ_{PL} = 43%) and columnar hexagonal phases (Figure **11b**), their isomorphic temperature ranges differed from 79 – 126 ˚C for one isomer to 63 - 95 ˚C for the other.

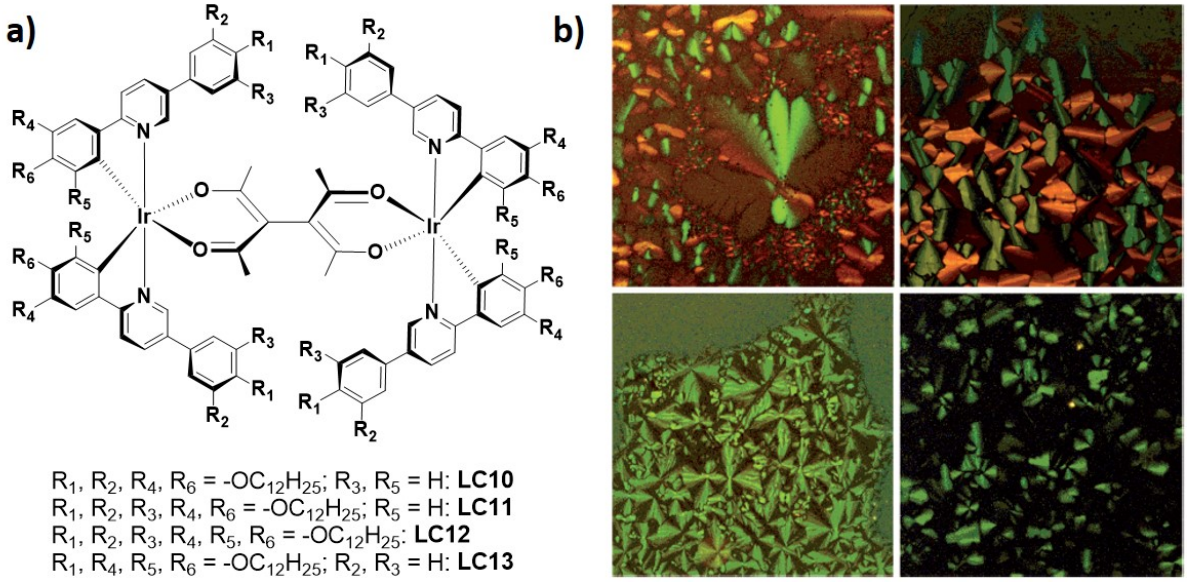

Figure **11**. **a)** Chemical structures of **LC10**, **LC11**, **LC12** and **LC13**. **b)** optical micrograph (on cooling) of complexes: **LC11** isomer 1, 100 ˚C (top-left); **LC11** isomer 2, 60 ˚C (top-right); **LC11** isomer 1, 100 ˚C (top-left); **LC10** racemate, 85 ˚C (bottom-left); **LC13**, 133 ˚C (bottom-right). Image **b)** is adapted with permission. Copyright 2012, Wiley-VCH.[92]

Baranoff and co-workers[93] recently reported a modular approach to the design of mesomorphic phosphorescent iridium complexes. In their design, rod-shaped difluorobiphenyl cyclohexyl mesogenic groups were grafted onto the non-chromophoric acac ligand of the core structure [Ir(C^N)$_2$(acac)] in complexes **LC14**, **LC15**, **LC16** and **LC17** (Figure **12**). The C^N ligands (ppy and dFppy) dictated the photophysical properties of the complexes while the mesogenic units of the functionalized acac ligands controlled the mesomorphic properties of the materials.

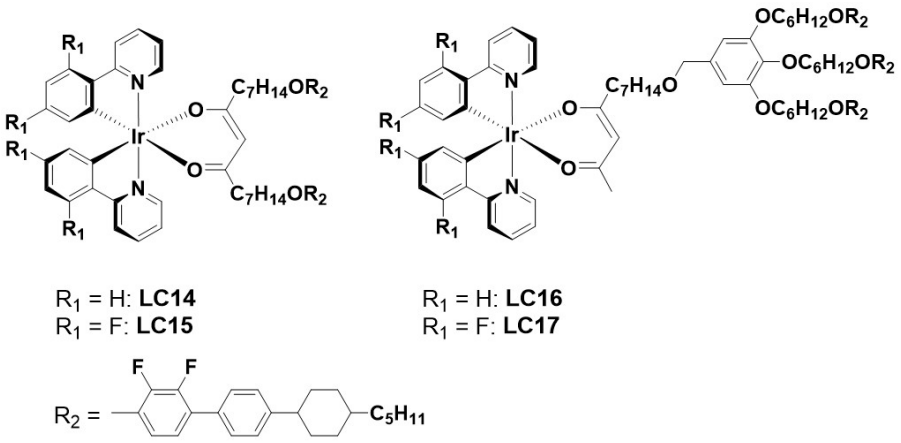

Figure **12**. Chemical structures of **LC14**, **LC15**, **LC16** and **LC17**.

In degassed DCM solution, the complexes **LC14** and **LC16** bearing dFppy C^N ligands exhibited sky-blue emissions centered at λ_{PL} = 482 nm, with Φ_{PL} of 64% and 65% and τ_{PL} = 1.2 μs and 1.0 μs, respectively. **LC15** and **LC17** bearing ppy as the C^N ligands, showed red-shifted emission compared to the previous two LCs centered at λ_{PL} = 517 nm, with Φ_{PL} of 51%

and 45% and τ_{PL} = 1.4 μs and 1.6 μs, respectively. As the functionalization of the acac ligand had little effect on the emission properties of the complexes in solution, the photophysical properties of **LC14**, **LC15**, **LC16** and **LC17** were very similar to those exhibited by the corresponding reference complexes [Ir(ppy)$_2$(acac)] and [Ir(dFppy)$_2$(acac)]. Each of **LC14**, **LC15**, **LC16** and **LC17** exhibited a smectic A mesophase with melting points between 150 ˚C and 170 ˚C. However, due to the unsymmetrical nature of **LC16** and **LC17**, the mesophase of these two complexes were found to be enantiotropic.

Kozhevnikov, Bruce and co-workers[94] recently reported the luminescent and mesomorphic properties of a series of metal complexes (Zn(II), Co(III), Rh(III), Ir(III), Eu(III) and Dy(III)) based on the mesomorphic ligand 5,5″-di(3,4,5-trialkoxyphenyl)terpyridine. Among this series of liquid crystals, the Ir(III) LCs, **LC18** and **LC19** (Figure **13**), exhibited enantiotropic columnar mesophases (Col$_h$) at temperatures higher than 140 ˚C that were dependent on the 5,5″-di(3,4,5-trialkoxyphenyl)terpyridine ligand, with little influence of the iridium metal center.

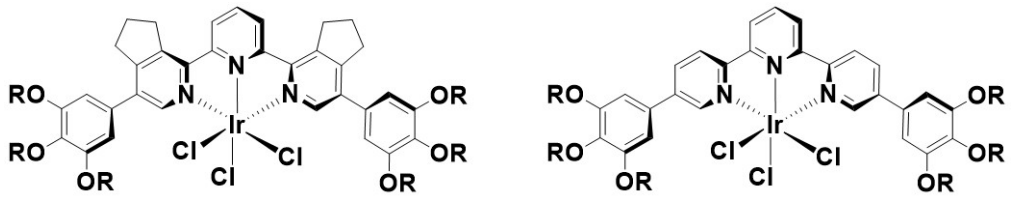

Figure **13**. Chemical structures of **LC18** and **LC19**.

In degassed hexane **LC18** and **LC19** exhibited broad ^{3}MLCT emissions, respectively, at 621 and 622 nm, with Φ_{PL} of 40% and 8% and τ_{PL} of 1.5 and 1.2 μs. The higher Φ_{PL} of **LC18** compared to **LC19** is attributed to the presence of the fused cyclopentane rings on the

terpyridine ligand, which increased the rigidity of the Ir(III) complex thereby reducing non-radiative decay pathways. In neat thin films at 298 K **LC18** emitted at λ_{PL} = 619 nm while complex **LC19** was found to be non-emissive. For **LC18**, the thin film photophysics were unchanged up to 100 ˚C while a 36 nm bathochromic shift was observed from 100 ˚C to 176 ˚C (λ_{exc} = 375 nm). This high temperature bathochromic shift was attributed to the reorganisation of **LC18** upon entering the liquid crystal phase and generating an excimer-like emission. Excimer emission was also observed for Pt(II) liquid crystals bearing the 5,5″-di(3,4,5-trialkoxyphenyl)terpyridine ligand scaffold.[95]

2.3. Luminescent gels

Macroscopically, gels consist of viscoelastic solid-like materials comprised of an elastic cross-linked network and a solvent trapped within the 3D matrix of the gel network by physical or chemical forces.[96, 97] Traditional gel chemistry is dominated by polymers formed through covalent bonds. Of more recent interest are fibrous gel networks, called "supramolecular gels", that can be constructed from small molecules that are interlinked through non-covalent interactions such as hydrogen bonding, π-π interactions, metal coordination or host-guest inclusion.[98] Gels have been used in diverse applications such as tissue engineering and wound healing, drug delivery, templating self-assembled morphologies, molecular electronics and sensing.[14, 99] Metal introduction in gel networks has been motivated as a way of tuning their properties with examples of gels containing metallo-porphyrins, ferrocene, platinum, ruthenium, gold and copper complexes having been described in the literature.[100] In this section of the review we summarize the recent developments in phosphorescent gels based on cyclometalated Ir(III) complexes.

By combining the blue-emitting 1,8-naphtalimide-based gelator **G1** with the orange-emitting iridium complex **G2** (Figure **14a**), Yi and co-workers[101] reported a white-emitting two-components supramolecular gel. **G1** exhibited an excellent ability to gelate a series of polar or apolar organic solvents (*e.g.,* cyclohexane, ethyl acetate, acetonitrile, acetone, methanol, propanol and dimethyl sulfoxide). Scanning electron microscopy (SEM) images of the xerogels of **G1** showed the formation of interweaving fibers (Figure **14b**). **G1** could also efficiently form gel networks in acetonitrile in the presence of the iridium complex **G2** in a molar ratio **G1**:**G2** = 3:1. This xerogel had almost the same fiber framework as that of the neat **G1** xerogel, with the iridium complex **G2** assembled into nanoparticles of 20 – 50 nm dispersed into the gel fibers. **G1** exhibited a blue fluorescence at λ_{PL} = 430 nm with a Φ_{PL} of 26.7% in MeCN, while after gelation its emission was slightly red-shifted at λ_{PL} = 440 nm. The iridium complex **G2**, on the other hand, exhibited a structured orange emission at λ_{PL} = 533, 570 nm with a Φ_{PL} of 2.2%. Upon photoexcitation of **G1** in MeCN, inefficient energy transfer (with efficiency of approximately 0.5 - 5%) to the iridium complex **G2** was promoted. However, due to the close proximity of the chromophores **G1** and **G2** in the gel fibers, the efficiency of the energy transfer increased up to 60 – 70%, leading to white light emission from the gel network of composition **G1**:**G2** = 3:1 (CIE coordinates, x: 0.31, y: 0.39, Figure **14c**).

It had previously been reported that Ir(III) complexes functionalized with carbonyl units can react with cysteine to give non-emissive complexes.[102] Addition of cysteine to complex **G2** in MeCN resulted in a red-shift of the emission of the iridium complex from 533 nm to 579 nm with a dramatic decrease in intensity due to the formation of the thiazolidine species. When cysteine (from 0 to 40 equiv.) was added to the white-emitting gel **G1**:**G2**, the gradual quenching of the orange emission of **G2** gave rise to a pronounced color change of the gel from

white to blue. As a result, the emission properties exhibited by gel **G1**:**G2** can be exploited for the detection of cysteine.

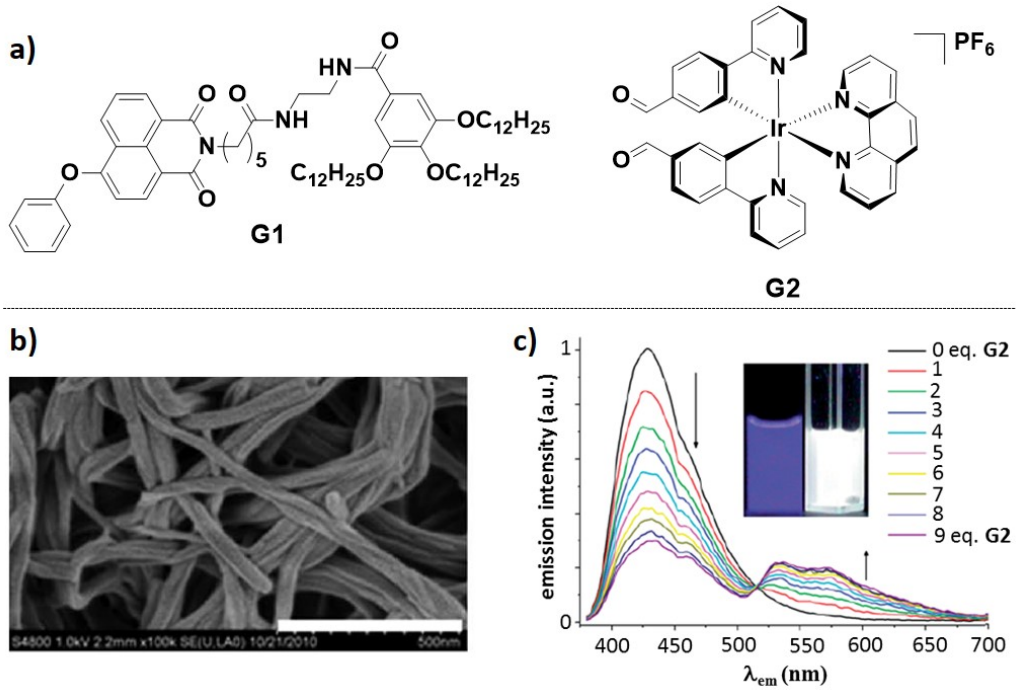

Figure **14**. a) chemical structures of gelator **G1** (left) and the iridium complex **G2** (right). **b)** SEM images of xerogel **G1** in acetonitrile at 298 K. **c)** Emission spectral changes of **G1** as a result of the addition of **G2** from 0.1 to 9 equivalents. Insets are images of the blue emitting **G1** and white emitting gel **G1**:**G2**. Images **b)** and **c)** are adapted from Ref. [101] with permission from The Royal Society of Chemistry.

Szerb, Donnio and co-workers[103] reported that cationic Ir(III) complexes of composition $[Ir(ppy)_2(bpy)]^+X^-$ spontaneously self-assembled into ordered aqueous gel phases when containing aliphatic carboxylate counterions, X^-, of the type of RCO_2^- (R: CH_3, C_2H_5, C_5H_{11}, C_7H_{15}, Figure **15a**). When dissolved in water at a concentration of 2.5 wt%, complexes **G3**, **G4** and **G5** formed gel networks (Figure **15b**), exhibiting similar blue-shifted emissions, respectively, at λ_{PL} = 540 nm, λ_{PL} = 538 nm and λ_{PL} = 536 nm with modestly higher Φ_{PL} of 15%, 15% and 17% compared to the corresponding isotropic solutions at lower concentration (1 wt% in degassed aqueous solution, **G3**: λ_{PL} = 564 nm, Φ_{PL}: 9%, **G4**: λ_{PL} = 554 nm, Φ_{PL}:

11%, **G5**: λ_{PL} = 540 nm, Φ_{PL}: 16%). By contrast, due to the long C_7H_{15} aliphatic chain present on the counterion of **G6**, the complex was found to be poorly soluble in water and it formed only turbid suspensions when dissolved in aqueous solution. The aggregation process of **G3**-**G5** into gels was investigated by wide- and small-angle x-ray scattering (WAXS and SAXS) and small-angle neutron scattering (SANS) measurements. At concentrations higher than 1.8 wt%, the gelification of **G3**-**G5** occurred with close packing of supramolecular columns, sheathed in their solvation shells into 2D-rectangular lattices surrounded by their counterions. The overall organization of the gels **G3**-**G5** is classified as a lamellar-columnar phase (Figure **15c**).

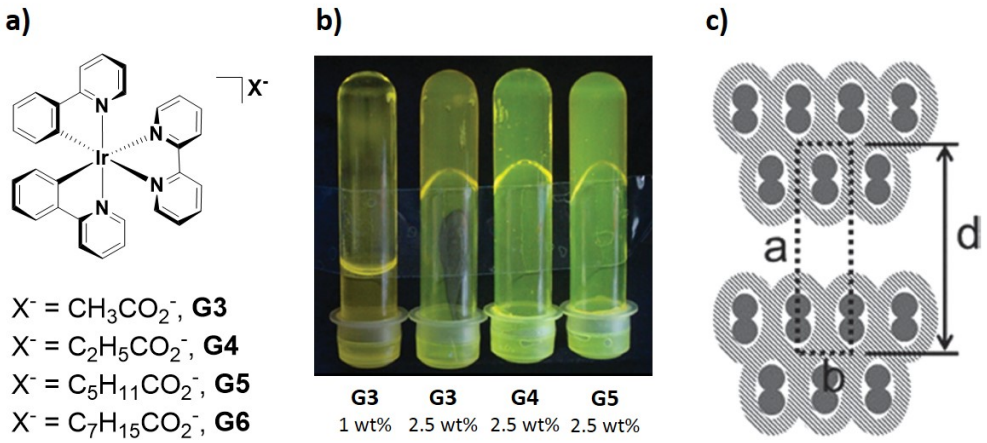

Figure **15**. **a)** Chemical structures of complexes **G3**-**G6**; **b)** images from left to right of anisotropic solution of **G3** at concentration of 1 wt%, gel of **G3**, **G4** and **G5** at concentration of 2.5 wt%; **c)** schematic representation of the proposed organization of the Ir(III) complexes in the gel phase. Strand (solid gray) associated laterally into double rows incorporating water and counterions (dashed gray). Images **b)** and **c)** are adapted with permission. Copyright 2013, Wiley-VCH.[103]

The quasi-spherical shape of octahedral Ir(III) complexes is intrinsically unfavorable for face-to-face stacking and linearly polarized emission and therefore the number of emissive Ir(III) liquid crystals and gels reported to date are still limited. This contrasts, for example, with cyclometalated Pt(II) complexes that have square planar geometries and interact through both π-π and Pt-Pt bounding interactions, thus exhibiting good alignment with high polarization ratio.[104, 105] As a result, the number of reports of luminescent liquid crystals and gels to date based on Ir(III) complexes are much fewer in number than those based on Pt(II) chromophores.

2.4. Surfactant-based structures

The term surfactant defines molecules soluble in both organic solvents and water. They generally consist of a polar headgroup and an apolar tail that confer amphiphilic behavior to the systems.[21] One of the characteristic feature of surfactants is their ability to self-assemble, under certain conditions, into well-define aggregate structures such as micelles, colloids or highly symmetric volume phases through amphiphilic interactions.[106] Recent advances in nanoscience and colloidal technology have strongly driven the development of colloidal structures with integrated multifunctional properties.[11] In this context, iridium-based surfactants, when opportunely designed, have shown the ability to self-assemble into colloidal structures, giving rise to amphiphilic networks with enhanced photophysical properties.

De Cola and co-workers[107] reported the first examples of iridium and ruthenium metallo-surfactants assembled in micellar systems. Both the Ir(III) complex **MS1** $[Ir(dFppy)_2(alk\text{-}bpy)]Cl$ and the Ru(II) complex **MS2** $[Ru(bpy)_2(alk\text{-}bpy)]2Cl$ (Figure **16a**) contain a 2,2'-bipyridine ligand functionalized at the 4,4'-positions with seventeen methylene units (alk-bpy)

as the hydrophobic part of the structure. The photophysical properties of **MS1** and **MS2** in water below their critical micelle concentrations (CMC), respectively, of 5 μM and 3 μM, resembled those of the reference complexes $[Ir(dFppy)_2(bpy)]Cl$, **3b** (Figure **2**) and $[Ru(bpy)_3]Cl_2$. **MS1** exhibited, as a monomeric species, a broad emission at λ_{PL} = 635 nm with a Φ_{PL} of 3.0% and a τ_{PL} of 360 ns. At a concentration of 0.15 mM (above the CMC limit), the emission intensity of **MS1** was almost unchanged (Φ_{PL} = 3.3%) but its emission lifetime became bi-exponential in nature, with a short component due to the non-aggregated form of τ_{PL} = 400 ns, and a longer component of τ_{PL} = 860 ns that arises from the self-assembled species. Similarly, the emission intensity of **MS2** at a concentration of 0.01 mM was slightly enhanced (Φ_{PL} = 4.5%) with longer bi-exponential lifetime decay components of τ_{PL} = 175 ns and 475 ns compared to the emission properties of **MS2** in its monomeric form (Φ_{PL} = 2.5%, τ_{PL} = 160 ns). The enhanced emissions with long lifetime components in both **MS1** and **MS2** observed at concentrations higher than their CMC are attributed to their micellar aggregation that reduce the non-radiative vibrational modes of the complexes as a function of their closer packing. When **MS1** and **MS2** were mixed in a 1:1 ratio at 0.025 mM each, the complexes aggregated into mixed micellar system, and when excited at 350 nm, only the characteristic emission of the ruthenium complex **MS2** was observed at 645 nm. Thus, efficient Förster energy (ET) transfer from the iridium donor to the ruthenium acceptor was promoted in the assembled mix micelles (Figure **16b**); ET was not observed when the two complexes were mixed at a concentration below their CMC.

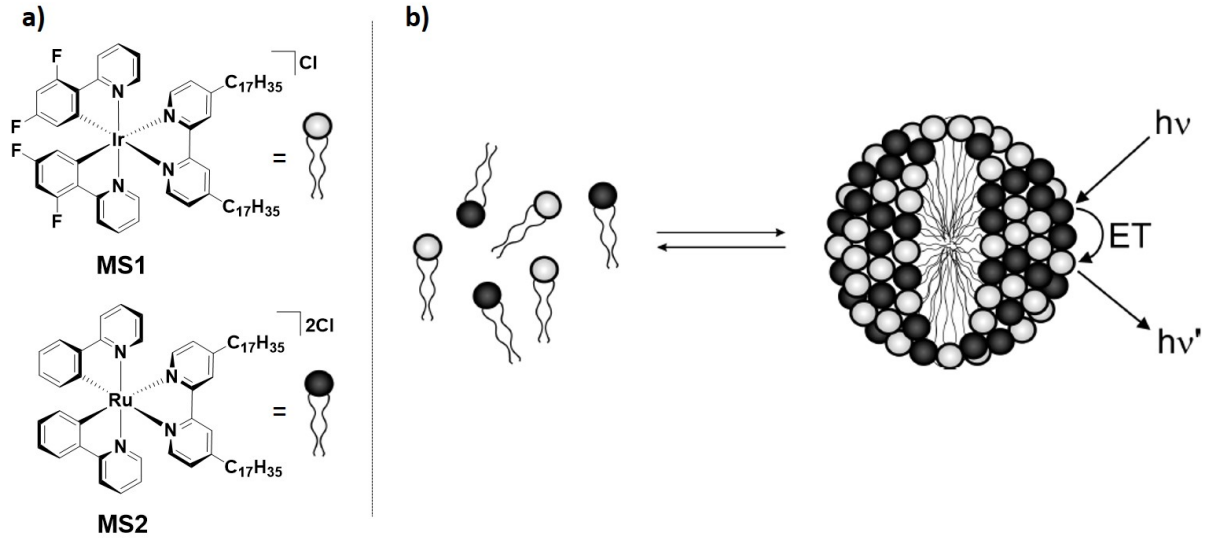

Figure **16**. **a)** Chemical structure of the metallo-surfactants **MS1** and **MS2**. **b)** self-aggregation of **MS1** and **MS2** into mix micelle and schematic illustration of ET from donor Ir to acceptor Ru. Image **b)** is adapted with permission from Ref. [107]. Copyright 2008, American Chemical Society.

The Ir(III) complex **MS3** (Figure **17a**) was designed similarly to **MS1**, to have a polar charged iridium head and long aliphatic tail appended to the ligands with the complex of composition $[Ir(ppy)_2(N^N)]PF_6$, where N^N is 2,2'-bipyridine functionalized with six apolar long aliphatic chains, bis-[4,4'-bis(3,4,5-trydodecyloxybenzoyloxymethyl)-2,2'-bipyridyl)].[108] As observed for **MS1**, **MS3** exhibited high tendency to aggregate in water through interactions between the hydrophobic chains, resulting in a blue-shifted emission at λ_{PL} = 565 nm with higher Φ_{PL} of 25.6% and longer bi-exponential emission decays of 210 ns, 700 ns compared to the emission exhibited in THF, where no aggregation was observed (λ_{PL} = 605 nm, Φ_{PL} = 4.5%, τ_{PL} = 113 ns).

In contrast to **MS1** and **MS3** that consist of a neutral hydrophobic tail attached to the ancillary ligand and a cationic Ir(III) complex as the headgroup, **MS4** and **MS5** (Figure **17b**) are characterized by a reverse design strategy where the Ir(III) core is neutral of composition of

[$Ir(ppy)_2$(alk-pic)], and the picolinate ligand (alk-pic) is substituted with long alkyl chains bearing a terminal mono-anionic sulfate group and sodium as counter cation.[109] At a low concentration of 0.01 mM in water, complexes **MS4** and **MS5** both exhibited weak emission centered respectively at λ_{PL} = 650 nm and λ_{PL} = 646 nm with Φ_{PL} < 0.1% accompanied by very short emission lifetimes τ_{PL} < 20 ns. At higher concentrations between 1 mM and 0.1 mM both **MS4** and **MS5** showed at first good solubility in water giving clear solutions, followed by a visible formation of colloidal samples within 2h. Compared to the mononuclear species, the colloidal samples of **MS4** and **MS5** exhibited enhanced and blue-shifted emissions, respectively, at λ_{PL} = 509 nm and λ_{PL} = 531 nm with Φ_{PL} of ca. 1% and bi-exponential τ_{PL} of 111 ns and 261 ns for **MS4** and 24 ns and 87 ns for **MS5**. The size, morphology and stability of the aggregates were determined by dynamic light scattering (DLS) and scanning electron microscopy (SEM), both of which evidenced the formation of particles with average radii of 300 – 1300 nm. In addition, Zeta potential analyses showed that **MS4** and **MS5** at a concentration of 1.9 mM both have highly negative surfaces towards the water phase (-37 and -57 mV, respectively). Therefore, the surfactant molecules gave rise to aggregates where the neutral and hydrophobic iridium complexes were preferentially inside the colloidal structure while the anionic sulfate moieties faced the solvent. Consequently, the protection of the iridium chromophores inside the colloidal systems accounted for the enhanced emission properties of **MS4** and **MS5** observed at high concentration.

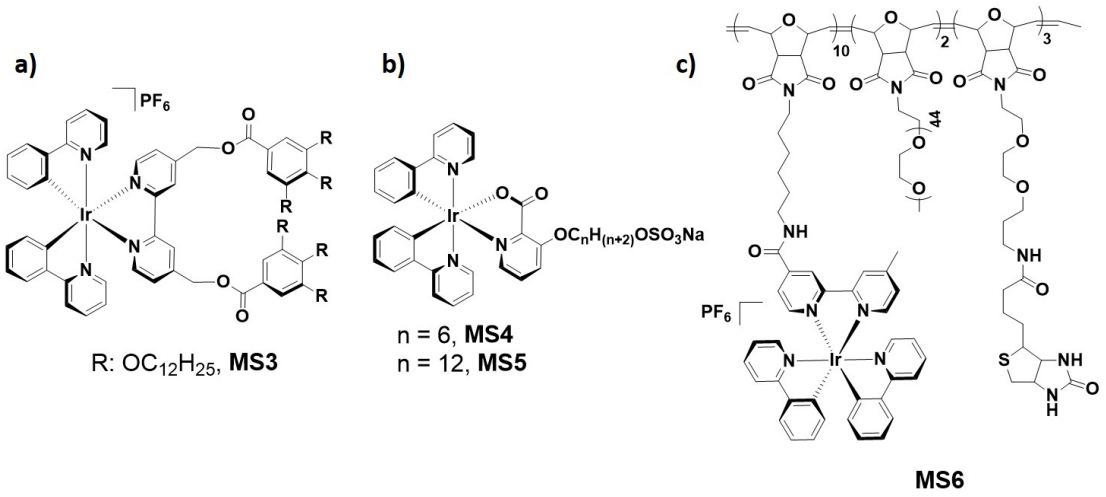

Figure **17**. **a)** Chemical structures of **a) MS3**; **b) MS4** and **MS5** and **c)** copolymer **MS6**.

Luminescent mesoporous silicas were prepared by assembling the neutral iridium complex *fac*-[Ir(ppy)$_3$] with two structure-directing agents (SDA), the cationic cetyltrimethyl ammonium bromide (CTAB) and the non-ionic poly(ethylene glycol)-*block*-poly(propylene glycol)-*block*-poly(ethylene glycol) (P123).[110] The Ir(III) complex was firstly trapped into the micelles formed by the SDAs. The micelles were then used as templates to form mesoporous silicas. XRD and nitrogen sorption measurements provided evidence for the preferential inclusion of the Ir(III) luminophore into the hydrophobic channels of the mesostructures, without any substantial changes in the hexagonal symmetry of the silica. The resulting hybrid material showed a blue-shifted iridium-based emission at λ_{PL} = 509 nm with higher Φ_{PL} of 72% and longer bi-exponential τ_{PL} of 576 ns and 1077 ns compared to the emission observed for *fac*-[Ir(ppy)$_3$] as a pristine powder (λ_{PL} = 534 nm, Φ_{PL} = 12%, τ_{PL} = 38 ns) where aggregation-caused quenching is prevalent.

Phosphorescent materials based on templated synthesis of mesoporous silica using micellar solution of the Ir(III) metallosurfactant [Ir(dFptrBz)$_2$(ppy-hd)]Cl (dFptrBz is 1-benzyl-4-(2,4-difluorophenyl)-1*H*-1,2,3-triazole and bpy-hd is 4,4'-diheptadecyl-2,2'-bipyridine), **MS7** in CTAB were also investigated by Stucchi de Camargo, De Cola and co-workers[111] (Figure **18**). **MS7** exhibited a broad emission at approximately λ_{PL} = 500 nm with a Φ_{PL} of 85% and a τ_{PL} = 1043 ns in degassed EtOH-H_2O (1:1 v/v) at a concentration of 10^{-5} M. Micellar solutions of **MS7:CTAB** (1:8000 ratio) also exhibited a broad emission at λ_{PL} = 500 nm with lower Φ_{PL} of 42% and a τ_{PL} = 1040 ns. Due to the rigidification of the system and/or more restricted access of oxygen inside the pores of the host silica material, **MS7:TEOS** exhibited an emission at λ_{PL} = 460, 500 nm with a Φ_{PL} of 45% and significantly longer bi-exponential lifetime of τ_{PL} = 1037 ns, 4200 ns compared to the micellar solution **MS7:CTAB**.

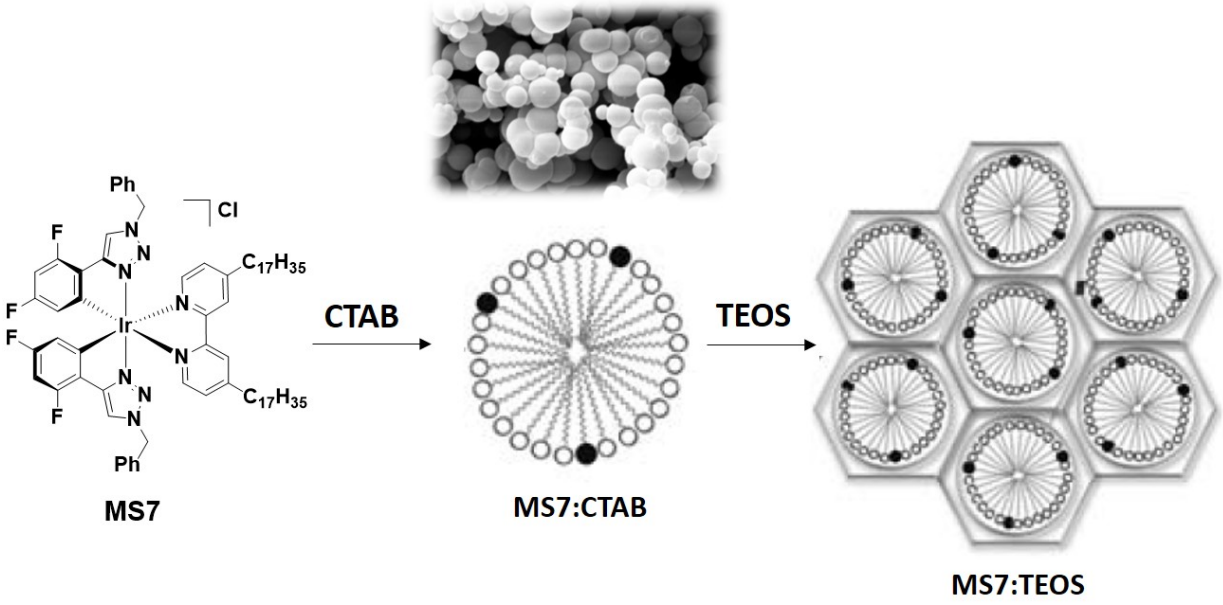

Figure **18**. Chemical structure of **MS7** and representation of the micellar system **MS7:CTAB** and the silica material **MS7:TEOS**. Inset is a SEM micrograph image of **MS7:CTAB** (1:1500 ratio). Adapted from Ref. [111] with permission from The Royal Society of Chemistry.

A different type of micellar system was reported by Mauzeroll, Sleiman and co-workers.[112] Through a ring-opening metathesis polymerization (ROMP), a tri-block polymer, **MS6** (Figure **17c**) containing an iridium complex with a core structure of composition of $[Ir(ppy)_2(bpy)]^+$ as the luminescent unit, oligoethylene glycol, and biotin as biorecognition unit for binding streptavidin (Figure **17c**) was prepared. As the Ir(III) blocks are hydrophobic and the PEG-based block is water soluble, the self-assembly of the polymer into a micellar system was possible upon addition of water to an acetonitrile solution of the polymer. Atomic force microscopy (AFM) evidenced the formation of nanoparticles with an average diameter of 20 – 50 nm, where the iridium complexes were located in the core of the micelles, while the biotin recognition units were situated at the surface. As observed for **MS1**-**MS5**, the emission of the iridium complex in **MS6** was blue-shifted at λ_{PL} = 562 nm with slightly higher Φ_{PL} of 34% compared to its monomeric emission in MeCN (λ_{PL} = 579 nm, Φ_{PL} = 28%). Copolymer **MS6** was used for bio-detection[113] and for electrogenerated chemiluminescence.[112]

Two examples of supramolecular polymers incorporating Ir(III) core structures $[Ir(C\hat{}N)_2(pic)]$[114] and $[Ir(dFC\hat{}N)_2(pic)]$[115] (pic is a picolinate ligand, and C^N and dFC^N are 2-phenylpyridinato- and 2-(2,4-difluorophenyl)pyridinato- derived cyclometalating ligands) used in OLEDs were reported by Huang, Zhu and co-workers. These systems take advantage of the efficient non-bonding assembly between both the bis(dibenzo-24-crown-8)-functionalized Ir(III) complexes-based monomers with the bis(dibenzylammonium)-tethered co-monomer. The formation of the polymeric assemblies was evidenced by ^{1}H NMR spectroscopy and viscosity measurements. Atomic Force Microscopy (AFM) measurements revealed that the assemblies exhibited a high tendency to form homogeneous and good film morphologies. The supramolecular polymer incorporating the complex $[Ir(C\hat{}N)_2(pic)]$

exhibited in neat film a structured emission at λ_{PL} = 416, 562, 604 nm with a Φ_{PL} of 17%. OLEDs fabricated with this polymer showed a turn-on voltage of 6.6 V, a luminous efficiency of 14.6 cd· A^{-1} at a luminance of 450 cd· m^{-2} and an EQE_{max} of 6.9%. The polymer incorporating the complex [Ir(dFC^N)$_2$(pic)] exhibited in neat film sky-blue structured phosphorescence with λ_{PL} = 476, 497 nm and a high Φ_{PL} of 78%. OLEDs fabricated with this polymer showed a turn-on voltage of 5.6 V, luminous efficiency of 6.89 cd· A^{-1} at a current density of 2.1 mA· cm^{-1} and an EQE_{max} of 3.96%.

2.5. Hydrogen bonding- and π-π-directing supramolecular networks

Hydrogen bonding and aromatic π-π-stacking interactions are particularly powerful building motifs employed in crystal engineering. Relevant examples of hydrogen bonding-directing supramolecular assembly of iridium(III) chromophore were reported by Talarico, Ghedini and co-workers[116] (Figure **19**). The Ir(III) complexes [Ir(ppy)$_2$(en)]X (en = ethylenediamine), with X^-: ClO_4^- (**H1**), PF_6^- (**H2**), Cl^- (**H3**) and BH_4^- (**H4**), assembled into different supramolecular networks depending on the nature of the counterions and the crystallization conditions. Two different types of crystalline materials classified as "non-channeled" and "channeled" were obtained. Non-channeled structures primarily involved intermolecular interactions between the NH_2 functionalities of the en ligand and the counterions (Figure **19a**). These types of frameworks were obtained from complexes **H1** and **H2** when crystallized through diffusion of Et_2O into methanol solutions, and from **H4** when crystallized through diffusion of water into an acetone solution. More interesting from a supramolecular point of view are the 3D-channeled networks exhibited by **H2** and **H3** when both crystallized through vapor diffusion of water into their methanol or acetone solutions, respectively. These 3D-networks assembled by multiple N-H···F intermolecular

interactions, that formed two types of hexagonal channels along the crystallographic *c* axis (Figure **19b**): (i) empty hydrophilic channels where PF_6^- or Cl^- ions and en ligands were projected inwards and (ii) hydrophobic channels, defined by the ppy ligand, accommodating templating solvent molecules. The complexes **H1**-**H4** exhibited identical photophysical properties in deoxygenated acetone solution (λ_{PL} = 502 nm, Φ_{PL} = 68%, τ_{PL} = 1.6 μs). In the crystalline state, on the other hand, their photophysical properties strongly depended upon their supramolecular organizations. Compared to the acetone emissions, non-channeled networks exhibited red-shifted emissions between 517 nm and 520 nm with lower Φ_{PL} of proximately 20%. Channeled networks also exhibited red-shifted emissions between 518 nm and 526 nm, but the emissions of these crystals were weak with Φ_{PL} ranging between 1 and 4%. The high degrees of inter-chromic interactions in the crystal networks accounted for the red-shifted emissions and the low Φ_{PL} observed for **H1**-**H4** in their crystalline states.

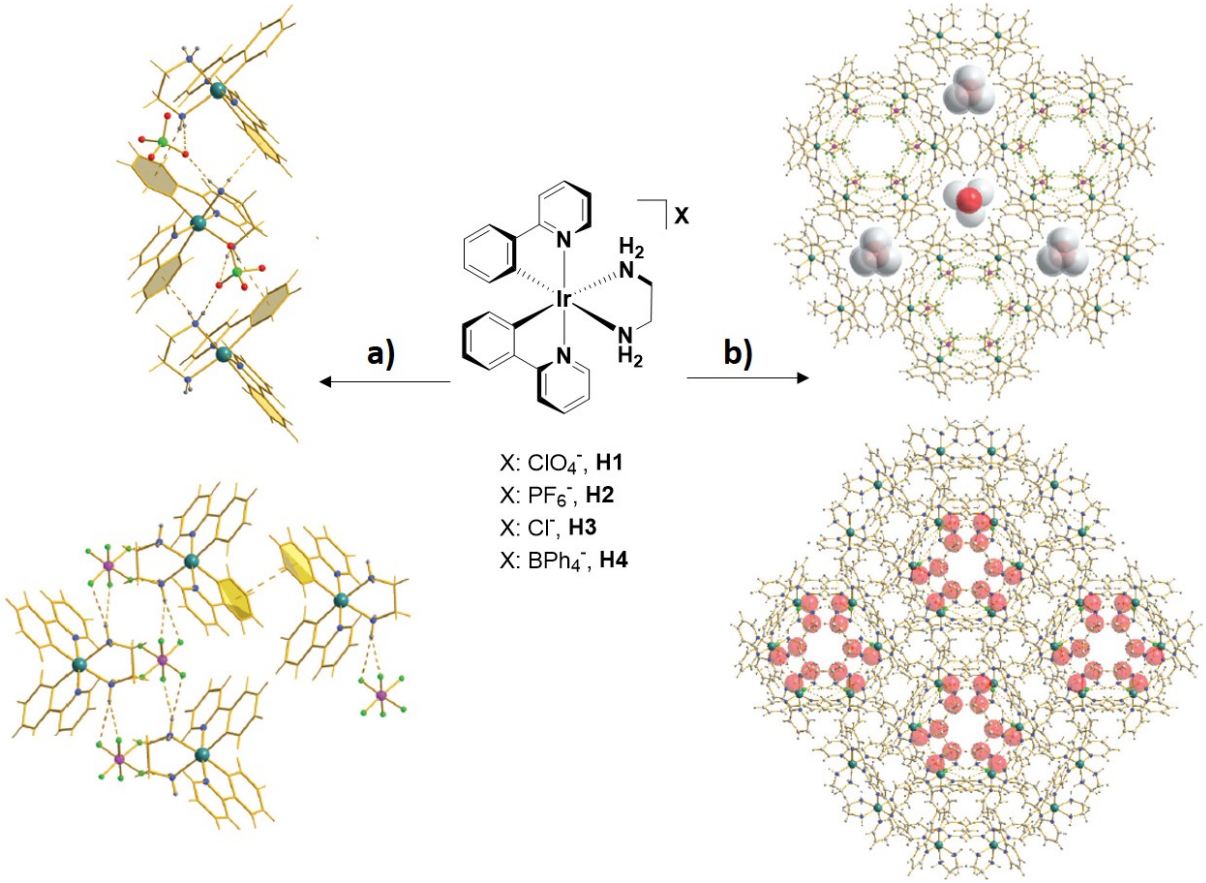

Figure **19**. Chemical structure of the Iridium complexes **H1-H4**; **a)** illustration of the 1D motif in **H1** along the c crystallographic axis (top) and **H2** along the *a* crystallographic axis (bottom). **b)** illustration of the crystal packing of **H2** (top) and **H3** (bottom) showing the channeled networks along the c crystallographic axis. van der Walls radii (red and white balls) for the crystallization solvent molecules are showed. Adapted from Ref. [116] with permission from The Royal Society of Chemistry.

Our group reported two iridium complexes of the composition of $[Ir(dfphtl)_2(btl)]PF_6$ (**H5**) and $[Ir(dfphtl)_2(btl)]Cl$ (**H6**) (dfphtl is 1-benzyl-4-(2,4-difluorophenylato)-1*H*-1,2,3-triazole and btl is 1,1'-dibenzyl-4,4'-bi-1*H*-1,2,3-triazolyl) that exhibit the formation of 1D-networks dictated by the hydrogen bonding motifs involving the triazole units (Figure **20**).[117, 118] Both **H5** and **H6** crystallized in the triclinic space group $P\bar{1}$ and exhibited similar H-bonding

motifs. The btl ligands formed C-H hydrogen bonds to the anions PF_6^- in **H5** and Cl^- in **H6** and a molecule of water, while the dfphtl triazole C-H groups acted as C-H hydrogen bond donors, forming C-N···N bonds to one of the nitrogen atom of the btl ligand (Figure **20b**). Complexes **H5** and **H6** were not photostable at room temperature neither in solution nor in the solid state.[117, 119] However, at 77 K in 2-MeTHF glass state **H6** exhibited a weak emission at λ_{PL} = 393, 419 nm.

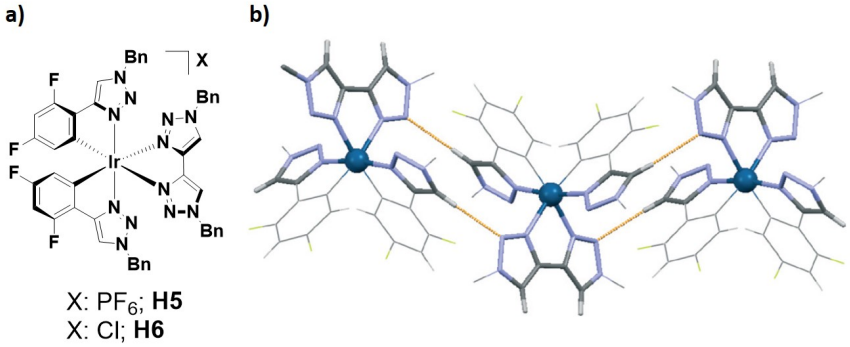

Figure **20**. **a)** Chemical structures of complexes **H5** and **H6** and **b)** view of the X-ray structure of **H5** showing the C-N···N hydrogen bonds propagating parallel to the *c* crystallographic axis. Image **b)** is adapted from Ref. [118] with permission from The Royal Society of Chemistry.

Holdt and co-workers have shown that homoleptic octahedral Ni(II) and Fe(III) complexes bearing the 1,12-diazaperylene (dap) ligand and PF_6^- or BF_4^- as the counterion in $[M(dap)_3]^{2+}$ are able to form supramolecular assemblies in their crystalline state with honeycomb structures via π-π stacking interaction.[120] Homoleptic tetrahedral Cu(I) complexes of 2,11-alkylated dap ligand are similarly able to form supramolecular columnar assemblies through π-π interactions.[121] The work has been subsequently extended to investigate the self-assembly in the solid state of heteroleptic diazaperylene Ir(III) complexes $[Ir(C^N)_2(dap)]PF_6$ (where C^N are isophenylisoquinoline, benzoquinoline, 1-phenylpyrazole and 2-(thiophen-2-yl)-pyridine).[122] Among this family of complexes, $[Ir(piq)_2(dap)]PF_6$ (where piq is

isophenylisoquinoline, **H7**) gave a three-dimensional assembly in the crystalline state (Figure **21a**). Complex **H7** indeed exhibited π-π–stacking interactions involving both the dap and piq ligands, leading to the formation of rectangles consisting of four cationic complexes, assembled together through both π-π and CH-π interactions (Figure **21b**). This particular crystal packing gave rise channels of 6.4 Å in height and 3.3 Å in width along the crystallographic ***c*** axis (Figure **21c**). Complex **H7** however was non emissive both in solution and in the crystalline state.

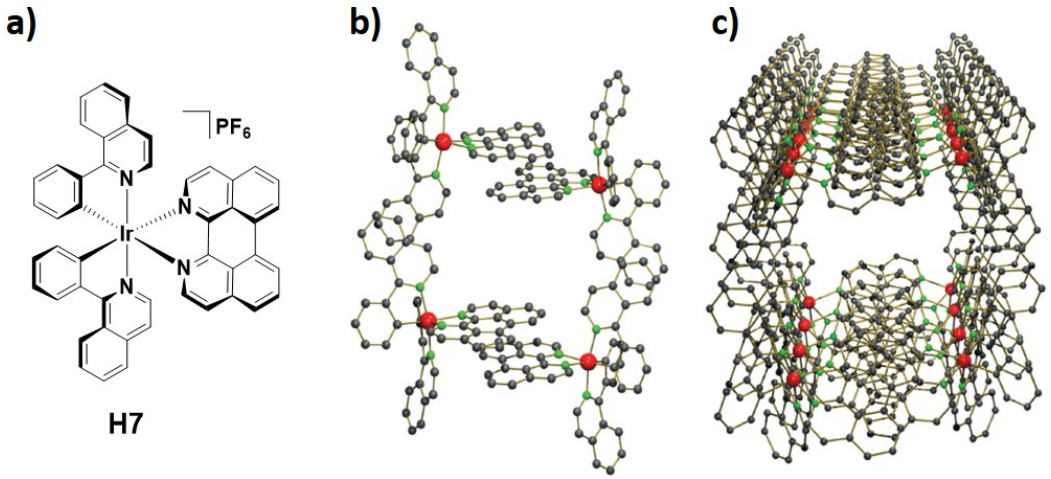

Figure **21**. **a)** chemical structure of **H7**; **b)** illustration of the molecular rectangle exhibited by the x-ray structure of **H7** by π-π stacking aggregation; **c)** illustration of the channels exhibited by the x-ray structure of **H7**. Hydrogen and counterions are omitted for clarity. Images **b)** and **c)** are adapted from Ref. [122] with permission from The Royal Society of Chemistry.

3. Coordination-driven self-assembly

Coordination-driven self-assembly, which is based on the formation of metal-ligand bonds, has proven to be a powerful method to prepare supramolecular well-defined nanostructures of varying shapes, sizes and functional properties, featuring considerable synthetic advantages

such as facile and rapid construction of the final products and high yields.[123-125] In this section, we highlight the use of Ir(III) complexes as luminescent scaffolds in coordination-driven self-assembly by describing the recent examples of luminescent coordination polymers, metal-organic frameworks (MOFs), discrete structures, capsules and cages.

3.1. Coordination polymers, metal-organic frameworks and discrete structures

Coordination polymers (CPs) and metal-organic frameworks (MOFs) are highly crystalline and porous materials constructed from metal ions or clusters usually bound to carboxylate or nitrogen capped organic linkers to form extended one-dimensional (1D), two-dimensional (2D) and three-dimensional (3D) networks.[17, 27, 126, 127] Because of the high surface area and structural tunability, Ir(III)-based CPs and MOFs have been primarily used as functional materials for gas storage and purification, sensing and catalysis.

Lin and co-workers[128] reported the first examples of the incorporation of two Ir(III) complexes of the form of *fac*-[Ir(ppy-c)$_3$] (ppy-c is 3-(pyridin-2-yl)benzoic acid in **L1** and 4-(pyridin-2-yl)benzoic acid in **L2**, Figure **22**), into Zn-based coordination polymers. Reaction of Zn(NO$_3$)$\cdot$ 6H$_2$O with **L1** and **L2** in DMF/H$_2$O at 90 ˚C for 24 h afforded, respectively, single crystals of [Zn$_4$(μ_4-O)(**L1**)$_2$]$\cdot$ 6DMF$\cdot$ H$_2$O, **P1** (Figure **22a**) and [Zn$_3$(**L2**)$_2$(DMF)(H$_2$O)$_3$]$\cdot$ 2DMF$\cdot$ 3H$_2$O, **P2** (Figure **22b**).

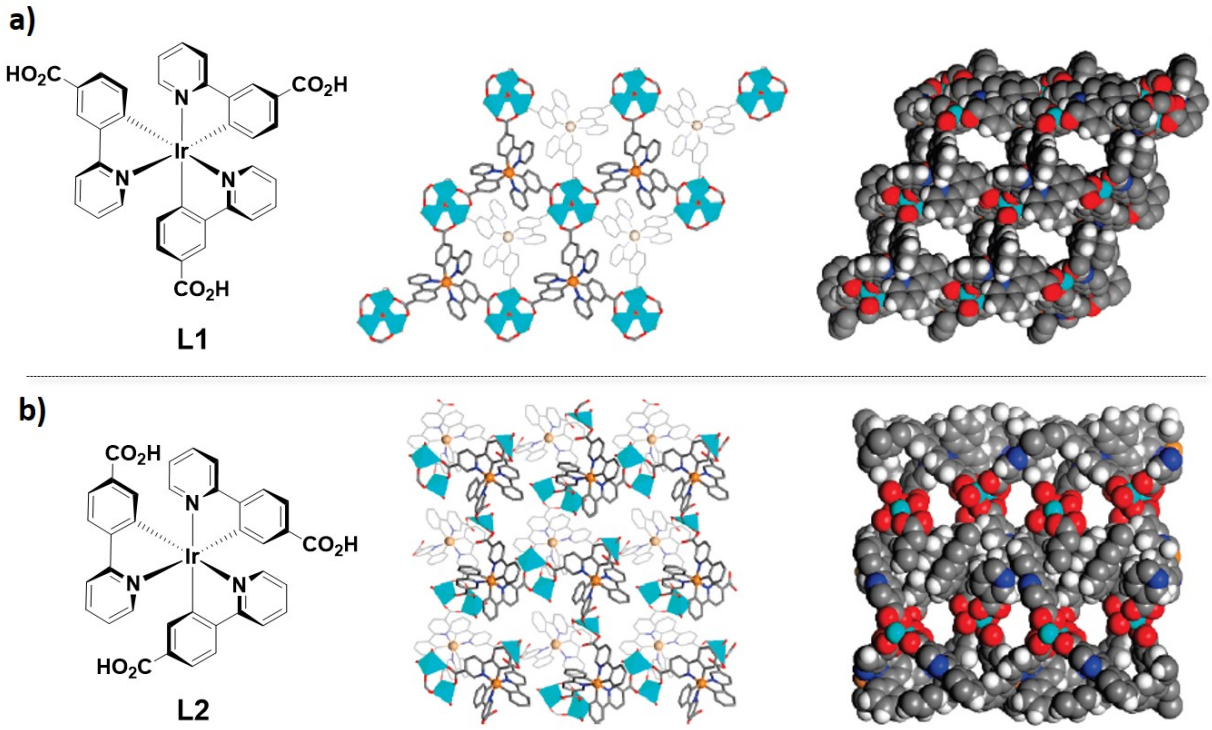

Figure **22**. From left to right: **a)** chemical structure of metalloligand **L1**; a top view of the 2D bilayer of the x-ray structure of **P1** and space-filling model of the x-ray structure of **P1**. **b)** chemical structure of metalloligand **L2**; a top view of the 2D bilayer of the x-ray structure of **P2** and space-filling model of the x-ray structure of **P2**. Adapted with permission from Ref. [128]. Copyright 2010, American Chemical Society.

P1 crystallized in a trigonal $R\bar{3}$ space group where the carboxylate groups from six adjacent **L1** ligands coordinate to four Zn centers to form 2D-bilayers $[Zn_4(\mu_4\text{-}O)(\mathbf{L1})_2]$. The crystal packing of the 2D layers along the crystallographic *c* axis created open channels of dimensions of 7.9 Å × 4.3 Å (Figure **22a**). By contrast, **P2** crystallized in the triclinic $P\bar{1}$ space group where both the carboxylate groups coordinate to the Zn to generate both mononuclear and dinuclear complexes where in the latter case three carboxylate groups bridge the two Zn centers, forming 2D-bilayers that packed along the *a*-axis. The largest channels of **P2** were of 4 Å × 3 Å run along the *b*-axis (Figure **22b**). **P1** exhibited high N_2 uptake at 77 K and CO_2 uptake at 273 K.

However, due to its smaller porosity no N_2 or CO_2 uptake was observed for **P2**. The solid-state emission of **P1** was red-shifted at λ_{PL} = 540 nm compared to that of **L1** (λ_{PL} = 520 nm), while the emission of **P2** was blue-shifted at λ_{PL} = 550 nm compared to that of **L2** (λ_{PL} = 575 nm) (Table **1**). Both **P1** and **P2** were sensitive to O_2 via the expected efficient and reversible luminescence quenching of the Ir(III) phosphors. When polymers **P1** and **P2** and metalloligands **L1** and **L2** were subjected to a gradual increase in O_2 partial pressure (from 0.05 to 1.0 atm), their luminescence intensity gradually decreased and, after addition of 1.0 atm of O_2, the quenching efficiencies of **P1**, **P2**, **L1** and **L2** were, respectively, 59% and 41%, 16% and 8%. As oxygen can be trapped within the pores of **P1** and **P2** and thus in persistent close contact with the Ir(III) luminophores, the emission quenching efficiencies of **P1** and **P2** were correspondingly higher than those of **L1** and **L2**.

Four Ir(III) coordination polymers $[Zn(\mathbf{L3})_2]\cdot 3DMF\cdot 5H_2O$ (**P3a**), $[Cd(\mathbf{L3})_2(H_2O)_2]\cdot 3DMF\cdot 6H_2O$ (**P3b**), $[Co(\mathbf{L3})_2(H_2O)_2]\cdot 2DMF\cdot 8H_2O$ (**P3c**) and $[Ni(\mathbf{L3})_2(H_2O)_2]\cdot 3DMF\cdot 6H_2O$ (**P3d**) were formed by using $[Ir(ppy)_2(H_2dcbpy)]PF_6$ (H_2dcbpy is 4,4'-dicarboxy-2,2'-bipyridine) as the bridging metalloligand (**L3**, Figure **23a**) and Zn^{2+}, Cd^{2+}, Co^{2+} and Ni^{2+} as metal ions.[129] **P3a** exhibited an orthorhombic geometry ($Pna2_1$ space group) that consisted of **L3** ligand coordinated to the Zn centre through the carboxylate groups in a 1:2 ratio, with DMF and water molecules trapped in the cavities of the extended structure in the solid state. This particular packing generated channels of rectangular shape (Figure **23b**). Similarly, polymers **P3b**, **P3c**, **P3d**, gave rise to 1D-chains with metal(II) ions in distorted orthorhombic geometries (Pnma space group) where Cd(II), Co(II) and Ni(II) were each, respectively, bound to six oxygen atoms, four of which were from four carboxylate groups of **L3** and two of which were from water molecules (Figure **23b**). **P3a**, **P3b**, **P3c**, **P3d** each

exhibited CT emission from single crystals at λ_{PL} = 613 nm, λ_{PL} = 595 nm, λ_{PL} = 587 nm and λ_{PL} = 600 nm, respectively with Φ_{PL} values of 27.4%, 19.3%, 0.1% and 0.2%, respectively (λ_{PL} = 613 nm and Φ_{PL} of 17.8% for **L3** in the solid state, Table **1**). As reported for **P1** and **P2**, polymers **P3a**, **P3b**, **P3c**, **P3d** also exhibited reversible oxygen-sensing properties. Indeed, at 1 atm of O_2 the emission quenching efficiencies from their single crystals were, respectively, 46%, 74%, 57% and 52%. The emission spectra and photos in Figure **23c** show the emission quenching of **P3b** upon gradual addition of oxygen.

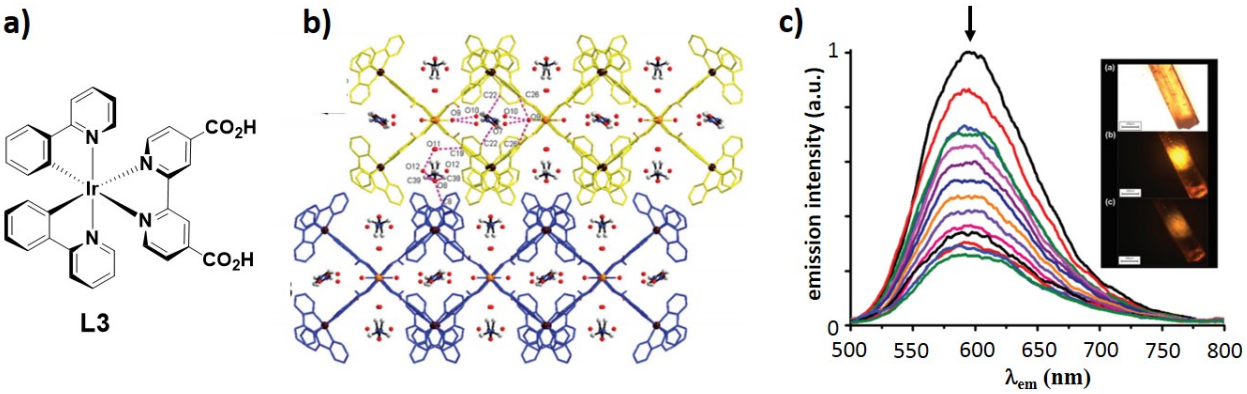

Figure **23**. **a)** Chemical structure of **L3**; **b)** illustration of two layers (in yellow and blue) of the 3D cadmium-bridged structure of **P3b** with open channels. **c)** Emission quenching of **P3b** upon addition of an increased amount of O_2. Insets are images of the emissions from the crystal **P3b**, with 100% N_2, and with 100% O_2. Images **b)** and **c)** are adapted from Ref. [129] with permission from The Royal Society of Chemistry.

In a subsequent report, the same group developed an electrochemical method to produce the Ir(III)-Zn(II) coordination polymer [Zn(**L3**)$_2$]· 3DMF· 5H_2O (**P3a**) with greater control over the crystal growing process. With this improved synthetic method, polymer **P3a** exhibited higher crystal stability and enhanced oxygen sensing performance.[130] Indeed, when electrochemically produced, **P3a** exhibited a high selectivity towards the absorption of O_2 with an emission quenching efficiency as high as 95%. Once oxygen was trapped within the pores

of **P3a**, the gradual addition of glucose to the crystals of **P3a** restored its emission at λ_{PL} = 596 nm upon excitation at 405 nm. As the consumption of oxygen due to the combustion reaction between glucose and O_2 was linearly correlated to the reduction of the emission quenching of **P3a**, quantitative detection of glucose within the concentration range of 0.05 – 6.0 mM was also possible.

Three luminescent coordination polymers were synthetized by assembling metalloligand **L3** with Mg(II) ions, respectively, in H_2O, DMF and DEF (DEF is N,N-diethylformamide) to form $[Mg(\mathbf{L3})_2]\cdot 3.5H_2O$ (**P3e**), $[Mg(\mathbf{L3})_2(DMF)_2]\cdot 3.5H_2O$ (**P3f**) and $[Mg(\mathbf{L3})_2(DEF)(H_2O)]\cdot 3H_2O$ (**P3g**).[131] Single crystal x-ray diffraction analyses revealed that the three coordination polymers were allomeric and formed similar 1D chain structures in which the Mg atoms coordinated in an octahedral geometry to four carboxylate oxygen atoms from four **L3** ligands and two oxygen atoms from solvent molecules (Figure **24**). Polymers **P3e**, **P3f** and **P3g** all exhibited in the solid state broad emission centered at λ_{PL} = 544 nm, λ_{PL} = 554 nm and λ_{PL} = 570 nm, respectively, with Φ_{PL} of 14.6%, 18.1% and 2.4% and τ_{PL} of 7.7 μs, 13.3 μs and 7.7 μs, respectively (Table **1**). Therefore, the different electron-donating abilities of the solvents, which increases in the order H_2O < DMF < DEF, exerted a strong influence on the emission energies of the polymers.

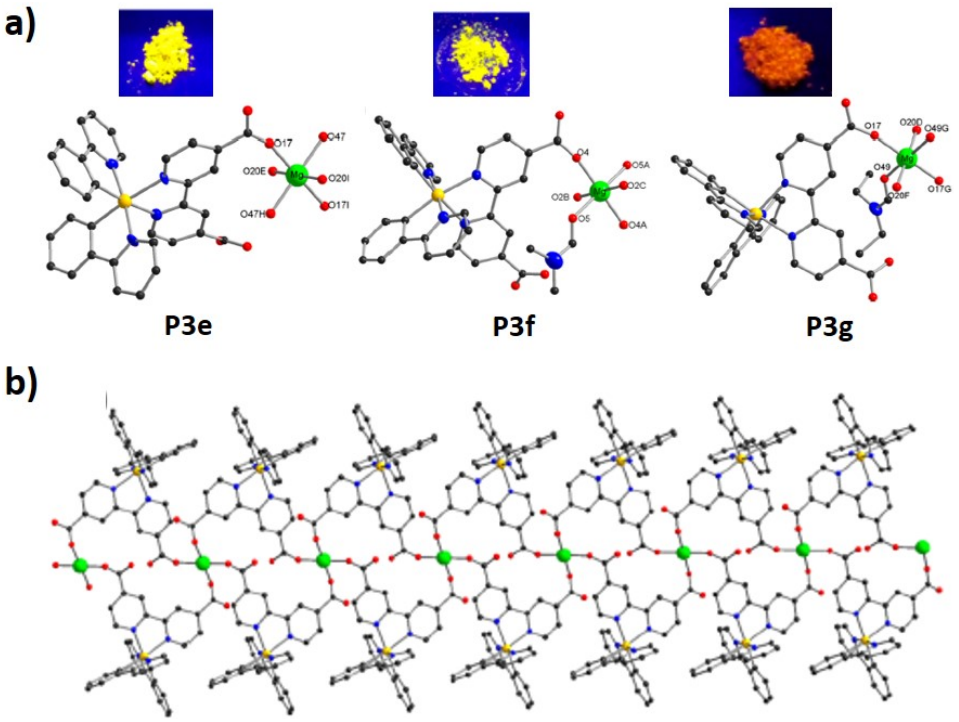

Figure **24**. **a)** view of the coordination environments of the Mg(II) ions in **P3e**, **P3f** and **P3g**. Insets are images of the powder emissions upon UV irradiation. **b)** View of the 1D chains exhibited by the coordination polymers. Adapted with permission from Ref. [131]. Copyright 2016, American Chemical Society.

Metalloligand **L3** was also used in heteronuclear Ir(III)-Ln(III) coordination polymers as a light-harvesting antenna to sensitize Ln(III)-based near-infrared (NIR) luminescence from Gd^{3+}, Yb^{3+}, Er^{3+} and Nd^{3+} ions.[132] The polymers **Ir-Gd**, **Ir-Yb**, **Ir-Er** and **Ir-Nd** are all isostructural and each crystallized in a triclinic $P\bar{1}$ space group where one Ln(III) center is seven-coordinate by five carboxylate oxygen atoms from five **L3** ligands and two hydroxylic groups from NaOH added to prepare to polymers, generating a pentagonal bipyramid coordination geometry. In the reference **Ir-Gd** polymer, as the Gd^{3+} ions cannot accept energy from the Ir excited state because of the absence of energy levels below 3200 cm^{-1}, the solid-state emission of **Ir-Gd** showed the characteristic ^{3}MLCT/^{3}LLCT emission of the Ir(III)

luminophore at λ_{PL} = 610 nm with a τ_{PL} of 8.1 μs (**L3** emits in the solid state at λ_{PL} = 592 nm with a τ_{PL} of 7.8 μs). For the other three luminescent polymers **Ir-Ln** (Ln: Yb, Er, Nb), the Ir-based emission centred at 610 nm was largely quenched, indicating that Dexter d → f energy transfer from the Ir(III) units to the Ln^{3+} ions was efficiently promoted. The fastest energy transfer rate was observed for the **Ir-Nd** polymer, with a calculated quenching rate constant (k_q) of 6.8 × 10^6 s^{-1}, while for **Ir-Yb** and **Ir-Er**, k_q of 5.0 × 10^5 s^{-1} and 6.0 × 10^6 s^{-1} were, respectively, obtained.

A related example of a Ir(III)-Ln(III) discrete structure was reported by Zheng and co-workers[133] by microwave reaction between the iridium complex $[Ir(ppy)_2(dppH)]$, **L4** (dppH is 2-pyridyl phosphonic acid) and $Dy(CF_3SO_3)_3$ in MeOH at 100 ˚C. The composition of the resultant structure, **P4**, was identified to be $[Dy(\mathbf{L4})_6](CF_3SO_3)]\cdot 8H_2O$ by x-ray diffraction (Figure **25**). The assembly **P4** exhibited a broad emission in the solid state centred at λ_{PL} = 531 nm, which is slightly blue-shifted compared to the emission in the solid-state of the iridium complex **L4** (λ_{PL} = 538 nm) (Table **1**). Given that the emission of the Ir(III) complex was not quenched, energy transfer from Ir(III) to Dy(III) did not take place. **P4** exhibited field-induced slow magnetization relaxation originating from both the Ir(III) and Dy(III) components.

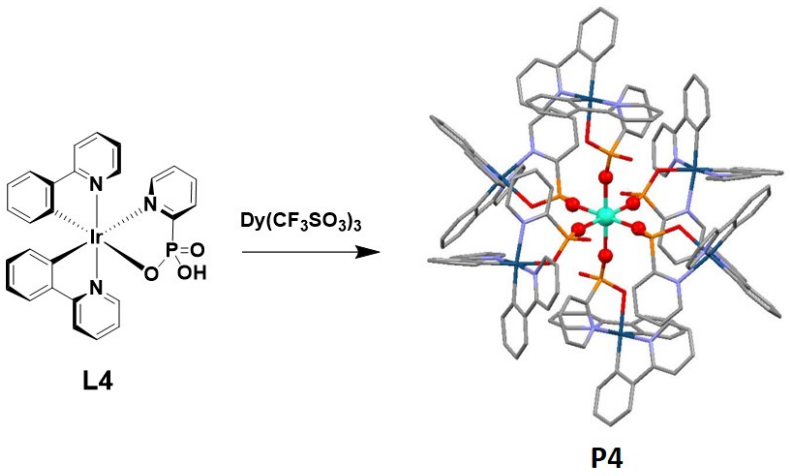

L4 **P4**

Figure **25**. Chemical structure of complex **L4** and X-ray structure of the Ir(III)-Dy(III) assembly **P4**. The red balls illustrate the octahedral coordination around the Dy ion (in light-blue).

Crystallisation of PPN**3a** (Figure **2a**, PPN is *bis*(triphenylphosphine) iminium cation) in the presence of excess of the Ln ions Gd, Nd, Eu led to the formation of assemblies based on Ir-CN-Ln bonding, which generated in the solid state either $Ir_2Ln_2(\mu\text{-}CN)_4$ square assemblies or linear trinuclear species with Ir-CN-Ln-NC-Ir cores.[134] In the Ir-Eu and Ir-Nd assemblies the vibronic emission of PPN**3a** in the solid state at λ_{PL} = 484, 507 nm was substantially quenched due to energy transfer to the lower-lying f-f states on these Ln ions. By contrast, similar to that observed for the **Ir-Gd** polymer previously described,[132] in the $Ir_2Gd_2(\mu\text{-}CN)_4$ complex the Gd cannot accept the energy from the Ir chromophore and therefore no energy transfer was promoted.

A heterogeneous coordination polymer, **P3h**, based on the assembly between metalloligand **L3** and Y^{3+} ions (Figure **26**) was used as a catalyst for the photochemical reduction of CO_2.[135] Similar to the Ir(III)-Ln(III) polymers previously described, **P3h** crystallizes in a triclinic $P\bar{1}$ space group where the Y atom is seven-coordinate with a coordination sphere consisting of five carboxylate oxygen atoms from five **L3** ligands and two hydroxyl groups from NaOH added to prepare the polymers, generating a pentagonal bipyramid coordination geometry (Figure **26a**). The neighboring Y centers are alternatively linked via two hydroxide ions from NaOH and two carboxylate groups from two **L3** ligands, giving rise to a 1D-$[Y(OH)_2(CO_2)_2]_\infty$ chain structure (Figure **26b**). Neighboring chain structures pack together through non-bonding Ir···Y interactions, forming the 3D supramolecular frameworks illustrated in Figure **26c**. Energy transfer from the Ir to Y centers was not possible due to the mismatching

of their respective energy levels. Indeed, **P3h** displayed in the crystal state a strong Ir-based emission centered at λ_{PL} = 592 nm, with a bi-exponential emission decay with the longest component of τ_{PL} = 29.0 μs (Table **1**). The emission decay of **P3h** was found to be almost four times longer than that exhibited by **L3** (τ_{PL} = 7.8 μs). **P3h** exhibited remarkable photocatalytic activity for CO_2 reduction under visible-light irradiation (λ_{exc} = 475 nm). The quantum yield of $HCOO^-$ production was 1.2% with a high turnover frequency (TF) of 118.8 μmol (g of cat.)$^{-1}$ h^{-1}.

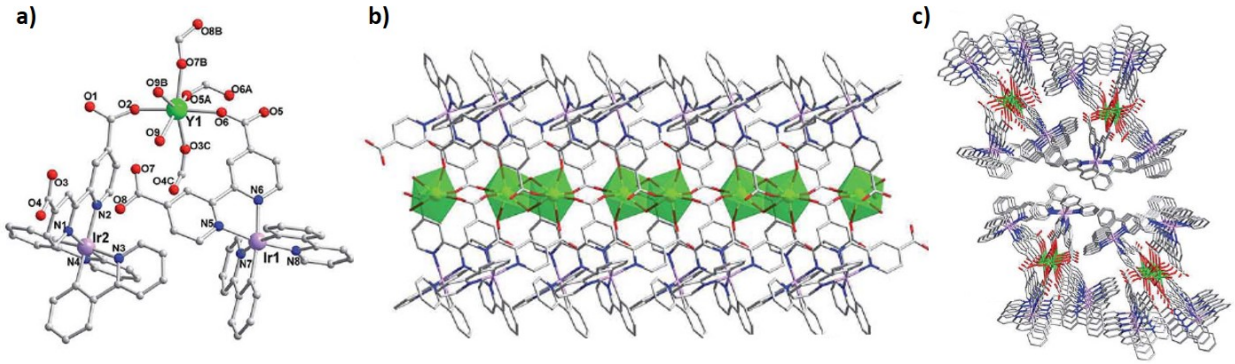

Figure **26**. x-ray structure of **P3h** illustrating: **a)** pentagonal bipyramid coordination geometry of the Y(III) ions; **b)** view of 1D-chain structures and **c)** view of 3D networks. Adapted from Ref. [135] with permission from The Royal Society of Chemistry.

The detection of nitroaromatic explosives on ppm scale is evidently of great importance for national security and defence. Luo and co-workers reported a highly luminescent heteronuclear MOF of composition [Zn(**L3**)$_2$]· 3DMF· 5H_2O (**MOF1**).[136] **MOF1** crystallized in the non-centrosymmetric space group $Pna2_1$ where the Zn centre adopts a tetrahedral geometry coordinated to four carboxylate O atoms from four **L3** ligands thereby forming a 3D porous network. **MOF1** exhibited an Ir-based emission that was red-shifted at λ_{PL} = 602 nm with an enhanced Φ_{PL} of 23.6% and a longer τ_{PL} of 14.3 μs compared to that observed for **L3** (Table **1**).

Similar to the behavior of polymers **P3a**, **P3b**, **P3c** and **P3e**, **P3f** and **P3g**, the enhanced emission of **MOF1** compared to **L3** is attribute to the enhanced rigidity and symmetry experienced by the Ir(III) luminophores in the coordination frameworks, which reduces non-radiative decay modes. **MOF1** exhibited good sensing abilities towards nitroaromatic compounds. Remarkably, when aromatic compounds with high nitro content such as TNT (trinitrotoluene) were diffused into the crystal at a concentration of 625 ppm, the emission of **MOF1** was quenched by 60%-70% via electron transfer from the Ir(III) luminophores to the nitroaromatic acceptors.

Lin and co-workers[137] successfully incorporated three iridium-based water-oxidation catalysts, [Ir(Cp*)(dcppy)Cl] (**L5**), [Ir(Cp*)(dcbpy)Cl]Cl (**L6**) and $[Ir(dcbpy)_2(OH_2)_2]OTf$ (**L7**) (Figure **27a**) (where Cp* is pentamethylcyclopentadienyl, dcppy is 2-phenylpyridine-5,4'-dicarboxylic acid, dcbpy is 2,2'-bipyridine-5,5'-dicarboxylic acid and OTf is trifluoromethyl sulfonate) into the octahedral $Zr_6O_4(OH)_4(bpdc)_6$ framework UiO-67 (bpdc is *para*-biphenyldicarboxylate), forming, respectively, **MOF2**, **MOF3** and **MOF4** (Figure **27a**). When these materials were tested as photocatalysts for water oxidation by using cerium ammonium nitrate (CAN) as the oxidant, turnover frequencies (TOFs) of 4.8, 1.9 and 0.4 h^{-1} for **MOF2**, **MOF3** and **MOF4** were, respectively, reported. Higher TOFs of 7.5 and 94.5 h^{-1} were, however, observed when the Ir(III) complexes bearing elongated linear bridging ligands **L8** and **L9** (Figure **27b**) were, respectively, incorporated into the octahedral zirconium frameworks (**MOF5** and **MOF6**).[138] The higher TOFs of **MOF5** and **MOF6** compared to **MOF2**-**MOF4** were attributed to the extended networks generated with wider channel sizes where the hydrated Ce^{4+} ions can freely diffuse without steric hindrance, thus promoting overall higher catalytic efficiency.

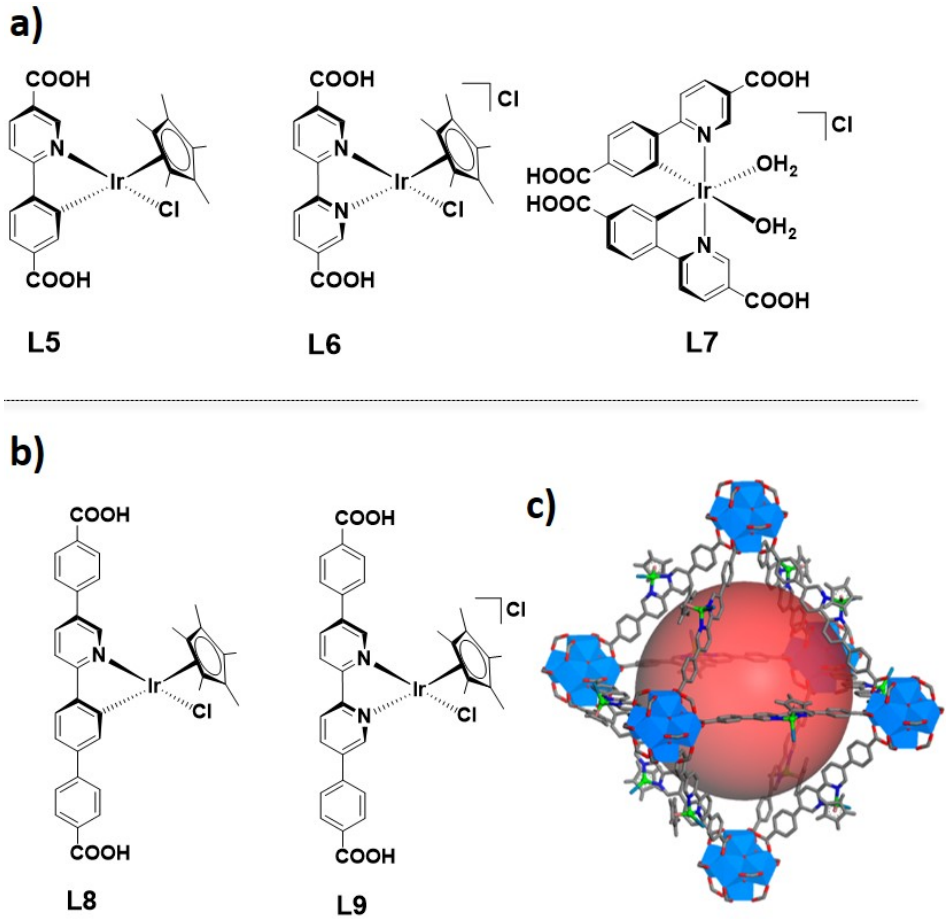

Figure **27**. **a)** Chemical structures of the Ir(III) metalloligands **L5**, **L6** and **L7**. **b)** Chemical structures of the extended Ir(III) metalloligands **L8** and **L9**. **c)** Structure model for **MOF6** showing the octahedral cage of 1 nm in diameter. Zr, blue polyhedron; Ir, green balls; Cl, dark green, C, grey; N, blue. The red ball in the middle represents the cage cavity. Image **c)** is adapted with permission from Ref. [138]. Copyright 2012, American Chemical Society.

In a subsequent work, Pt nanoparticles of 2-3 nm and 5-6 nm in diameter were loaded into MOFs constructed with the metalloligands **L10** and **L11** (respectively in Figure **28a** and **28b**) and the $Zr_6(\mu_3O)_4(\mu_3OH)_4(\text{carboxylate})_{12}$ secondary units (**Pt-MOF7** and **Pt-MOF8**, respectively).[139] The resulting **Pt-MOF7** and **Pt-MOF8** MOFs were used as efficient photocatalysts for hydrogen evolution from water by synergistic photoexcitation of the MOF

frameworks and electron-injection into the Pt-nanoparticles. The larger channels of **Pt-MOF8**, resulting from the use of the elongated ancillary ligand on **L11**, promoted enhanced catalytic efficiency of **Pt-MOF8** compared to **Pt-MOF7** under visible light irradiation, with triethylamine (TEA) serving as a sacrificial reducing agent. Over 48h, **Pt-MOF8** and **Pt-MOF7** exhibited, respectively, TONs of 2400 and 7000 h^{-1}. The MOF materials proved to be very stable and could be collected back after catalytic experiments and recycled for use at least three further times without loss of activity.

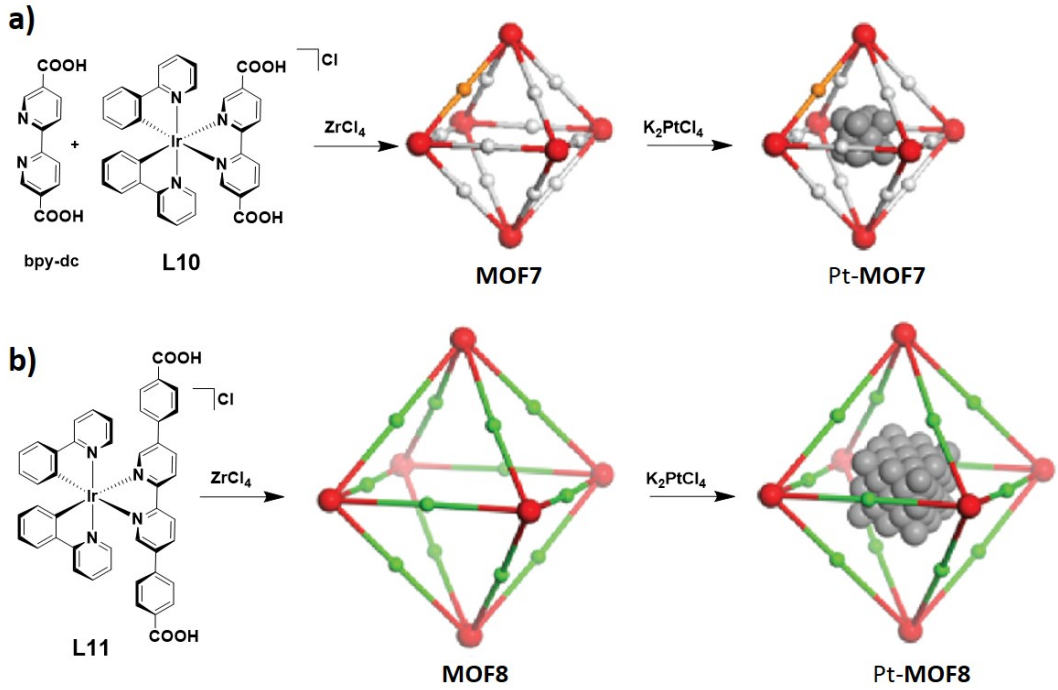

Figure **28**. Schematic representation of the formation of: **a)** Pt-**MOF7** and **b)** Pt-**MOF8**. Red balls are Zr atoms, white linkers are bpy-dc, yellow linkers are **L10**, green linkers are **L11** and in grey are Pt nanoparticles. Adapted with permission from Ref. [139]. Copyright 2012, American Chemical Society.

A supramolecular system composed of the iridium complex $[Ir(ppy)_2(pytl\text{-}\beta CD)]Cl$ (pytl-βCD is 1-substituted-1*H*-1,2,3-triazol-4-yl)pyridine functionalised with a β-cyclodextrin unit)

as the photosensitiser, viologen functionalised with two adamantyl moieties as the electron-relay and cyclodextrin coated platinum nanoparticles as the catalyst, was also tested for photoinduced hydrogen evolution from water.[140] The system was designed to assemble through adamantane – cyclodextrin non-covalent interactions and therefore to give rise to photoinduced electron transfer from the iridium chromophore to the Pt nanoparticle *via* the viologen bridge (Figure **29**). Interestingly, with ethylendiaminetetra-acetic acid (EDTA) serving as a sacrificial donor, this supramolecular system could produce almost 32 μmoles (approximately 0.75 ml) of H_2 per hour from 10 ml of H_2O, which was a higher yield than the analogous supramolecular system involving a ruthenium chromophore in Ru-bpy/viologen/Pt.[141]

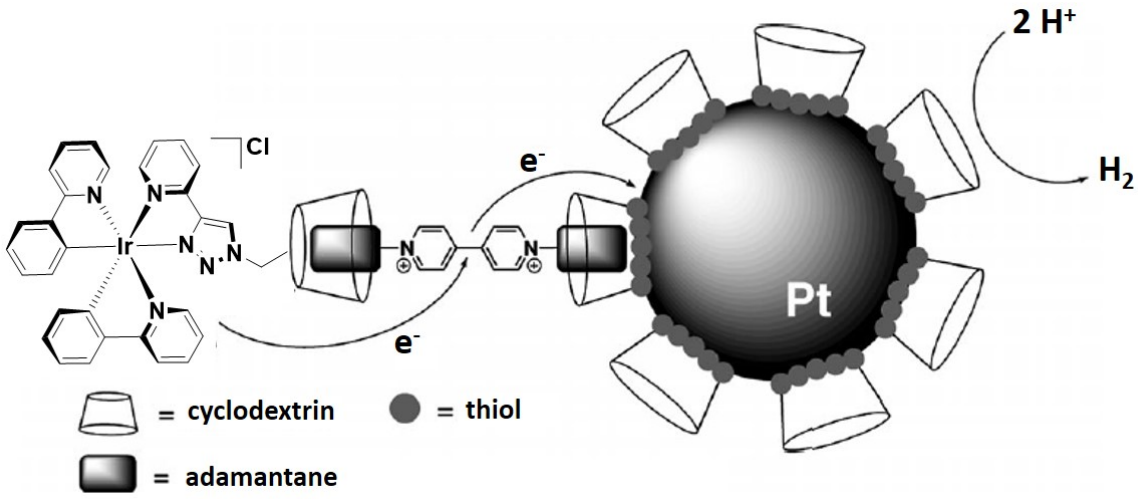

Figure **29**. Illustration of the supramolecular assembly Ir/viologen/Pt used for photoproduction of H_2. Adapted with permission. Copyright 2012, Wiley-VCH.[140]

Two Ir(III) metalloligands containing six carboxylic acid groups appended at the 4,4'-positions of both the ppy and bpy ligands in the homoleptic complex *fac*-[Ir(ppy-dc)$_3$] (**L12)** (ppy-dc is 2-(3-carboxyphenyl)isonicotinic acid) and the heteroleptic complex [Ir(ppy-dc)$_2$(bpy-dc)] (**L13**, Figure **30a,b**), have been recently assembled with [Ni(cyclam)](ClO$_4$)$_2$

(cyclam is 1,4,8,11-tetraazacyclotetradecane), forming two networks of cubic topologies (**MOF9** and **MOF10**).[142] **MOF9** and **MOF10** both crystallized in trigonal space groups (R-3 and R-3c, respectively) where the Ni(II) cations are in octahedral coordination environments bound to four nitrogen atoms of the cyclam ligand and to two carboxylate groups from two **L12** and **L13** metalloligands, respectively, along the z-axis. As illustrated in Figure **30c**, the crystal packing of **MOF9** and **MOF10** gave rise to two sets of interlocked primitive cubic networks. The materials exhibited small pore sizes and therefore poor ability to absorb CO_2 and N_2. For example, at 298 K and 1 atm, the sorption capacity of **MOF9** for CO_2 was 13.2 cm^3g^{-1}, while that of **MOF10** was 29.6 $cm^3 \cdot g^{-1}$. The luminescence properties of **MOF9** and **MOF10** were not investigated.

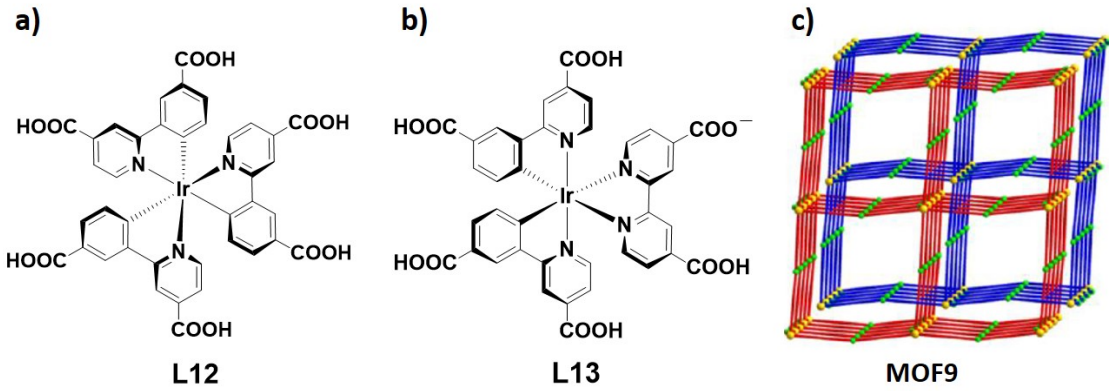

Figure **30**. **a)** Chemical structure of **L12**; **b)** chemical structure of **L13** and **c)** illustration of the interlocked cubic topology exhibited by the crystal structures of **MOF9** and **MOF10**.[142] Image **c)** is adapted with permission. Copyright 2017, Wiley-VCH.[142]

Three iridium-based MOFs of composition $[Cd_3(\mathbf{L1})_3]_2(DMF)_2(H_2O)_4] \cdot 6H_2O \cdot 2DMF$ (**MOF11**), $[Cd_3(\mathbf{L1})_3]_2(DMA)_2(H_2O)_2] \cdot 0.5H_2O \cdot 2DMA$ (**MOF12**) and $[Cd_3(\mathbf{L1})_3]_2(DEF)_2(H_2O)_2] \cdot 8H_2O \cdot 2DEF$ (**MOF13**) (**L1** is reported in Figure **22**, DMA is *N*,*N*-

dimethylacetamide and DEF is *N*,*N*-diethylformamide) were recently reported by Zheng and co-workers.[143] X-ray single-crystal structure analyses revealed that **MOF11**, **MOF12** and **MOF13** are isostructural and crystallized in the monoclinic space group $P2_1/n$, showing a three dimensional framework where complex **L1** bridges three Cd^{2+} ions through its six carboxylate oxygen atoms (Figure **31**).

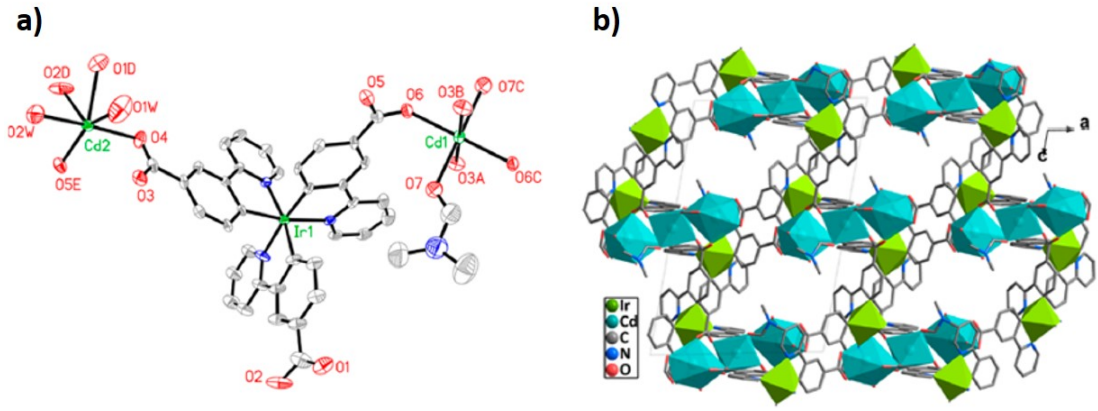

Figure **31**. **a)** Building units of **MOF11** and **b)** View of the 3D structure of **MOF11**, showing the channels along the *b*-axes. Solvent molecules are removed for clarity. Image is adapted with permission from Ref. [143]. Copyright 2018, American Chemical Society.

The powder emission of **MOF11** was broad, originating from a ^{3}MLCT state, and red-shifted at λ_{PL} = 519 nm with longer τ_{PL} of 2.95 μs (Table **1**) compared to the powder emission exhibited by complex **L1** (λ_{PL} = 488, 510 nm, τ_{PL} of 1.93 μs). The red-shifted emission observed for **MOF11** is due to coordination of the Cd^{2+} ions to the iridium complex, which decrease the LUMO thereby giving rise to a smaller optical gap, while the increased rigidity reduces non-radiative decay and accounts for the longer τ_{PL} in **MOF11** compared to that of **L1**. **MOF11** was found to be soluble in water and emissive at 515 nm. The sensing ability of **MOF11** towards metal cations (Na^+, Mg^{2+}, K^+, Ca^{2+}, Cr^{3+}, Mn^{2+}, Fe^{3+}, Co^{2+}, Ni^{2+}, Cu^{2+} and Zn^{2+}) and various anions (F^-, Cl^-, Br^-, I^-, BrO_3^-, IO_3^-, NO_3^-, CO_3^{2-}, SO_4^{2-}, PF_6^-, HPO_4^{2-} and $Cr_2O_7^{2-}$) were investigated by emission spectroscopy both in water and in PMMA-doped films. Among this series of

analytes, **MOF11** exhibited selective sensing for the cation Fe^{3+} and the anion $Cr_2O_7^{2-}$ with detection limits of 67.8 and 145.1 ppb for Fe^{3+} and $Cr_2O_7^{2-}$, respectively. **MOF11** also exhibited selective sensing of adenosine triphosphate (ATP^{2-}) over both adenosine diphosphate (ADP^{2-}) and adenosine monophosphate (AMP^{2-}). Indeed, following gradual addition of ATP^{2-} to an aqueous solution **MOF11** or exposing a PMMA-doped film of **MOF11** to vapors of ATP^{2-} a significant phosphorescent quenching of **MOF11** was observed; no emission quenching was observed when either ADP^{2-} and ATP^{2-} were added to **MOF11**.

An example of a heterometallic paddlewheel structure (**P5**) was reported by Hosseini and co-workers[144] by assembling an Ir(III) dipyrrin derivative bearing an appended carboxylic acid (**L14**) with Cu(II) ions (Figure **32**). Single crystals of **P5** suitable for x-ray diffraction were obtained by slow diffusion of a MeOH solution of $Cu(OAc)_2$ into a DMF solution of **L14**, leading to the formation after two weeks of dark red crystals of composition of [(**L14**)$_4$$Cu_2$(DMF)($H_2O$)]. **P5** crystallized in a in a triclinic $P\bar{1}$ space group where two Cu(II) cations form the paddlewheel motif bridged by the carboxylate groups of four **L14** molecules, and one DMF molecule and one water molecule occupy the remaining two axial positions (Figure **32**). Complex **L14** exhibited a weak emission at λ_{PL} = 710 nm in degassed DCM (Table **1**). However, complex **P5** was rather insoluble or unstable in common organic solvents and therefore, its emission properties could not be investigated.

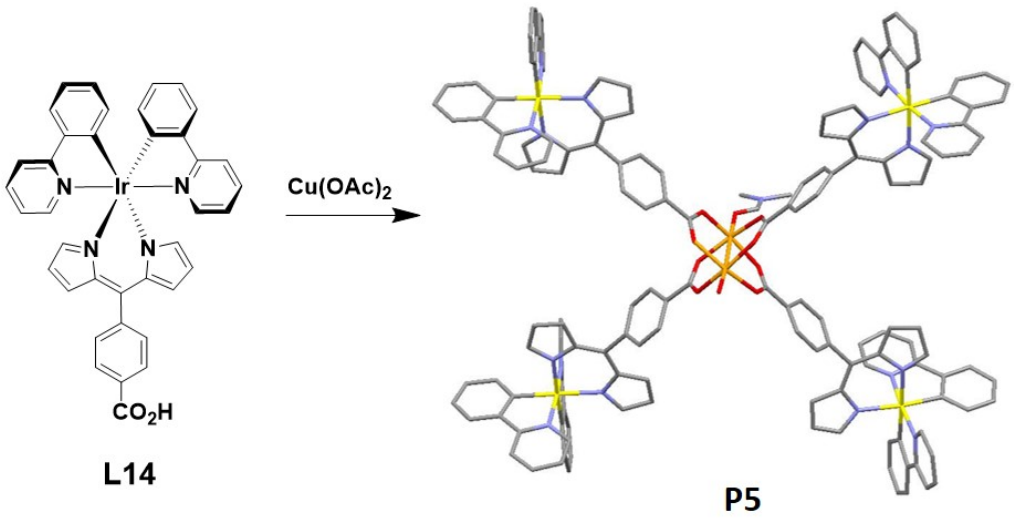

Figure **32**. Formation of the paddlewheel structure **P5** by reacting the iridium complex **L14** with Cu(II) ions. The x-ray structure of **P5** is shown (carbon, oxygen, copper and iridium atoms are shown respectively in grey, red, orange and yellow).

More recently the same group reported two homochiral heterometallic coordination networks involving cyclometalated Ir(III) chiral metallotectons.[145, 146] Enantiopure Δ- and racemic *rac*-Ir(III) complexes, Δ-, *rac*-**L15** and Δ-, *rac*-**L16**, of composition of Δ-, *rac*-$[Ir(C^N)_2(py\text{-}alk\text{-}bpy)]PF_6$ (where C^N is ppy in **L15** and dFppy in **L16** and py-alk-bpy is 5,5'-bis(pyridine-4-ylethynyl)-2,2'-bipyridine) were assembled, respectively, with Cu(I)[145] and Cd(II)[146] ions (Figure **33a** and **33b**, respectively). When an EtOH solution of $[Cu(NCMe)_4]BF_4$ was left to slowly diffuse into an MeCN solution of *rac*-**L15**, single crystals suitable for x-ray diffraction were obtained. The structural investigation of these crystals revealed the formation of a grid-type network (Figure **33a**), where Cu(II) ions, formed during the crystallization process from oxidation of Cu(I) under ambient conditions, adopted a slightly distorted octahedral geometry, with four pyridyl units of four **L15** molecules occupying the square base of the octahedron and two BF_4^- ions occupying the axial positions. Interestingly, each grid was intrinsically chiral as only one enantiomer of **L15** was present. However, consecutive homochiral sheets were packed with alternation of Δ-**L15** and Λ-**L15** leading thus to achiral

crystal. No single crystals were obtained when the enantiopure Δ-**L15** was used in the assembly. Metalloligand *rac*-**L15** exhibited a mixed ^{3}MLCT/^{3}LLCT emission in the solid state at λ_{PL} = 677 nm with a Φ_{PL} of 3% (Table **1**), while no emission could be detected from the grid-type network.

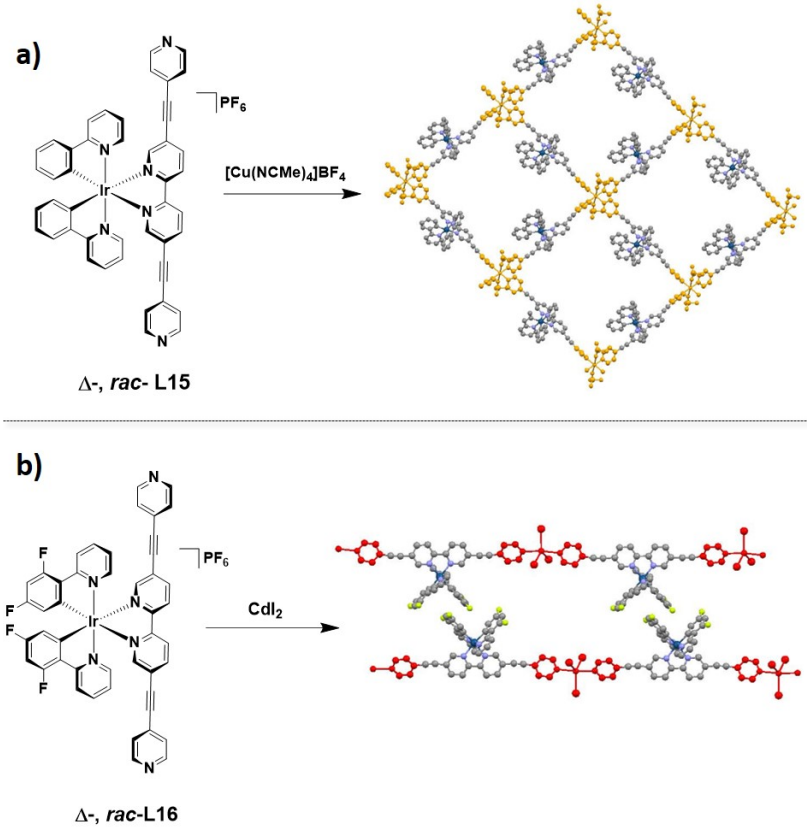

Figure **33**. **a)** Self-assembly between metalloligands Δ-, *rac*-**L15** and Cu(I) ions yielding the Ir-Cu grid-type network. In orange is illustrated the coordination around the Cu(I) ions.[145] **b)** Self-assembly between metalloligands Δ-, *rac*-**L16** and Cd(II) ions yielding the Ir-Cd linear network. In red is illustrated the coordination around the Cd(II) ions.

Diffusion of an EtOH solution of CdI_2 through an EtOH/$Cl_2CHCHCl_2$ buffer layer containing two drops of trifluoroethanol and 4,4,4-trifluorobutanol into a solution of either Δ- and *rac*-**L16** in 1,1,2,2-tetrachloroethane led to the slow formation of orange single crystals. X-ray analyses of the crystals obtained by the assembly of both complexes Δ-**L16** and *rac*-**L16** and

CdI_2 demonstrated the formation identical structures. These resembled infinite 1D networks where the Cd centers adopted a trigonal bipyramidal coordination geometry with the two terminal pyridine moieties of Δ-**L16** and *rac*-**L16** occupying the apical positions, and three iodine atoms located at the trigonal base (Figure **33b**). In the case of the network involving *rac*-**L16**, consecutive homochiral planes of opposite chirality were packed in a parallel fashion, resulting in the formation of non-chiral crystals. By contrast, the assembly of enantiopure Δ-**L16** with CdI_2 resulted in the formation of a chiral 1D network. Metalloligand *rac*-**L16** exhibited structured emission in both degassed THF and in the solid state with two maxima at λ_{PL} = 570, 605 nm, but with divergent Φ_{PL} of 19% (τ_{PL} of 1.47 μs) and 2%, respectively (Table **1**); no lifetime data were reported in the solid state. The racemic and enantiopure Ir(III)-Cd(II) coordination networks exhibited structured emission in the solid state with two emission maxima red-shifted at λ_{PL} = 575, 620 nm and with lower Φ_{PL} < 1% compared to *rac*-**L16**. The red-shifted emissions of the Ir-Cd networks are attributed to the lowering of their LUMO energy levels as a result of the binding of the Lewis-acidic Cd(II) ions to the pyridine moieties of **L16**.

Table **1**. Relevant photophysical properties at 298 K of Ir(III) metalloligands, CPs and MOFs

	medium	**λ_{PL} (nm)**	**Φ_{PL} (%)**	**τ_{PL} (μs)**	**reference**
L1	powder	520	-	1.9	128, 143
L2	powder	575	-	-	128
L3	powder	613	17.8	7.8	129, 131, 132, 135, 136
L4	powder	538	-	-	133
L14	DCM	710	-	-	144
***rac*-L15**	powder	677	3		145
***rac*-L16**	powder, (THF)	570, 605	2	(1.5)	146
P1	powder	540	-	-	128
P2	powder	550	-	-	128
P3a	crystal	613	27.4	-	129
P3b	crystal	595	19.3	-	129
P3c	crystal	587	0.1	-	129

P3d	crystal	600	0.2	-	129
P3e	powder	544	14.6	7.7	131
P3f	powder	554	18.1	13.3	131
P3g	powder	570	2.4	7.7	131
P3h	crystal	592	-	29.0	135
P4	powder	531	-	-	133
MOF1	powder	602	23.6	14.3	136
MOF11	powder	519		2.9	143

3.2. Macrocycles, capsules and cages

In the previous section, we documented extended structures incorporating iridium metalloligands. Here, we summarize discrete cage-like structure incorporating iridium. Coordination capsules and cages, formed through the self-assembly of arrays of metal ions and bridging ligands, have been areas of great interest in supramolecular chemistry during the last two decades.[147-149] Small guest molecules have been shown to be sequestered within the cavities of these cages and their host-guest interactions have been exploited in the context of sensing, gas storage and purification, and for catalysis.[150, 151] In recent years a small number of photophysically active capsules and cages that include Ir(III) metalloligands as luminescent units have been reported. In addition, iridium half-sandwich complexes of Cp*Ir (Cp* is penthamethylcyclopentadienyl) have been extensively used in macrocyclic chemistry to form a wide range of 2D-assemblies, including molecular squares, rectangles and triangles, with application in catalysis.[152-154] As these macrocycles have been already reported in pertinent review articles, they are not included herein.

A luminescent tetranuclear square-like macrocycle was reported by Baranoff and co-workers.[155] This macrocycle (**M1**, Figure **34a**) was synthetized in one step by reacting the

dimeric complex $[Ir(ppy)_2Cl]_2$ with two equivalents of tetrabutyl ammonium cyanide (TBACN) in the presence of a small excess of AgOTf in DCM. The geometry of **M1** was identified by x-ray diffraction (Figure **34a**). **M1** could be defined as a cyclic tetramer where the four Ir(III) centers and the bridging ambidentate cyano ligands form a chiral structure. Interestingly, while each iridium unit could be either the Λ- or Δ-isomer, giving a total of nine possible optical isomers, only two isomers were observed in the crystal structure, namely the [-Δ-Λ-Δ-Λ] and the mirror image [-Λ-Δ-Λ-Δ]. **M1** exhibited a bright green structured luminescence with maxima at 496 nm and 521 nm in degassed MeCN, with a Φ_{PL} of 66% and a bi-exponential τ_{PL} of 40 ns, 2320 ns (Table **2**). The emission of **M1** was red-shifted and slightly quenched when compared to the reference $TBA[Ir(ppy)_2(CN)_2]$, which likewise showed structured emission in degassed MeCN at λ_{PL} = 470, 502 nm, with Φ_{PL} of 79%. Solution-processed OLEDs fabricated by using **M1** as the emitter achieving a maximum external quantum efficiency (EQE) of 10.2% (λ_{EL} = 497 nm).

Shiu and co-workers[156] reported the self-assembly of the Ir(III) complex $[Ir(ppy)_2(4\text{-}pyCO_2H)_2]NO_3$ (4-$pyCO_2H$ is 4-pyridine carboxylic acid), **L17** with the Arrhenius base $Mg(OH)_2$ in the presence of KPF_6, yielding quantitatively the cage structure of composition $[(\mathbf{L17})_3(Mg(OH_2)_3)_2]K_2(PF_6)_3$, **C1** (Figure **34b**). The x-ray crystal structure of **C1** comprised of a cationic coordination cage exhibiting a large trigonal bipyramidal geometry that encapsulated the quintuple ionic aggregate $K_2(PF_6)_3^-$ formed in solution from KPF_6 (Figure **34b**). The neutralization of **C1** with KOH and $Mg(OH)_2$ in MeOH or EtOH promoted the degradation of the coordination cage and the subsequent formation of a zig-zag coordination polymer of composition $[(\mathbf{L17})_4MgK_2]_n$, which was itself also characterised by x-ray diffraction. The

emission properties of the coordination cage **C1** and the related coordination polymer were not investigated.

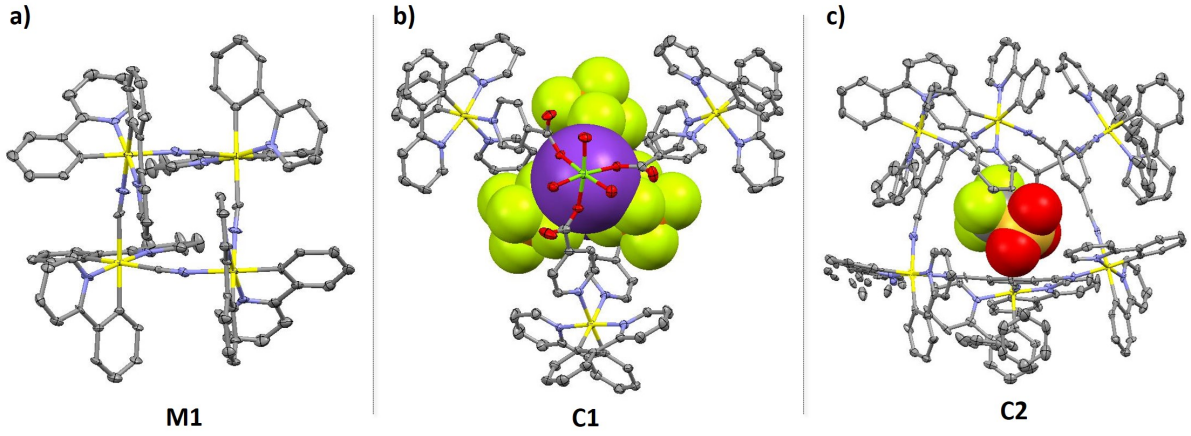

Figure **34**. X-ray crystal structures of: **a) M1** and **b) C1** and **c) C2**. C, N and Ir atoms are respectively shown in grey, blue and yellow. The guests $K_2(PF_6)_3$ in **b)** and OTf molecule in **c)** are illustrated in space-fill mode.

Lusby and co-workers[157] reported the first example of a 3D luminescent Ir(III) capsule of composition of $[(Ir(ppy)_2)_6(tcb)_4](OTf)_6$ (tbc is 1,3,5-tricyanobenzene) (**C2**, Figure **34c**). To eliminate the problem of mixed stereoisomer formation during the self-assembly, the *rac*-$[Ir(ppy)_2Cl]_2$ dimer was firstly resolved into its enantiopure Λ,Λ- and Δ,Δ-stereoisomers through chromatographic resolution of serine-based complexes, the amino acid acting as a chiral ancillary ligand thereby forming a diastereomeric mixture of products. Reaction of either Λ,Λ- and Δ,Δ-$[Ir(ppy)_2Cl]_2$ with tcb quantitatively yielded the enantiopure Λ_6- and Δ_6-**C2**. Vapor diffusion of benzene into a saturated DCM solution of Δ_6-**C2** afforded suitable crystals for x-ray diffractions. Within the crystal structure of Δ_6-**C2** a triflate anion is encapsulated within the octahedral cavity of **C2** (Figure **34c**). Interestingly, despite the weak emission (Φ_{PL} < 1%) observed for the bis(benzonitrile) reference complex $[Ir(ppy)_2(NCPh)_2]OTf$ at λ_{PL} = 525 nm, a broad and red-shifted emission at 575 nm with an unusually enhanced Φ_{PL} of 4% was

detected for **C2** in deareated tetrachloroethane (Table **2**). The capsule exhibited an affinity for the encapsulation of perfluorinated anions following the sequence: PF_6^- > OTf^- ~ $CF_3BF_3^-$ > BF_4^-.

The self-assembly between square planar palladium(II) or platinum(II) metal ions and complementary bent ligands containing specifically positioned distal pyridine moieties, first demonstrated by Fujita and co-workers,[158] has been used as a technology to prepare myriad molecular capsules and cages.[124, 149] Recently, our group[159] has reported the first examples or metallocages through $N_{(pyridine)}$-Pd coordination. Ir(III) homochiral supramolecular cages of composition Λ_8-, Δ_8-, and *rac*-$[Ir_8Pd_4]^{16+}$ were obtained through the self-assembly between two families of Ir(III) metalloligands of the form of $Ir(C\hat{}N)_2(qpy)]BF_4$ and Pd^{2+} ions (Figure **35a**,**b**; C^N is mesppy = 2-phenyl-4-mesitylpyridinato in **L18**, and dFmesppy = 2-(4,6-difluorophenyl)-4-mesitylpyridinato in **L19**).[160] The metalloligands **L18** and **L19** were prepared in their racemic forms and also as their Λ- and Δ-enantiomers.[161] The assembly of ***rac*-L18** and ***rac*-L19** with Pd^{2+} ions yielded racemic cages *rac*-$[Ir_8Pd_4]^{16+}$ (***rac*-C3** and ***rac*-C4**, respectively), while when Λ- and Δ-**L18** and Λ- and Δ-**L19** were assembled with Pd(II) ions, enantiopure cages Λ_8- and Δ_8-$[Ir_8Pd_4]^{16+}$ were obtained (**Λ**-, **Δ-C3** and **Λ**-, **Δ-C4**, respectively).[159] The enantiopurity of metalloligands **Λ**-, **Δ-L18** and **Λ**-, **Δ-L19**, and metallocages **Λ**-, **Δ-C3** and **Λ**-, **Δ-C4** were confirmed by CD spectroscopy. As the chirality of the iridium metal did not impact the overall self-assembly process, metalloligand exchange was observed when either of the homochiral cages **Λ-** or **Δ-C3** were mixed with the homochiral cage **Δ-C4** at 85 ˚C for 12h, promoting the formation of a statistical mixture of heteronuclear cages of composition $[(\mathbf{\Lambda}, \mathbf{\Delta}\text{-}\mathbf{L18})_n(\mathbf{\Delta}\text{-}\mathbf{L19})_mPd_4](BF_4)_{16}$ (n + m = 8, from **Λ-**, **Δ-L18** : **Δ-L19** = 7 : 1 to **Λ-**, **Δ-L18** : **Δ-L19** = 1 : 7).

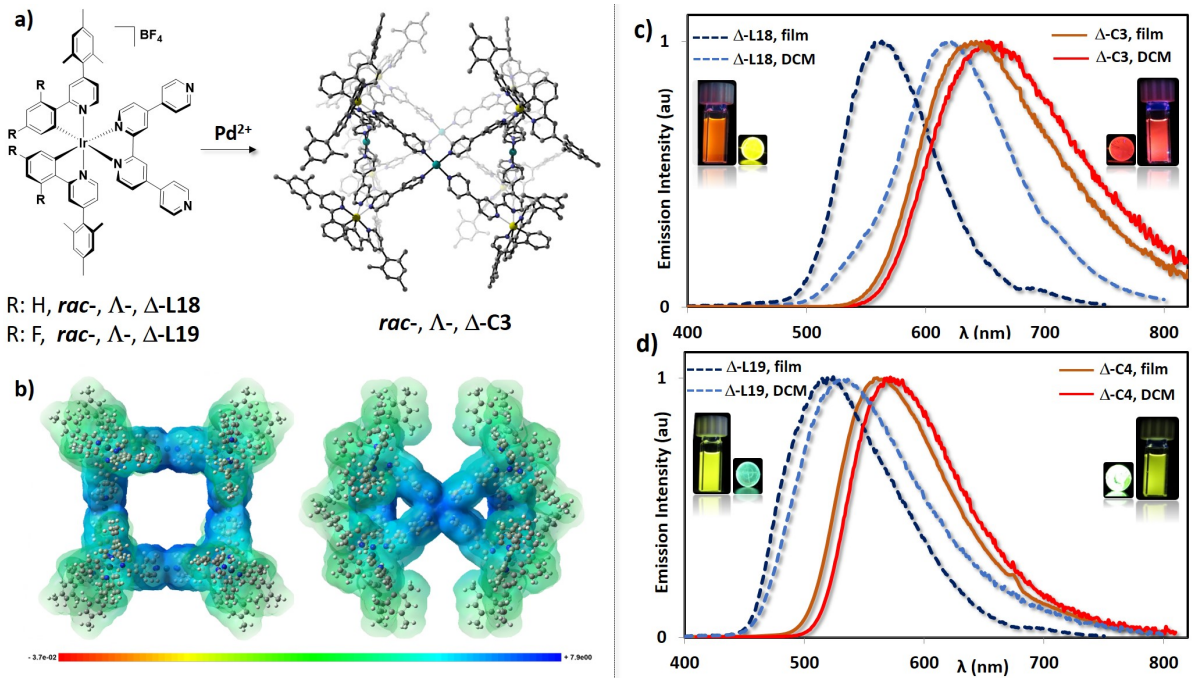

Figure **35**. **a)** Self-assembly between the metalloligands ***rac***-, **Λ**-, **Δ-L18** and ***rac***-, **Λ**-, **Δ-L19** and Pd^{2+} ions yielding cages ***rac***-, **Λ**-, **Δ-C3** and ***rac***-, **Λ**-, **Δ-C4**. For clarity, only the calculated structure of **Δ-C3** obtained is shown. **b)** Molecular electrostatic potential [HF/6-31G(d)] map of **Δ-C3** with front (left) and central (right) views. The most positive potential regions are shown in deep blue. Normalized emission spectra of: **c) Δ-L18** and **Δ-C3** and **d) Δ-ML19** and **Δ-C4**. Dotted dark-blue lines: PMMA-doped film with 5 wt% of metalloligands **Δ-L18** and **Δ-L19** spin-coated on quartz substrates; Dotted light-blue lines: deareated DCM solution of **Δ-L18** and **Δ-L19**; Solid orange lines: PMMA-doped film with 5 wt% of **Δ-C3** and **Δ-C4** spin-coated on quartz substrates; Solid red lines: deaerated DCM solution of **Δ-C3** and **Δ-C4**.[159]

The photophysical properties of the metalloligands ***rac***-, **Λ**-, **Δ-L18** and ***rac***-, **Λ**-, **Δ-L19**, and metallocages ***rac***-, **Λ**-, **Δ-C3** and ***rac***-, **Λ**-, **Δ-C4** were investigated both in DCM solution and in polymethyl methacrylate (PMMA) doped films (Figure **35c**,**d**) (Table **2**). In deaerated DCM,

cages ***rac***-, **Λ**-, **Δ**-**C3** and ***rac***-, **Λ**-, **Δ**-**C4** exhibited red-shifted emissions, respectively, at 655 nm and 561 nm, with lower Φ_{PL} of 5% and 14%, and shorter τ_{PL} of 202 ns and 825 ns, compared to those of the corresponding metalloligands ***rac***-, **Λ**-, **Δ**-**L18** and ***rac***-, **Λ**-, **Δ**-**L19** (*e.g.*, ***rac***-**L18**: λ_{PL} = 620 nm, Φ_{PL} = 14%, τ_{PL} = 300 ns; ***rac***-**L19**: λ_{PL} = 527 nm, Φ_{PL} = 34%, τ_{PL} = 1000 ns). As a result of the less polar environment and the rigidification conferred by the PMMA host polymer, the emissions of **L18**, **L19**, **C3** and **C4** in the thin films were blue-shifted, respectively, at 564 nm, 518 nm, 643 nm and 531 nm (Figures **35c**,**d**), with enhanced Φ_{PL} of 28%, 41%, 10% and 16% and longer multi-exponential τ_e compared to their photophysical behavior in DCM. The red-shifted emissions of the cages **C3** and **C4** in both DCM and PMMA-doped films compared to the corresponding metalloligands was interpreted to be the result of coordination of the Lewis acidic Pd^{II} to the iridium complex thereby lowering the LUMO energies of **L18** and **L19** localized on the qpy ligand, [160] [159] [158] [158] [157] [156] [155] [152] [136] [136] [138] [137] [136] [135] [134] [133] [133] [132] [131] [130] [130] [129] [128] [128] [127] [126] [125] [124] [123] [122] [121] [120] [119] [118] [117] [116] [115] and giving rise to smaller optical gaps. Interestingly, cage **C3** could encapsulate within its cavity large anionic guests including the blue-emitting complex $NBu_4[Ir(dFppy)_2(CN)_2]$, giving rise to host-guest photoinduced interactions. These results will be discussed in the following chapter.

Hardie, Zysman-Colman and co-workers[162] reported the assembly of CTV-type ligands (CTV is cyclotriveratrylene), (±)-*tris*(isonicotinoyl)-cyclotriguaiacylene (**L20**), or (±)-*tris*(4-pyridyl-methyl)-cyclotriguaiacylene (**L21**), with $[Ir(ppy)_2(NC)_2]^+$, forming metallo-cryptophane cages of compositions of $[(Ir(ppy)_3)_3(\mathbf{L20})_2](BF_4)_3$ (**C5**) and $[(Ir(ppy)_3)_3(\mathbf{L21})_2](BF_4)_3$ (**C6**, Figure **36a**). The geometry of **C5** was revealed by x-ray crystallography (Figure **36b**). The cage has three pseudo-octahedrally coordinated Ir(III)

centers, each bearing two ppy ligands and two pyridyl groups from two **L20** ligands in a *cis*-arrangements. The two **L20** ligands are bridged between three Ir(III) centers, acting as vertices. Interestingly, despite iridium-centred Λ- and Δ-enantiomers and the M and P enantiomers of the CTV ligands that were present in the reaction mixture, and thus twelve possible stereoisomeric cages, the cage exhibited homochiral self-sorting, and only the enantiomeric MM-ΛΛΛ and PP-ΔΔΔ cages were observed, both in the x-ray structure of **C5** and by NMR in solution after several months, where the self-sorting was found to be very slow. The self-sorting in solution was found to be accelerated by the presence of R-camphor or S-camphor as chiral guests.

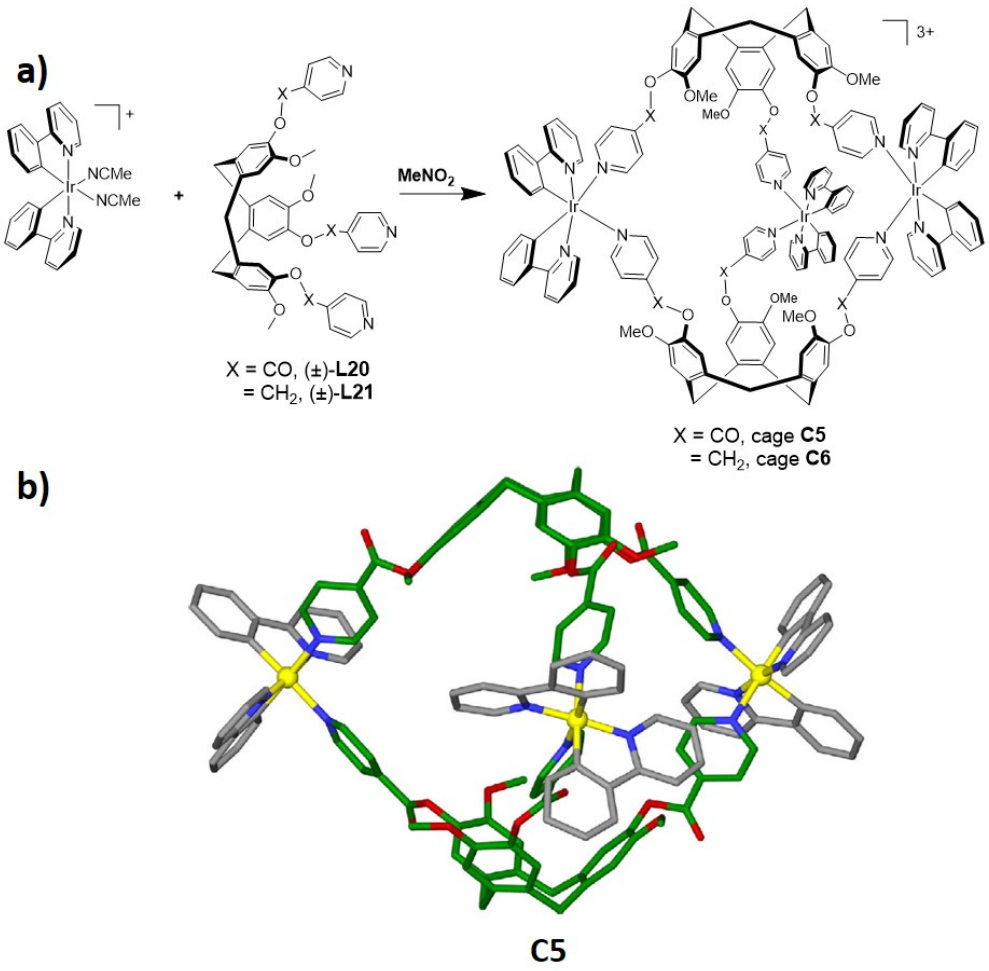

Figure **36**. **a)** Chemicals structures of ligands **L20** and **L21** and cages **C5** and **C6**. **b)** X-ray structure of cage **C5**.[162]

Cages **C5** and **C6** are emissive in solution, as bulk powders and in PMMA-doped films (Figure **37a,b**) (Table **2**). The emission of **C5** in the powder was red-shifted (λ_{PL} = 648 nm) compared to that in DCM (λ_{PL} = 604 nm). In both media low Φ_{PL} of 1% and short bi-exponential emission decays were observed. Due to the increased conjugation into the CTV scaffold as a result of the carbonyl linker to the distal pyridine, **C5** exhibited red-shifted emission compared to **C6** but with similar though red-shifted photophysical behavior compared to the monomeric $[Ir(ppy)_2(4\text{-}pyCO_2Et)_2]^+$ (4-$pyCO_2$Et = 4-ethyl isonicotinate) (λ_{PL} = 560 nm; Φ_{PL} = 2%). As a result of the reduction of non-radiative vibrational motion in PMMA-doped thin films, the emission of **C5** was blue-shifted and more structured at λ_{PL} = 514 nm with an enhanced emission and longer photoluminescence decays (Φ_{PL} = 5.5%, τ_{PL} = 634 ns, 2319 ns) compared to the emission in DCM. The photoluminescence of **C6** in DCM was found to be structured and blue-shifted at λ_{PL} = 516 nm with higher Φ_{PL} of 15% and longer τ_{PL} = 523, 887 ns compared to **C5**. Unlike that observed for **C5**, the emissions of **C6** as a powder and in PMMA-doped films were similar to that in DCM (in powder: λ_{PL} = 519 nm, Φ_{PL} = 1.6%, τ_{PL} = 141, 1175 ns; in thin film: λ_{PL} = 515 nm, Φ_{PL} = 10%, τ_{PL} = 688, 3042 ns).

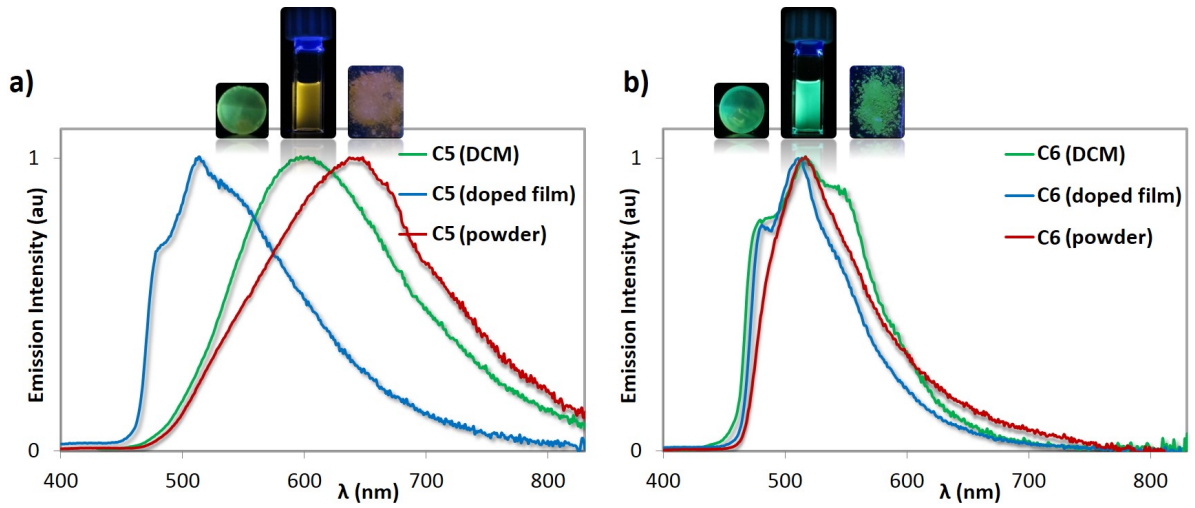

Figure **37**. Normalized photoluminescence spectra of **a) C5** and **b) C6**. Green lines are deaerated DCM solutions, light-blue lines are PMMA-doped films with 5wt% of cages spin-

coated on a quartz substrate; red lines are bulk powders. Insets are images of the samples under UV irradiation.[162]

By functionalizing the three arms of the CTV core with three bipyridines instead of pyridines as in the preceding example, emissive polynuclear systems composed of cationic Ir(III) complexes bearing core fragments of $[Ir(ppy)_2]^+$ and/or $[Ir(dFppy)_2]^+$ coordinated to the CTV through the bpy ligands were also reported (Figure **38**).[163] In mixed systems containing both the $[Ir(ppy)_2]^+$ and the $[Ir(dFppy)_2]^+$ luminescent units linked to a single CTV core, the Ir(III) chromophores behaved as isolated centers, with no optoelectronic communication between them. This is an unusual behavior for multimetallic Ir(III)-chromophoric complexes, since energy transfer between metal centers is commonly observed.

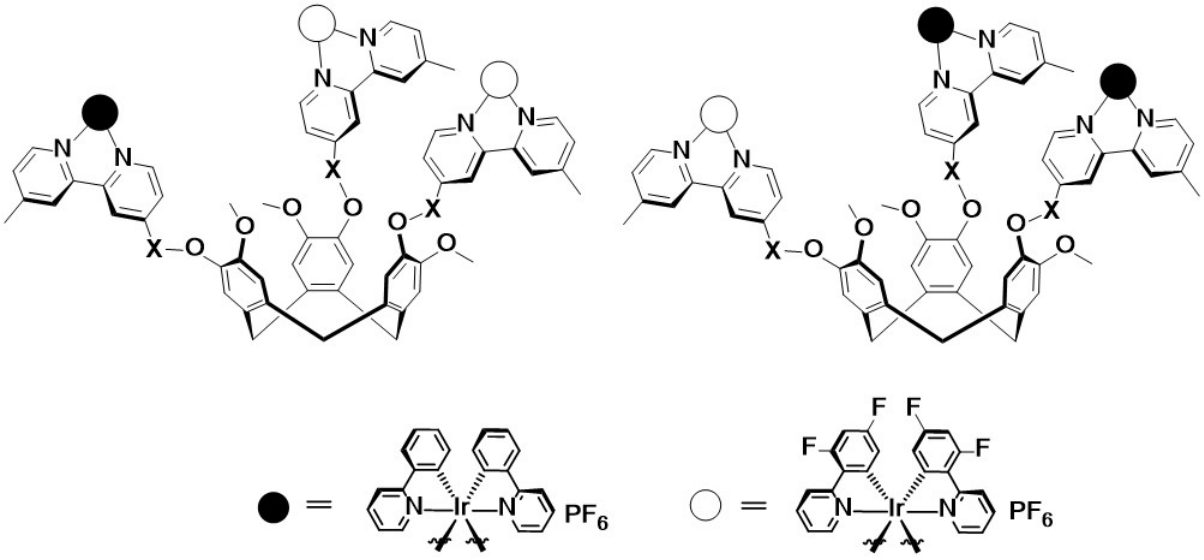

Figure **36**. Illustration of the chemical structures of the multimetallic Ir(III)-luminophoric complexes.[163]

Duan and co-workers recently reported the multicomponent self-assembly of two pentanuclears Ir(III)-Zn(II)[164] (**C7a**) and Ir(III)-Co(II)[165] (**C7b**) heterometal-organic polyhedrons. Polyhedron **C7a** was obtained by the reaction of *fac*-tris(4-(2-pyridinyl)phenylpyridinato)iridium (**L22**) and 2-formylpyridine, via a subcomponent self-

assembly in the presence of $Zn(BF_4)_2 \cdot 6H_2O$ in acetonitrile under nitrogen (Figure **39a**). Similarly, polyhedron **C7b** was formed by mixing **L22** with 2-formylpyridine in the presence of $Co(ClO_4) \cdot 6H_2O$ in a 2:6:3 ratio in acetonitrile (Figure **40a**). Suitable single crystals for x-ray diffraction of both **C7a** and **C7b** were obtained through slow vapor diffusion of diethyl ether into MeCN solutions of the polyhedrons. X-ray crystallography analyses revealed the formation of discrete cages of composition of Ir_2M_3 (where M is Zn in **C7a** and Co in **C7b**) that exhibited a trigonal bipyramidal geometry. In both structures, the three M atoms form the equatorial plane and the two iridium atoms occupied the axial positions.

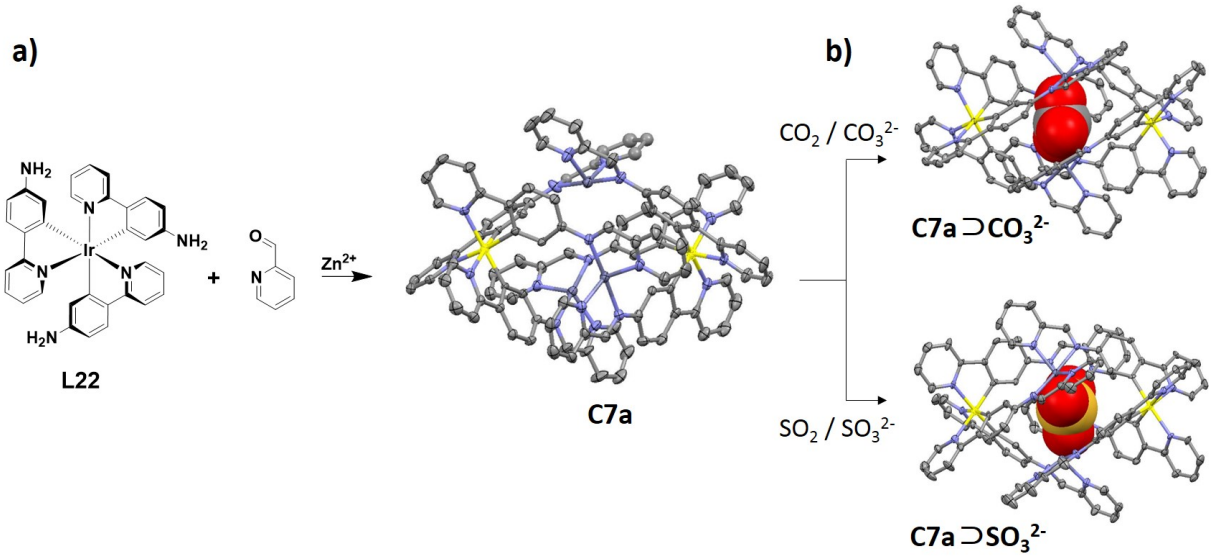

Figure **39**. **a)** formation of polyhedron **C7a** from the assembly of **L22**. **b)** x-ray structures of **C7a** encapsulating CO_3^{2-} and SO_3^{2-} shown with space-fill representations.

In Nature, carbon anhydrases (CAs) are common enzymes that contain active Zn^{2+} sites that are coordinated by three histidine residues and a water or hydroxide molecule and catalyze the reversible hydration of CO_2 to CO_3^{2-}.[166] Interestingly, **C7a** exhibits an adequate hydrophobic cavity and coordination geometry around the Zn atoms to mimic the active site of natural CAs. Vapor diffusion of diethyl ether into a MeCN solution of **C7a** under a CO_2 atmosphere, yielded single crystals suitable for x-ray diffraction. The crystallographic analyses revealed that CO_2

was converted into CO_3^{2-} and encapsulated into the cavity of **C7a** (**C7a⊃CO_3^{2-}**, Figure **39b**). **C7a⊃CO_3^{2-}** exhibited the same polyhedral structure as **C7a** with each of the three Zn atoms coordinating to one mono-dentate oxygen atom from CO_3^{2-} forming a [$Zn_3(\mu_3$-$CO_3^{2-})$] core, which was protected inside the cavity of the polyhedron. Similarly, **C7a** was found to be able to capture SO_2 and convert it into SO_3^-. The x-ray crystal structure of **C7a** encapsulating **SO_3^{2-}** (**C7a⊃SO_3^{2-}**, Figure **39b**) was also obtained. The formation of the host-guest systems **C7a⊃CO_3^{2-}** and **C7a⊃SO_3^{2-}** was observed not only in the solid state but also in MeCN solution by ^{1}H NMR spectroscopy and ESI-MS spectrometry. Emission spectroscopy provided further evidence of the encapsulation of CO_3^{2-} within **C7a**. The weak Ir(III)-centered emission exhibited by **C7a** at 508 nm (Table **2**) was gradually quenched within 18 minutes as a result of the formation of **C7a⊃CO_3^{2-}** upon pumping gaseous CO_2 into the MeCN solution of **C7a**.

When treatment of capsule **C7b** with one equivalent of carbonate dianions in MeCN solution, the formation of the host-guest assembly **C7b⊃CO_3^{2-}** was observed both by x-ray diffraction (Figure **40**) and ESI-MS spectrometry. Interestingly, the empty cage **C7b** was able to convert in high yield (86-96%) 2-aylpyridines to their α-trichloromethylated products when the system was photoirradiated with a 26 W fluorescent lamp (Figure **40b**). However, when **C7b⊃CO_3^{2-}** or only the single components **L22** or $Co(ClO_4)\cdot 6H_2O$ were tested as photocatalysts, no conversion was observed (Figure **40c**). These results unequivocally demonstrate that in order to photocatalyze the conversion of 2-aylpyridines, it is necessary to combine the photoactivity of the Ir(III) chromophores with the coordinatively unsaturated Co(II) centers. **C7b** offers a rigid platform to keep the Ir(III) complexes in close proximity to the Co(II) metal ions,

increasing the effective reaction concentration within the local micro-environment, and thus promoting high photoconversion of the substrates.

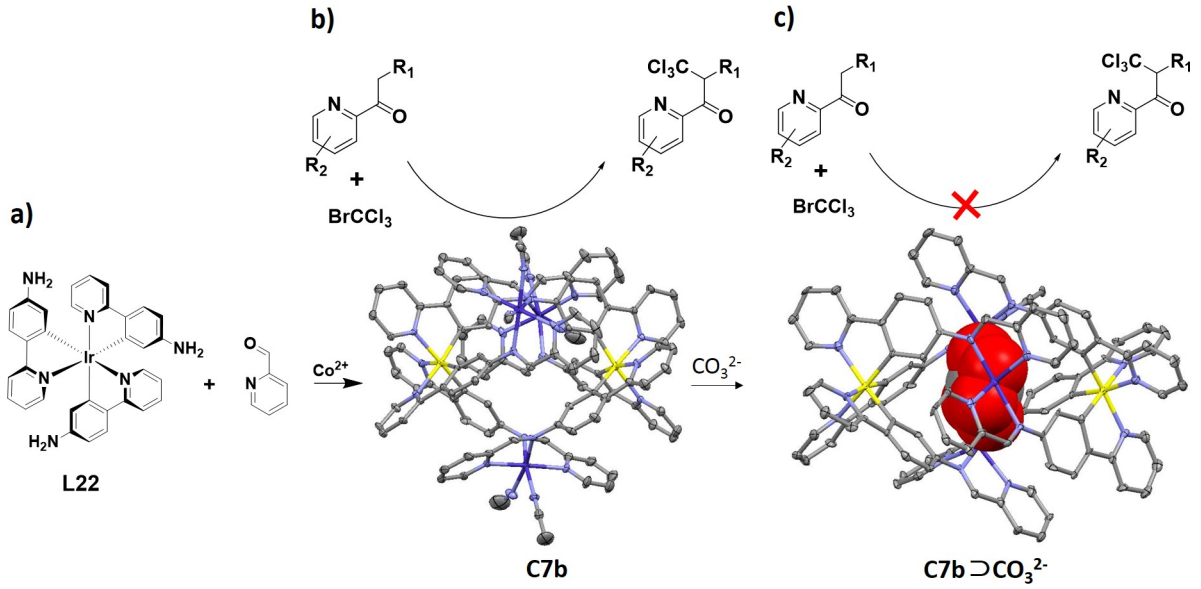

Figure **40**. **a)** Synthesis and x-ray crystal structure of polyhedral **C7b**. **b)** illustration of the photocatalyzed α-trichloromethylation of acylpyridine promoted by **C7b** (1 wt%). **c)** no photoreaction occurred when CO_3^{2-} ions was encapsulated into the cavity of **C7b**.

Table **2**. Relevant photophysical properties at 298 K of Ir(III) metalloligands, capsules, cages and macrocycles

	medium	**λ_{PL} (nm)**	**Φ_{PL} (%)**	**τ_{PL} (μs)**	**reference**
C2	TCE	575	4	-	157
***rac*-, Λ-, Δ-C3**	DCM, (film)[a]	655 (643)	5 (10)	0.20 (0.27, 0.72)	159
***rac*-, Λ-, Δ-C4**	DCM, (film)[a]	561 (531)	14 (16)	0.83 (0.24, 1.19)	159
C5	DCM, (film)[a], [powder]	604 (514) [648]	1 (5.5) [1.0]	0.06, 0.13 (0.63, 2.31) [0.06, 0.20]	162
C6	DCM, (film)[a], [powder]	516 (515) [519]	15 (10) [1.6]	0.52, 0.89 (0.69, 3.09) [0.14, 1.18]	162
C7a	MeCN	508	-	-	164
***rac*-, Λ-, Δ-L18**	DCM, (film)[a]	620 (564)	14 (28)	0.30 (0.34, 1.04)	159
***rac*-, Λ-, Δ-L19**	DCM, (film)[a]	527 (518)	34 (41)	1.00 (0.24, 1.18)	159
M1	MeCN	496, 521	66	0.04, 2.32	155

[a]PMMA-doped thin film spin-coated with 5 wt% of cage.

4. Encapsulation of Ir(III) chromophores

Several studies have demonstrated that the photophysical properties of luminescent Ir(III) metal complexes emitting from CT states strongly depend on the local environment.[101, 107, 111, 167] In this context, the encapsulation of iridium complexes into the cavities of photoactive cages, capsules or MOFs has been demonstrated to be an efficient approach to tuning of the emission properties of the assembly as a function of host-guest energy transfer.

Umakoshi and co-workers[168]. encapsulated $[Ir(ppy)_2(bpy)]Cl$ (**L23**) within a hexameric resorcinarene hydrogen-bonded capsule (Figure **41a**) and observed that the capsule provided a hydrophobic environment and also effectively hampered non-radiative decay, thereby inducing a change in the emission of **L23** from orange (λ_{PL} = 609 nm) to yellow (λ_{PL} = 582 nm) while enhancing both the Φ_{PL} and the τ_{PL} of the encapsulated iridium guest in degassed chloroform (encapsulated **L23**: Φ_{PL} = 32%, τ_{PL} = 860 ns; free **L23**: Φ_{PL} = 20%, τ_{PL} = 420 ns) (Figure **41b**).

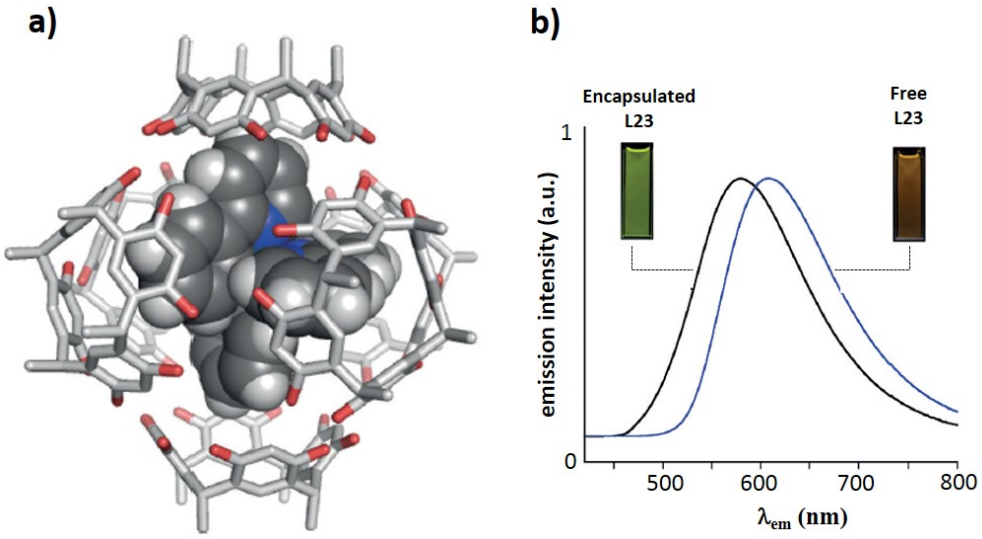

Figure **41**. **a)** Molecular model of the resorcinarene capsule encapsulating **L23** (space-fill representation). **b)** normalized emission spectra of free **L23** (blue line) and encapsulated **L23** (black line) collected at 298 K in $CHCl_3$ (λ_{exc} = 400 nm). Image **b)** is adapted with permission. Copyright 2016, Wiley-VCH.[168]

Similarly, the emission of the Ir(III) complex $[Ir(ppy\text{-}CHO)_2(bpy)]^+$ (**L24**, where ppy-CHO is 4-(2-pyridylbenzaldehyde), Figure **42a**) was remarkably enhanced and blue-shifted upon its encapsulation into the cavity of the cucurbituril [Q10] host (Figure **42b**,**c**).[169] Indeed, in aqueous buffer solution (pH 4.7), complex **L24** exhibited a weak emission at 593 nm, which was enhanced 80-fold and blue-shifted to 543 nm after its encapsulation (Figure **42b**). The temperature had a strong effect on the binding equilibrium; at 40 °C the host-guest assembly was found to be partially dissociated and thus its emission intensity and emission lifetime were, respectively, lower and shorter compared to those collected at 6 °C (at 40 °C: τ_{PL} = 100, 1750 ns; at 6 °C: τ_{PL} = 230, 3260 ns).

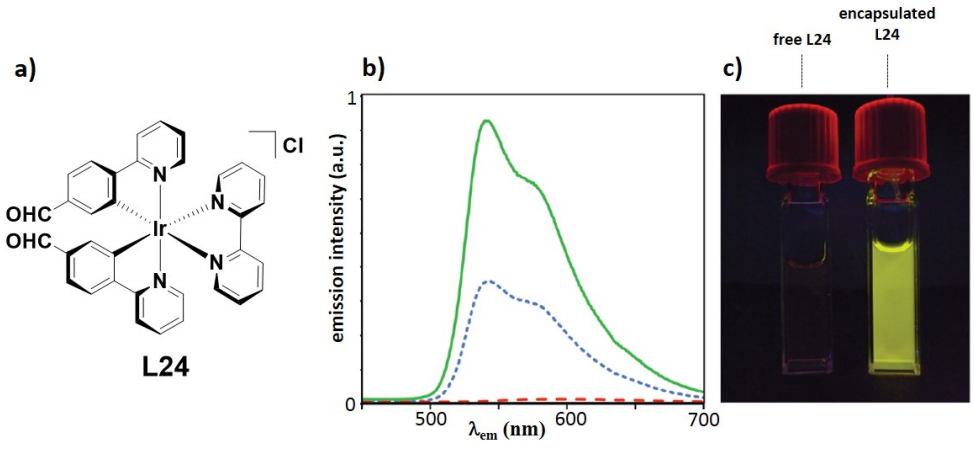

Figure **42**. **a)** chemical structure of **L24**. **b)** Emission spectra in aqueous buffer solution (pH 4.7) at 22 °C of **L24** (dashed red line), with added [Q10] in 1:1 molar ratio (dotted blue line) and with excess of [Q10] (solid green line). **c)** Emission from free **L24** (left) and **L24**

encapsulated into [Q10] host (right). Adapted from Ref. [169] with permission from The Royal Society of Chemistry.

The introduction of Ir(III) luminophores into the nanospace of inorganic host materials have also been explored. Wada and co-workers[170] introduced mixtures of the homoleptic *fac*- and *mer*-[Ir(ppy)$_3$] (**L25**) and *fac*- and *mer*-[Ir(dFppy)$_3$] (**L26**), into the cavity of a zeolite (Figure **43**). Depending on the Ir(III) species introduced into the zeolite, different emission colours were observed from the solid materials. Structured blue emission at λ_{PL} = 465, 488 nm was observed when **L26** was encapsulated, while green emission at λ_{PL} = 524 nm was observed from the zeolite encapsulating **L25** (Figure **43**). These emission profiles were consistent with those exhibited by the free complexes **L25** (λ_{PL} = 510 nm) and **L26** (λ_{PL} = 468, 482 nm) in MeCN.

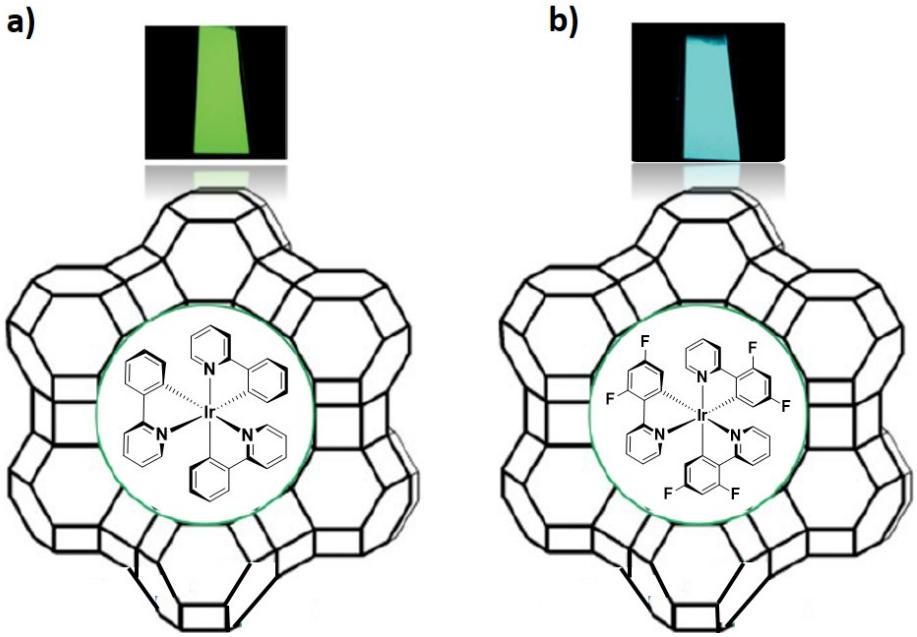

Figure **43**. Illustration of the encapsulation of the Ir(III) chromophores [Ir(ppy)$_3$], **a)** and [Ir(dFppy)$_3$], **b)** into the cavity of the zeolite cage. Insets are images of their emission colours. Adapted with permission. Copyright 2012, Wiley-VCH.[170]

In a subsequent work, the same group investigated the photoinduced electron transfer (PeT) processes from **L25**⊃Zeolite to propyl viologen sulfonate (PVS) in solution by using 1,1'-ethylene-2,2'-bipyridilynium ($2DQ^{2+}$), also incorporated into the zeolite cage, as an electron-relay molecule.[171] Their results demonstrated that upon photoirradiation, electron transfer from **L25** to $2DQ^{2+}$ occurred in the zeolite framework, forming the $2DQ^{\cdot +}$ radical cation and the $\mathbf{L25}^{\cdot -}$ radical anion. $2DQ^{\cdot +}$ transferred subsequently the electron to PVS is solution through a dark reaction, forming the $PVS^{\cdot -}$ radical anion. The regeneration of **L25** in its ground state was achieved through the addition of triethanolamine as a sacrificial reductant. The encapsulation of both **L25** and $2DQ^{\cdot +}$ in the cavity of the zeolite was found to be pivotal for promoting the PeT. Indeed, when the free species **L25**, $2DQ^{2+}$ and PVS were irradiated in solution, no PeT was observed.

A Periodic Mesoporous Organosilica derivative (PMO) bearing high density of the homoleptic Ir(III) complex [Ir(ppy)$_3$] (**4b** in Figure **2**) on the pore surface was investigated by Inagaki and co-workers.[167, 172] The PMO material was prepared by the polycondensation reaction between the ppy-bridge alkoxysilane precursor, 2-(4-triethoxysilylphenyl)-5-triethoxysilylpyridine and the cationic surfactant octadecyltrimethylammonium chloride (C_{18}TMACl). The subsequent cyclometalation reaction of [Ir(ppy)$_2$Cl]$_2$ with the ppy ligands of

PMO in an ethylene glycol solution in the presence of K_2CO_3 at 120 ˚C for 24 h yielded the PMO material with the Ir(III) complex [Ir(ppy)$_3$] included in its pores (Ir-PMO). Ir-PMO exhibited a broad phosphorescence at λ_{PL} = 550 nm with a Φ_{PL} of 3% and a bi-exponential emission lifetime of τ_{PL} = 250 ns, 1000 ns. These emission properties are characteristic for the meridional isomer *mer*-[Ir(ppy)$_3$], which is typically formed when cyclometalation reactions are conducted at relatively low temperature (< 140 ˚C).[173] Ir-PMO also acted as a light-harvesting antennae as the energy absorbed by the PMO framework upon photoexcitation at 300 nm was efficiently transferred to the Ir(III) complex following a Förster mechanism. Indeed, the emission of *mer*-[Ir(ppy)$_3$] in Ir-PMO was enhanced when excited at 300 nm (instead of at 380 nm) and the characteristic emission of the PMO framework at λ_{PL} = 420 nm was completely quenched.

The phosphorescence properties of PMO derivatives functionalized with the heteroleptic Ir(III) complex [Ir(ppy)$_2$(bpy]Cl (**4b**, Figure **2**) were also investigated.[174] Depending on the amount of **4b** loaded into the pores of the PMO, the emission properties of **4b**-PMO in the solid state were found to differ only slightly. With a low, medium and high **4b** loading, respectively, of 3.47 μmol g^{-1}, 20.4 μmol g^{-1} and 59.9 μmol g^{-1}, **4b**-PMO exhibited broad emission, respectively, at λ_{PL} = 527 nm, λ_{PL} = 530 nm and λ_{PL} = 535 nm with Φ_{PL} of 13%, 14% and 13% and τ_{PL} of 405 ns, 462 ns and 438 ns. In MeCN the emission of **4b**-PMO was red-shifted at λ_{PL} = 560 nm with Φ_{PL} of 7.0% and τ_{PL} of 784 ns. When a MeCN solution of tetracene was gradually added (from 0 to 0.4 mM) to a MeCN solution of **4b**-PMO, the emission intensity of **4b**-PMO at λ_{PL} = 527 nm was correspondingly quenched together with a shortenning of its emission lifetime from 784 ns to 107 ns. Förster energy transfer was therefore promoted from **4b**-PMO donor to the tetracene acceptor upon photoexcitation at 340 nm.

By encapsulating the yellow-emitting $[Ir(ppy)_2(bpy)]PF_6$ (**L27**) chromophore into the cavities of the blue-emitting fluorescent MOF $[(CH_3)_2NH_2]_{15}[(Cd_2Cl)_3(TATPT)_4]\cdot 12DMF\cdot 18H_2O$ (**MOF-H**, TATPT is a hexadentate carboxylate triazine ligand, 2,4,6-tris(2,5-dicarboxyphenylamino)-1,3,5-triazine), an efficient white-emitting assembly was obtained as reported by Li and co-workers.[175] The Ir(III) complex **L27** exhibited an adequate molecular size of approximately of 10 × 11 $Å^2$ to be encapsulated into the aperture of the pore windows of **MOF-H** (11 × 11 $Å^2$). **L27** showed a broad emission at λ_{PL} = 570 nm in degassed DMF, while **MOF-H** exhibited bright blue emission at λ_{PL} = 425 nm attributed to the emissive TATPT linker. When complex **L27** was loaded into the pores of **MOF-H** at various concentrations from 0.52 wt% to 8.8 wt%, the host-guest **MOF-H⊃L27** exhibited two emission maxima with various intensities at λ_{PL} = 425 nm and λ_{PL} = 530 nm (Figure **44a**), attributed, respectively, to the emissions of **MOF-H** and **L27** without energy transfer between the two. Due to the rigid confinement of **L27** into the cavities of **MOF-H**, the emission of **L27** in **MOF-H⊃L27** was blue-shifted by ca. 40 nm compared to that observed for the free complex in solution. Interestingly, at a concentration of 3.5 wt% of **L27**, **MOF-H⊃L27** exhibited pure white light emission with a high Φ_{PL} of 20.4% corresponding to CIE coordinates of x: 0.31, y: 0.33 (Figure **44b,c**). A WOLED (white organic-light emitting diode) of CIE coordinates of x: 0.30, y: 0.35 using this material and an InGaAsN ultraviolet chip were both successfully fabricated.

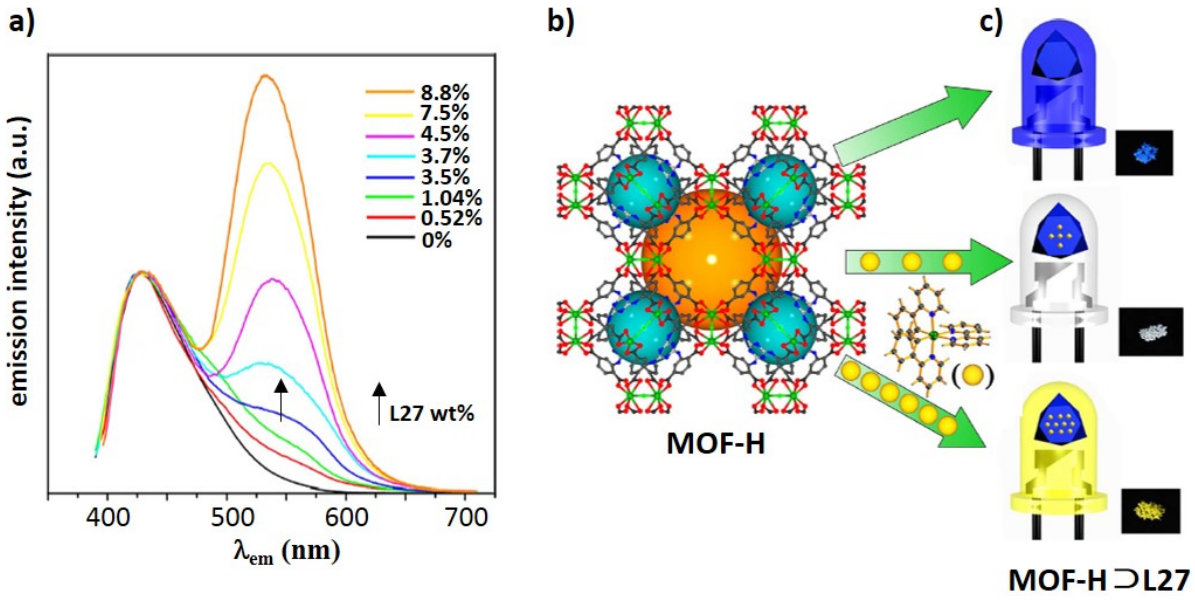

Figure **44**. **a)** Emission spectra of **MOF-H** and **MOF-H⊃L27** with different concentrations of **L27** (from 0.52 wt% to 8.8 wt%, λ_{ect} = 370 nm, 298 K); **b)** ball and stick representation of the 3D structure of **MOF-H** (orange and cyan spheres represent the void spaces); **c)** illustration of the blue, white and yellow emissions exhibited by **MOF-H⊃L27** with a concentration of **L27** respectively of 0%, 3.5% and 8.8 wt%. Adapted from Ref. [175], Springer Nature.

The red-emitting cage **C3** (Figure **35a**,**b**) we recently reported exhibited a diameter of approximately 18.8 Å (corresponding to the Pd···Pd distance) with an internal pocket volume of approximately 3480 Å^3, which was of sufficient size to include mononuclear Ir(III) complexes.[159] We thus targeted the encapsulation of the anionic blue-emitting $NBu_4[Ir(dFppy)_2(CN)_2]$ complex (**L28**) to study the nature of the energy transfer between the donor blue-emitting guest and the acceptor red-emitting cage **C3** (Figure **45**).[159] ^{1}H, ^{1}H DOSY and ^{19}F NMR investigations along with computational calculations revealed a strong binding of **L28** within the cavity of **C3** in **C3⊃L28** with an association constant K of $3.9 \times 10^6 \pm 0.2$ M^{-1}.

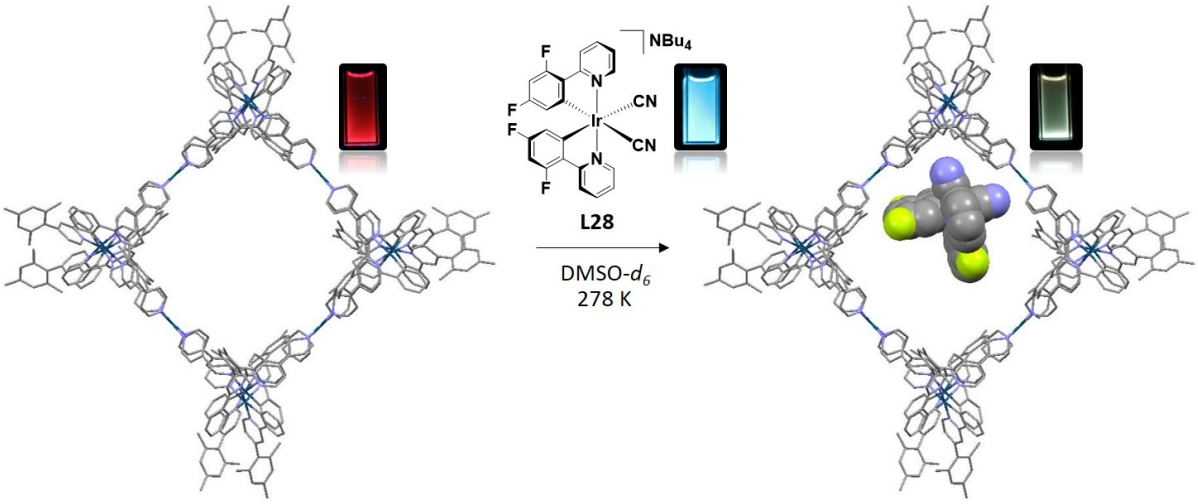

Figure **45**. Illustration of encapsulation of **L28** (space-fill representation) within the cavity of **C3**. The HF/6-31G(d) optimized host-guest structure **C3⊃L28** is shown. Insets are the emissions of the species under UV irradiation.[159]

The anionic complex **L28** exhibited a blue ^{3}LC emission in DMSO, with two maxima at 458 and 483 nm and a shoulder at 515 nm (blue line in Figure **46a**), a Φ_{PL} of 52%, and a τ_{PL} of 2915 ns. Titration of cage **C3** (from 0 to 120 μM) into a 100 μM degassed DMSO solution of **L28** at 298 K resulted in a gradual quenching of the blue emission of the donor **L28** together with a gradual enhancement of the emission of the red-emitting cage at 666 nm, with an isosbestic point observed at 565 nm (Figure **46a**). Upon photoexcitation of **C3⊃L28** at 360 nm, Dexter energy transfer from the blue-emitting **L28** to the red-emitting **C3** was therefore promoted.

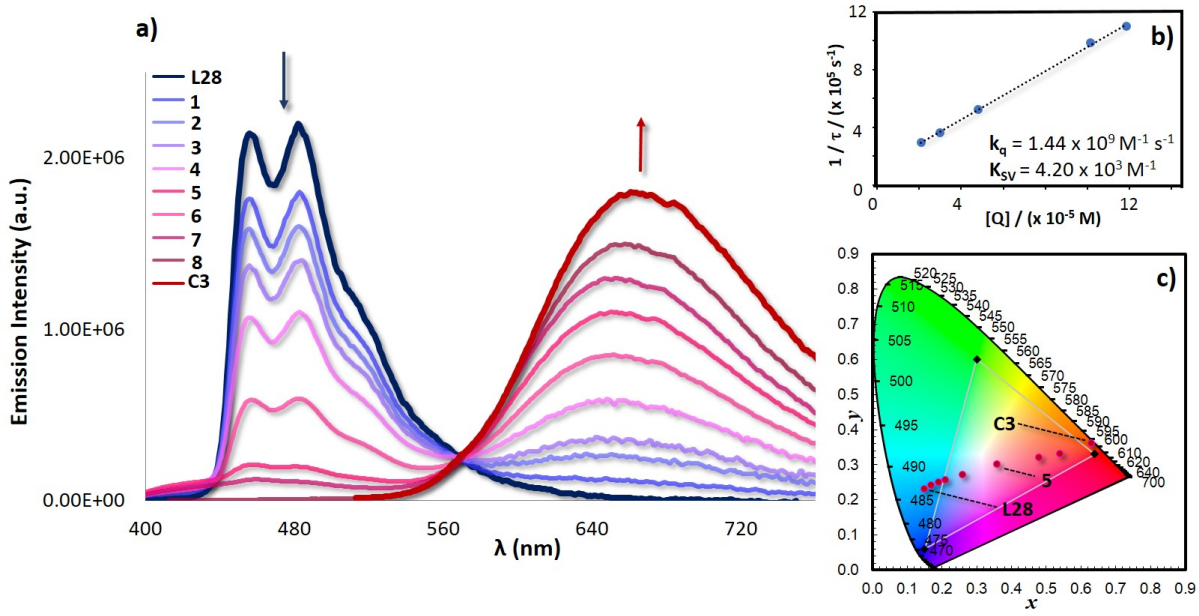

Figure **46**. **a)** Emission titrations of **C3** into a 100 μM solution of **L28** at 298 K in degassed DMSO; **b)** Stern-Volmer plot of the quenching study between **L28** and **C3**; **c)** CIE diagram indicating the change of emission colors during the emission titration.[159]

Stern-Volmer analysis (Figure **46b**) demonstrated that the energy transfer/quenching process in **C3**⊃**L28** was very efficient with a calculated quenching rate constant (k_q) of 1.44×10^9 $M^{-1}s^{-1}$ and a Stern-Volmer constant (K_{SV}) of 4.20×10^3 M^{-1}. The CIE diagram shown in Figure **46c** illustrates the change in the emission colors observed during the emission titration. Titration 5 (Figure **46c**) shows CIE coordinates of (0.36, 0.30), which are close to coordinates of pure white light (x: 0.31, y: 0.33).

5. Conclusions

The self-assembly of Ir(III) luminophores into supramolecular materials clearly offers possibilities for tuning the physical and optoelectronic properties of Ir(III) complexes and opens up opportunities for exploiting these materials in many applications, ranging from

catalysis to electroluminescent devices. Iridium-based soft materials generally exhibit highly organized structures with enhanced emission when compared to their mononuclear counterparts. Three-dimensional iridium-based polymers and MOFs are still in their infancy. However, it appears clear that the combination of the luminescent properties of Ir(III) chromophores and the large channel sizes exhibited by these classes of porous materials is of great interest for sensing and for solar-driven chemical transformations. Photoactive coordination cages and capsules incorporating Ir(III) chromophores are promising candidates as photoactive containers capable of photophysically interacting with guest molecules. On the other hand, stability, ligand design and control of the luminescent properties of the materials in the solid state are the major challenges to meet in order to expand the use and number of supramolecular Ir(III) assemblies. The relatively small number of examples included in this review article shows, however, that the field is relatively new, with most of the articles published only in the last decade. However, given the demonstrated functionality of these systems, their importance is sure to grow rapidly.

Acknowledgements. EZ-C acknowledges the University of St Andrews for financial support and the Engineering and Physical Sciences Research Council for financial support (EP/M02105X/1).

References

[1] D. Philp, J.F. Stoddart, Angew. Chem. Int. Ed. Engl., 35 (1996) 1154-1196.
[2] J.M. Grimes, J.N. Burroughs, P. Gouet, J.M. Diprose, R. Malby, S. Zientara, P.P.C. Mertens, D.I. Stuart, Nature, 395 (1998) 470-478.
[3] A.W. Roszak, T.D. Howard, J. Southall, A.T. Gardiner, C.J. Law, N.W. Isaacs, R.J. Cogdell, Science, 302 (2003) 1969-1972.

[4] L. Yang, A. Liu, S. Cao, R.M. Putri, P. Jonkheijm, J.J.L.M. Cornelissen, Chem. Eur. J., 22 (2016) 15570-15582.
[5] G.M. Whitesides, B. Grzybowski, Science, 295 (2002) 2418-2421.
[6] W.R. Wikoff, L. Liljas, R.L. Duda, H. Tsuruta, R.W. Hendrix, J.E. Johnson, Science, 289 (2000) 2129-2133.
[7] G. McDermott, S.M. Prince, A.A. Freer, A.M. Hawthornthwaite-Lawless, M.Z. Papiz, R.J. Cogdell, N.W. Isaacs, Nature, 374 (1995) 517-521.
[8] S. Bahatyrova, R.N. Frese, C.A. Siebert, J.D. Olsen, K.O. van der Werf, R. van Grondelle, R.A. Niederman, P.A. Bullough, C. Otto, C.N. Hunter, Nature, 430 (2004) 1058-1062.
[9] K. Goossens, K. Lava, C.W. Bielawski, K. Binnemans, Chem Rev, 116 (2016) 4643-4807.
[10] T. Wohrle, I. Wurzbach, J. Kirres, A. Kostidou, N. Kapernaum, J. Litterscheidt, J.C. Haenle, P. Staffeld, A. Baro, F. Giesselmann, S. Laschat, Chem Rev, 116 (2016) 1139-1241.
[11] D. Kim, S. Cheong, Y.G. Ahn, S.W. Ryu, J.K. Kim, J. Cho, Nanoscale, 8 (2016) 7000-7016.
[12] P.-P. Yang, X.-X. Zhao, A.-P. Xu, L. Wang, H. Wang, J. Mater. Chem. B, 4 (2016) 2662-2668.
[13] S.S. Babu, V.K. Praveen, A. Ajayaghosh, Chem Rev, 114 (2014) 1973-2129.
[14] Z. Qi, C.A. Schalley, Acc Chem Res, 47 (2014) 2222-2233.
[15] A. Winter, U.S. Schubert, Chem Soc Rev, 45 (2016) 5311-5357.
[16] L. Yang, X. Tan, Z. Wang, X. Zhang, Chem Rev, 115 (2015) 7196-7239.
[17] M.C. Das, S. Xiang, Z. Zhang, B. Chen, Angew Chem Int Ed Engl, 50 (2011) 10510-10520.
[18] D. Fujita, Y. Ueda, S. Sato, N. Mizuno, T. Kumasaka, M. Fujita, Nature, 540 (2016) 563-566.
[19] D. Fujita, H. Yokoyama, Y. Ueda, S. Sato, M. Fujita, Angew Chem Int Ed Engl, 54 (2015) 155-158.
[20] H.K. Bisoyi, Q. Li, Acc Chem Res, 47 (2014) 3184-3195.
[21] M. Antonietti, C. Göltner, Angew. Chem. Int. Ed. Engl., 36 (1997) 910-928.
[22] C.F. Faul, Acc Chem Res, 47 (2014) 3428-3438.
[23] E. Caló, V.V. Khutoryanskiy, Eur. Polym. J., 65 (2015) 252-267.
[24] A.S. Hoffman, Advanced Drug Delivery Reviews, 64 (2012) 18-23.
[25] V.K. Thakur, M.R. Kessler, Polymer, 69 (2015) 369-383.
[26] L. Sun, M.G. Campbell, M. Dinca, Angew Chem Int Ed Engl, 55 (2016) 3566-3579.
[27] J.-L. Wang, C. Wang, W. Lin, ACS Catalysis, 2 (2012) 2630-2640.
[28] T.H. Noh, O.-S. Jung, Acc. Chem. Res., 49 (2016) 1835-1843.
[29] Z. Hu, B.J. Deibert, J. Li, Chem Soc Rev, 43 (2014) 5815-5840.
[30] L. Xu, Y.X. Wang, H.B. Yang, Dalton Trans, 44 (2015) 867-890.
[31] M.W. Cooke, D. Chartrand, G.S. Hanan, Coord. Chem. Rev., 252 (2008) 903-921.
[32] S. Durot, J. Taesch, V. Heitz, Chem Rev, 114 (2014) 8542-8578.
[33] D.B. Amabilino, D.K. Smith, J.W. Steed, Chem Soc Rev, 46 (2017) 2404-2420.
[34] H. Xu, R. Chen, Q. Sun, W. Lai, Q. Su, W. Huang, X. Liu, Chem. Soc. Rev., 43 (2014) 3259-3302.
[35] T. Zhang, W. Lin, Chem. Soc. Rev., 43 (2014) 5982-5993.
[36] A.F. Henwood, E. Zysman-Colman, Chem. Commun., 53 (2017) 807-826.
[37] A.F. Henwood, E. Zysman-Colman, Top. Curr. Chem., 374 (2016) 36.
[38] D. Ma, T. Tsuboi, Y. Qiu, L. Duan, Adv Mater, 29 (2017) 1603253.
[39] J.C. Deaton, F.N. Castellano, Archetypal Iridium(III) Compounds for Optoelectronic and Photonic Applications, in: Iridium(III) in Optoelectronic and Photonics Applications, John Wiley & Sons, Ltd, 2017, pp. 1-69.

[40] Z. Liu, Z. Bian, C. Huang, Luminescent Iridium Complexes and Their Applications, in: H. Bozec, V. Guerchais (Eds.) Molecular Organometallic Materials for Optics, Springer Berlin Heidelberg, Berlin, Heidelberg, 2010, pp. 113-142.
[41] Y. You, S. Cho, W. Nam, Inorg Chem, 53 (2014) 1804-1815.
[42] D.-L. Ma, S. Lin, W. Wang, C. Yang, C.-H. Leung, Chem. Sci., 8 (2017) 878-889.
[43] K.K.-W. Lo, K.K.-S. Tso, Inorganic Chemistry Frontiers, 2 (2015) 510-524.
[44] C.K. Prier, D.A. Rankic, D.W.C. MacMillan, Chem. Rev., 113 (2013) 5322-5363.
[45] N.D. McDaniel, S. Bernhard, Dalton Trans., 39 (2010) 10021-10030.
[46] J.M. Thomsen, D.L. Huang, R.H. Crabtree, G.W. Brudvig, Dalton Trans., 44 (2015) 12452-12472.
[47] A.F. Henwood, E. Zysman-Colman, A Comprehensive Review of Luminescent Iridium Complexes Used in Light-Emitting Electrochemical Cells (LEECs), in: Iridium(III) in Optoelectronic and Photonics Applications, John Wiley & Sons, Ltd, 2017, pp. 275-357.
[48] E. Longhi, L. De Cola, Iridium(III) Complexes for OLED Application, in: Iridium(III) in Optoelectronic and Photonics Applications, John Wiley & Sons, Ltd, 2017, pp. 205-274.
[49] L. Flamigni, J.-P. Collin, J.-P. Sauvage, Acc. Chem. Res., 41 (2008) 857-871.
[50] V.L. Whittle, J.A.G. Williams, Dalton Trans., (2009) 3929-3940.
[51] A.M. Soliman, D. Fortin, P.D. Harvey, E. Zysman-Colman, Dalton Trans., 41 (2012) 9382-9393.
[52] A. Winter, U.S. Schubert, Polymeric Architectures Containing Phosphorescent Iridium(III) Complexes, in: Iridium(III) in Optoelectronic and Photonics Applications, John Wiley & Sons, Ltd, 2017, pp. 145-203.
[53] Q. Zhao, S.-J. Liu, W. Huang, Macromol. Rapid Commun., 31 (2010) 794-807.
[54] F. Xu, H.U. Kim, J.-H. Kim, B.J. Jung, A.C. Grimsdale, D.-H. Hwang, Prog. Polym. Sci., 47 (2015) 92-121.
[55] C. Wu, H.-F. Chen, K.-T. Wong, M.E. Thompson, J. Am. Chem. Soc., 132 (2010) 3133-3139.
[56] M. Mauro, K.C. Schuermann, R. Prétôt, A. Hafner, P. Mercandelli, A. Sironi, L. De Cola, Angew. Chem. Int. Ed., 49 (2010) 1222-1226.
[57] M. Sandroni, E. Zysman-Colman, Dalton Trans., 43 (2014) 3676-3680.
[58] K.N. Swanick, M. Sandroni, Z. Ding, E. Zysman-Colman, Chem. Eur. J., 21 (2015) 7435-7440.
[59] E.H. Doeven, E.M. Zammit, G.J. Barbante, C.F. Hogan, N.W. Barnett, P.S. Francis, Angew. Chem. Int. Ed., 51 (2012) 4354-4357.
[60] G.J. Barbante, N. Kebede, C.M. Hindson, E.H. Doeven, E.M. Zammit, G.R. Hanson, C.F. Hogan, P.S. Francis, Chem. Eur. J., 20 (2014) 14026-14031.
[61] E.H. Doeven, E.M. Zammit, G.J. Barbante, P.S. Francis, N.W. Barnett, C.F. Hogan, Chem. Sci., 4 (2013) 977-982.
[62] A. Ionescu, E.I. Szerb, Y.J. Yadav, A.M. Talarico, M. Ghedini, N. Godbert, Dalton Trans., 43 (2014) 784-789.
[63] V. Fiorini, A. D'Ignazio, K.D. Magee, M.I. Ogden, M. Massi, S. Stagni, Dalton Trans, 45 (2016) 3256-3259.
[64] S. Lamansky, P. Djurovich, D. Murphy, F. Abdel-Razzaq, R. Kwong, I. Tsyba, M. Bortz, B. Mui, R. Bau, M.E. Thompson, Inorg. Chem., 40 (2001) 1704-1711.
[65] S. Lamansky, P. Djurovich, D. Murphy, F. Abdel-Razzaq, H.-E. Lee, C. Adachi, P.E. Burrows, S.R. Forrest, M.E. Thompson, J. Am. Chem. Soc., 123 (2001) 4304-4312.
[66] Y. Chi, P.-T. Chou, Chem. Soc. Rev., 39 (2010) 638-655.
[67] C.E. Housecroft, E.C. Constable, Coord. Chem. Rev., 350 (2017) 155-177.
[68] R.D. Costa, G. Fernández, L. Sánchez, N. Martín, E. Ortí, H.J. Bolink, Chem. Eur. J., 16 (2010) 9855-9863.

[69] E.A. Plummer, A. van Dijken, J.W. Hofstraat, L. De Cola, K. Brunner, Adv. Funct. Mater., 15 (2005) 281-289.
[70] X. Yang, X. Xu, J.S. Dang, G. Zhou, C.L. Ho, W.Y. Wong, Inorg Chem, 55 (2016) 1720-1727.
[71] X. Yang, Z. Feng, J. Zhao, J.S. Dang, B. Liu, K. Zhang, G. Zhou, ACS Appl Mater Interfaces, 8 (2016) 33874-33887.
[72] A. M'Hamedi, A.S. Batsanov, M.A. Fox, M.R. Bryce, K. Abdullah, H.A. Al-Attar, A.P. Monkman, J. Mater. Chem., 22 (2012) 13529-13540.
[73] Y. Zheng, A.S. Batsanov, M.A. Fox, H.A. Al-Attar, K. Abdullah, V. Jankus, M.R. Bryce, A.P. Monkman, Angew Chem Int Ed Engl, 53 (2014) 11616-11619.
[74] M.Y. Wong, G. Xie, C. Tourbillon, M. Sandroni, D.B. Cordes, A.M.Z. Slawin, I.D.W. Samuel, E. Zysman-Colman, Dalton Trans., (2015) **DOI:** 10.1039/C1034DT03127J
[75] K. He, N. Su, Y. Junting, Y. Liu, W. Xiong, Z. Hao, D. Ma, W. Zhu, Tetrahedron, 72 (2016) 7164-7169.
[76] F. Dumur, G. Nasr, G. Wantz, C.R. Mayer, E. Dumas, A. Guerlin, F. Miomandre, G. Clavier, D. Bertin, D. Gigmes, Org. Electron., 12 (2011) 1683-1694.
[77] G. Nasr, A. Guerlin, F. Dumur, L. Beouch, E. Dumas, G. Clavier, F. Miomandre, F. Goubard, D. Gigmes, D. Bertin, G. Wantz, C.R. Mayer, Chem. Commun., 47 (2011) 10698-10700.
[78] C. He, K. Lu, W. Lin, J Am Chem Soc, 136 (2014) 12253-12256.
[79] H. Izumi, T. Torigoe, H. Ishiguchi, H. Uramoto, Y. Yoshida, M. Tanabe, T. Ise, T. Murakami, T. Yoshida, M. Nomoto, K. Kohno, Cancer Treatment Reviews, 29 (2003) 541-549.
[80] S. Chen, Y. Hong, Y. Liu, J. Liu, C.W. Leung, M. Li, R.T. Kwok, E. Zhao, J.W. Lam, Y. Yu, B.Z. Tang, J Am Chem Soc, 135 (2013) 4926-4929.
[81] Y. Ma, H. Liang, Y. Zeng, H. Yang, C.-L. Ho, W. Xu, Q. Zhao, W. Huang, W.-Y. Wong, Chem. Sci., 7 (2016) 3338-3346.
[82] S. Liu, A. Xu, Z. Chen, Y. Ma, H. Yang, Z. Shi, Q. Zhao, Opt Express, 24 (2016) 28247-28255.
[83] J.H. Vella, A. Parthasarathy, K.S. Schanze, J Phys Chem A, 117 (2013) 7818-7822.
[84] K. Binnemans, Chem. Rev., 105 (2005) 4148-4204.
[85] S.A. Hudson, P.M. Maitlis, Chem. Rev., 93 (1993) 861-885.
[86] P. Berdague, J. Courtieu, P.M. Maitlis, J. Chem. Soc., Chem. Commun., (1994) 1313-1314.
[87] M.A. Esteruelas, L.A. Oro, E. Sola, M.B. Ros, J.L. Serrano, J. Chem. Soc., Chem. Commun., (1989) 55-56.
[88] D.W. Bruce, D.A. Dunmur, M.A. Esteruelas, S.E. Hunt, R.L. Lagadec, P.M. Maitlis, J.R. Marsden, E. Sola, J.M. Stacey, J. Mater. Chem., 1 (1991) 251-254.
[89] S.T. Trzaska, T.M. Swager, Chem. Mater., 10 (1998) 438-443.
[90] E.I. Szerb, A.M. Talarico, I. Aiello, A. Crispini, N. Godbert, D. Pucci, T. Pugliese, M. Ghedini, Eur. J. Inorg. Chem., 2010 (2010) 3270-3277.
[91] A. Santoro, A.M. Prokhorov, V.N. Kozhevnikov, A.C. Whitwood, B. Donnio, J.A.G. Williams, D.W. Bruce, J. Am. Chem. Soc., 133 (2011) 5248-5251.
[92] A.M. Prokhorov, A. Santoro, J.A.G. Williams, D.W. Bruce, Angew. Chem. Int. Ed., 51 (2012) 95-98.
[93] Y. Wang, C.P. Cabry, M. Xiao, L. Male, S.J. Cowling, D.W. Bruce, J. Shi, W. Zhu, E. Baranoff, Chem. Eur. J., 22 (2016) 1618-1621.
[94] N.S. Kumar, M.Z. Shafikov, A.C. Whitwood, B. Donnio, P.B. Karadakov, V.N. Kozhevnikov, D.W. Bruce, Chemistry, 22 (2016) 8215-8233.

[95] V.N. Kozhevnikov, B. Donnio, D.W. Bruce, Angew. Chem. Int. Ed., 47 (2008) 6286-6289.
[96] J.W. Steed, Chem. Soc. Rev., 39 (2010).
[97] N.M. Sangeetha, U. Maitra, Chem Soc Rev, 34 (2005) 821-836.
[98] X. Du, J. Zhou, J. Shi, B. Xu, Chem Rev, 115 (2015) 13165-13307.
[99] C.D. Jones, J.W. Steed, Chem. Soc. Rev., 45 (2016) 6546-6596.
[100] M.-O.M. Piepenbrock, G.O. Lloyd, N. Clarke, J.W. Steed, Chem. Rev., 110 (2010) 1960-2004.
[101] X. Cao, Y. Wu, K. Liu, X. Yu, B. Wu, H. Wu, Z. Gong, T. Yi, J. Mater. Chem., 22 (2012) 2650.
[102] L. Xiong, Q. Zhao, H. Chen, Y. Wu, Z. Dong, Z. Zhou, F. Li, Inorg Chem, 49 (2010) 6402-6408.
[103] Y.J. Yadav, B. Heinrich, G. De Luca, A.M. Talarico, T.F. Mastropietro, M. Ghedini, B. Donnio, E.I. Szerb, Adv. Optical Mater., 1 (2013) 844-854.
[104] M. Mauro, A. Aliprandi, D. Septiadi, N.S. Kehr, L. De Cola, Chem Soc Rev, 43 (2014) 4144-4166.
[105] A. Aliprandi, D. Genovese, M. Mauro, L. De Cola, Chem. Lett., 44 (2015) 1152-1169.
[106] N. Vogel, M. Retsch, C.A. Fustin, A. Del Campo, U. Jonas, Chem Rev, 115 (2015) 6265-6311.
[107] A. Guerrero-Martínez, Y. Vida, D. Domínguez-Gutiérrez, R.Q. Albuquerque, L. De Cola, Inorg. Chem., 47 (2008) 9131-9133.
[108] A.M. Talarico, M. Ghedini, C.O. Rossi, E.I. Szerb, Soft Matter, 8 (2012) 11661-11669.
[109] M. Mauro, G. De Paoli, M. Otter, D. Donghi, G. D'Alfonso, L. De Cola, Dalton Trans., 40 (2011) 12106-12116.
[110] D. Aiello, A.M. Talarico, F. Teocoli, E.I. Szerb, I. Aiello, F. Testa, M. Ghedini, New J. Chem., 35 (2011) 141-148.
[111] M. de Barros e Silva Botelho, J.M. Fernandez-Hernandez, T.B. de Queiroz, H. Eckert, L. De Cola, A.S.S. de Camargo, J. Mater. Chem., 21 (2011) 8829-8834.
[112] U.M. Tefashe, K.L. Metera, H.F. Sleiman, J. Mauzeroll, Langmuir, 29 (2013) 12866-12873.
[113] K.L. Metera, K.D. Hänni, G. Zhou, M.K. Nayak, H.S. Bazzi, D. Juncker, H.F. Sleiman, ACS Macro Letters, 1 (2012) 954-959.
[114] A.-H. Liang, K. Zhang, J. Zhang, F. Huang, X.-H. Zhu, Y. Cao, Chem. Mater., 25 (2013) 1013-1019.
[115] A.-h. Liang, S. Dong, K. Zhang, X. Xiao, F. Huang, X.-H. Zhu, Y. Cao, Macromol. Rapid Commun., 34 (2013) 1301-1305.
[116] A.M. Talarico, E.I. Szerb, T.F. Mastropietro, I. Aiello, A. Crispini, M. Ghedini, Dalton Trans., 41 (2012) 4919-4926.
[117] L. Donato, P. Abel, E. Zysman-Colman, Dalton Trans., 42 (2013) 8402-8412.
[118] J.M. Rawson, L. Donato, E. Zysman-Colman, CrystEngComm, 16 (2014) 8531-8536.
[119] C.E. Welby, L. Gilmartin, R.R. Marriott, A. Zahid, C.R. Rice, E.A. Gibson, P.I. Elliott, Dalton Trans, 42 (2013) 13527-13536.
[120] S. Kammer, H. Müller, N. Grunwald, A. Bellin, A. Kelling, U. Schilde, W. Mickler, C. Dosche, H.-J. Holdt, Eur. J. Inorg. Chem., 2006 (2006) 1547-1551.
[121] S. Kammer, A. Kelling, H. Baier, W. Mickler, C. Dosche, K. Rurack, A. Kapp, F. Lisdat, H.-J. Holdt, Eur. J. Inorg. Chem., 2009 (2009) 4648-4659.
[122] S. Kammer, I. Starke, A. Pietrucha, A. Kelling, W. Mickler, U. Schilde, C. Dosche, E. Kleinpeter, H.-J. Holdt, Dalton Trans., 41 (2012) 10219-10227.
[123] L. Chen, Q. Chen, M. Wu, F. Jiang, M. Hong, Acc Chem Res, 48 (2015) 201-210.
[124] W. Wang, Y.X. Wang, H.B. Yang, Chem Soc Rev, 45 (2016) 2656-2693.

[125] P.J. Stang, B. Olenyuk, Acc. Chem. Res., 30 (1997) 502-518.
[126] S. Kitagawa, R. Kitaura, S. Noro, Angew Chem Int Ed Engl, 43 (2004) 2334-2375.
[127] C. Wang, D. Liu, Z. Xie, W. Lin, Inorg Chem, 53 (2014) 1331-1338.
[128] Z. Xie, L. Ma, K.E. deKrafft, A. Jin, W. Lin, J. Am. Chem. Soc., 132 (2010) 922-923.
[129] M.-L. Ho, Y.-A. Chen, T.-C. Chen, P.-J. Chang, Y.-P. Yu, K.-Y. Cheng, C.-H. Shih, G.-H. Lee, H.-S. Sheu, Dalton Trans., 41 (2012) 2592-2600.
[130] K.Y. Cheng, J.C. Wang, C.Y. Lin, W.R. Lin, Y.A. Chen, F.J. Tsai, Y.C. Chuang, G.Y. Lin, C.W. Ni, Y.T. Zeng, M.L. Ho, Dalton Trans, 43 (2014) 6536-6547.
[131] Y. Xu, L. Li, S. Zhang, S. Zhao, J. Luo, Crystal Growth & Design, 16 (2016) 406-411.
[132] L. Li, S. Zhang, L. Xu, Z.-N. Chen, J. Luo, J. Mater. Chem. C, 2 (2014).
[133] D. Zeng, M. Ren, S.S. Bao, L. Li, L.M. Zheng, Chem. Commun., 50 (2014) 8356-8359.
[134] N.M. Ali, V.L. MacLeod, P. Jennison, I.V. Sazanovich, C.A. Hunter, J.A. Weinstein, M.D. Ward, Dalton Trans., 41 (2012) 2408-2419.
[135] L. Li, S. Zhang, L. Xu, J. Wang, L.-X. Shi, Z.-N. Chen, M. Hong, J. Luo, Chem. Sci., 5 (2014).
[136] L. Li, S. Zhang, L. Xu, L. Han, Z.N. Chen, J. Luo, Inorg Chem, 52 (2013) 12323-12325.
[137] C. Wang, Z. Xie, K.E. deKrafft, W. Lin, J. Am. Chem. Soc., 133 (2011) 13445-13454.
[138] C. Wang, J.-L. Wang, W. Lin, J. Am. Chem. Soc., 134 (2012) 19895-19908.
[139] C. Wang, K.E. deKrafft, W. Lin, J. Am. Chem. Soc., 134 (2012) 7211-7214.
[140] P. Contreras Carballada, N. Mourtzis, M. Felici, S. Bonnet, R.J.M. Nolte, R.M. Williams, L. De Cola, M.C. Feiters, Eur. J. Org. Chem., 2012 (2012) 6729-6736.
[141] N. Mourtzis, P.C. Carballada, M. Felici, R.J. Nolte, R.M. Williams, L. de Cola, M.C. Feiters, Phys Chem Chem Phys, 13 (2011) 7903-7909.
[142] S.-L. Huang, N. Liu, Y. Ling, H.-K. Luo, Chem. Asian J., ASAP DOI: 10.1002/asia.201701339.
[143] K. Fan, S.-S. Bao, W.-X. Nie, C.-H. Liao, L.-M. Zheng, Inorg. Chem., 57 (2018) 1079-1089.
[144] C. Bronner, S.p.A. Baudron, M.W. Hosseini, Inorg. Chem., 49 (2010) 8659-8661.
[145] C. Xu, A. Guenet, N. Kyritsakas, J.-M. Planeix, M.W. Hosseini, Chem. Commun., 51 (2015) 14785-14788.
[146] C. Xu, A. Guenet, N. Kyritsakas, J.-M. Planeix, M.W. Hosseini, Inorg. Chem., 54 (2015) 10429-10439.
[147] M.D. Ward, P.R. Raithby, Chem. Soc. Rev., 42 (2013) 1619-1636.
[148] M.M.J. Smulders, I.A. Riddell, C. Browne, J.R. Nitschke, Chem. Soc. Rev., 42 (2013) 1728-1754.
[149] R. Chakrabarty, P.S. Mukherjee, P.J. Stang, Chem. Rev., 111 (2011) 6810-6918.
[150] S. Zarra, D.M. Wood, D.A. Roberts, J.R. Nitschke, Chem Soc Rev, 44 (2015) 419-432.
[151] M. Yoshizawa, J.K. Klosterman, M. Fujita, Angew. Chem. Int. Ed., 48 (2009) 3418-3438.
[152] Y.F. Han, W.G. Jia, W.B. Yu, G.X. Jin, Chem Soc Rev, 38 (2009) 3419-3434.
[153] N. Singh, D. Kim, D.H. Kim, E.H. Kim, H. Kim, M.S. Lah, K.W. Chi, Dalton Trans, 46 (2017) 571-577.
[154] L. Yang, A. von Zelewsky, H. Stoeckli-Evans, Chem. Commun., (2005) 4155-4157.
[155] E. Baranoff, E. Orselli, L. Allouche, D. Di Censo, R. Scopelliti, M. Gratzel, M.K. Nazeeruddin, Chem. Commun., 47 (2011) 2799-2801.
[156] C.T. Wang, L.C. Shiu, K.B. Shiu, Chemistry, 21 (2015) 7026-7029.
[157] O. Chepelin, J. Ujma, X. Wu, A.M.Z. Slawin, M.B. Pitak, S.J. Coles, J. Michel, A.C. Jones, P.E. Barran, P.J. Lusby, J. Am. Chem. Soc., 134 (2012) 19334-19337.
[158] M. Fujita, D. Oguro, M. Miyazawa, H. Oka, K. Yamaguchi, K. Ogura, Nature, 378 (1995) 469-471.

[159] D. Rota Martir, D. Escudero, D. Jacquemin, D.B. Cordes, A.M.Z. Slawin, H.A. Fruchtl, S.L. Warriner, E. Zysman-Colman, Chem. Eur. J., 23 (2017) 14358-14366.
[160] D. Rota Martir, G.J. Hedley, D.B. Cordes, A.M.Z. Slawin, D. Escudero, D. Jacquemin, T. Kosikova, D. Philp, D.M. Dawson, S.E. Ashbrook, I.D.W. Samuel, E. Zysman-Colman, Dalton Trans., 45 (2016) 17195-17205.
[161] D.R. Martir, C. Momblona, A. Pertegás, D.B. Cordes, A.M.Z. Slawin, H.J. Bolink, E. Zysman-Colman, ACS Applied Materials & Interfaces, 8 (2016) 33907-33915.
[162] V.E. Pritchard, D. Rota Martir, S. Oldknow, S. Kai, S. Hiraoka, N.J. Cookson, E. Zysman-Colman, M.J. Hardie, Chem. Eur. J., 23 (2017) 6290-6294.
[163] V.E. Pritchard, D. Rota Martir, E. Zysman-Colman, M.J. Hardie, Chem. Eur. J., 23 (2017) 8839-8849.
[164] X. Li, J. Wu, C. He, R. Zhang, C. Duan, Chem. Commun., 52 (2016) 5104-5107.
[165] X. Li, J. Wu, L. Chen, X. Zhong, C. He, R. Zhang, C. Duan, Chem. Commun., 52 (2016) 9628-9631.
[166] C.D. Boone, S. Gill, A. Habibzadegan, R. McKenna, International Journal of Chemical Engineering, 2013 (2013) 1-6.
[167] M. Waki, N. Mizoshita, T. Tani, S. Inagaki, Angew. Chem. Int. Ed., 50 (2011) 11667-11671.
[168] S. Horiuchi, H. Tanaka, E. Sakuda, Y. Arikawa, K. Umakoshi, Chem. Eur. J., 22 (2016) 17533-17537.
[169] L.R. Alrawashdeh, A.I. Day, L. Wallace, Dalton Trans, 42 (2013) 16478-16481.
[170] C. Xu, D. Mochizuki, Y. Hashimoto, T. Honda, Y. Tsukahara, T. Yamauchi, Y. Wada, Eur. J. Inorg. Chem., 2012 (2012) 3113-3120.
[171] C. Xu, D. Mochizuki, M.M. Maitani, Y. Wada, Eur. J. Inorg. Chem., 2014 (2014) 1470-1476.
[172] M. Waki, Y. Maegawa, K. Hara, Y. Goto, S. Shirai, Y. Yamada, N. Mizoshita, T. Tani, W.J. Chun, S. Muratsugu, M. Tada, A. Fukuoka, S. Inagaki, J Am Chem Soc, 136 (2014) 4003-4011.
[173] W.J. Finkenzeller, H. Yersin, Chem. Phys. Lett., 377 (2003) 299-305.
[174] D. Mochizuki, M. Sugiyama, M.M. Maitani, Y. Wada, Eur. J. Inorg. Chem., 2013 (2013) 2324-2329.
[175] C.-Y. Sun, X.-L. Wang, X. Zhang, C. Qin, P. Li, Z.-M. Su, D.-X. Zhu, G.-G. Shan, K.-Z. Shao, H. Wu, J. Li, Nat Commun, 4 (2013) 1-8.

TOC graphic